

**Yttrium Doped Bismuth Vanadium Oxide For Visible Light
Driven Hydrogen Production And Dye Degradation**

By

Muhammad Imran Rameel

Reg. No # 00000203843

Session 2017-21

Supervised by

Dr. Muhammad Hassan

**MASTER of SCIENCE in
Energy Systems Engineering**

**US-Pakistan Center for Advanced Studies in Energy
(USPCAS-E)**

National University of Sciences and Technology (NUST)

H-12, Islamabad 44000, Pakistan

April 2021

**Yttrium Doped Bismuth Vanadium Oxide For Visible Light
Driven Hydrogen Production And Dye Degradation**



By

Muhammad Imran Rameel

Reg. No. 00000203843

Session 2017-21

Supervised by

Dr. Muhammad Hassan

**A Thesis Submitted to the US-Pakistan Center for Advanced
Studies in Energy in partial fulfillment of the requirements for
the degree of**

**MASTER of SCIENCE in
Energy Systems Engineering**

**US-Pakistan Center for Advanced Studies in Energy
(USPCAS-E)**

National University of Sciences and Technology (NUST)

H-12, Islamabad 44000, Pakistan

THESIS ACCEPTANCE CERTIFICATE

Certified that final copy of MS/MPhil thesis written by **Mr. Muhammad Imran Rameel** (Registration No.203843), of USPCAS-E has been vetted by undersigned, found complete in all respects as per NUST Statues/Regulations, is within the similarity indices limit and is accepted as partial fulfillment for the award of MS/MPhil degree. It is further certified that necessary amendments as pointed out by GEC members of the scholar have also been incorporated in the said thesis.

Signature: _____

Name of Supervisor Dr. Muhammad Hassan

Date: _____

Signature: _____

Name of Co-Supervisor Dr. Abdullah Khan

Date: _____

Signature (HoD ESE) Dr. Naseem Iqbal

Date: _____

Signature (Dean/Principal) Dr Adeel Waqas

Date: _____

Certificate

This is to certify that work in this thesis has been carried out by **Mr. Muhammad Imran Rameel** and completed under my supervision in US-Pakistan Center for Advanced Studies in Energy (USPCAS-E), National University of Sciences and Technology, H-12, Islamabad, Pakistan.

Supervisor:

Dr. Muhammad
Hassan
USPCAS-E
NUST, Islamabad

GEC member 1:

Dr. Adeel Waqas
USPCAS-E
NUST, Islamabad

GEC member 2:

Dr. Nadia Shehzad
USPCAS-E
NUST, Islamabad

Co-Supervisor:

Dr. Abdullah Khan
Dept. Of Environment
Science
QAU, Islamabad

HOD-ESE:

Dr. Naseem Iqbal
USPCAS-E
NUST, Islamabad

Principal:

Dr. Adeel Waqas
USPCAS-E
NUST, Islamabad

Dedication

I dedicate my thesis to my beloved parents, my sister, my brother, my cousins and friends for their affection and support during my studies. Especially to my mother for always believing in me, praying for me and giving me courage.

Acknowledgment

First of all, to thanks to Allah Almighty for his countless blessings.

My gratitude to my supervisor Dr. Muhammad Hassan for giving the opportunity to conduct Research under his kind supervision.

My gratitude to Dr. A.M Kannan for proving opportunity to work under his supervision in Fuel Cells and batteries lab, ASU.

Many thanks to co-supervisor Dr. Abdullah Khan for guidance throughout the research and for opportunity to work in Renewable Energy Advancement Laboratory, QAU.

I would also like to extend my sincere gratitude to the GEC committee Dr. Adeel Waqas and Dr. Nadia Shehzad for their guidance and support.

I wish to acknowledge Engr. Ahad Hussain Javed for his support throughout the project.

Last but not least, my profound gratitude to my parents for being world best parents. They kept me going and provided all the support and encouragement throughout this journey.

Abstract

Fossil energy sources are continuously depleting and causing damage to the environment. The use of renewable energy options should be used to meet current and potential energy needs and to generate clean energy. Solar seems to be an attractive clean alternative energy source among renewable resources that can help increase our energy independence and reduce the implications of global warming. However solar suffers fluctuations so that need to be coupled with energy storage technologies. Energy storage in chemical bonds is most feasible and economical for solar energy storage, one of the attractive way to store electricity is to convert into storage fuels, such as hydrogen. Hydrogen production through water splitting is most used method but this is expensive, PEC waters splitting is cheapest way to produce hydrogen. Photo anode is one of the most important component of Photo-electrochemical water splitting. Bismuth vanadate is a promising photo catalyst for hydrogen production by splitting water molecules. Bismuth vanadate is also important photo catalyst for decolorizing the textile waste water. Dyes with bright color as reactive and acidic dyes are soluble in water and hard to remove, the removal of such color dyes from waste water is a difficult and complex task. Wastewater in the presence of dyes is a source for eutrophication and an unsightly contamination which can deliver by items through oxidation, hydrolysis or any other additional chemical process occurring in wastewater which are dangerous to both health and environment. Bismuth vanadate's photocatalytic performance is strongly influenced by high energy surface states i.e., unsaturated Bi atoms in structural framework and broken Bi-O bonds. The presence of these states makes photoactive materials susceptible to high charge-carriers recombination and poor in charge transport characteristics. To address this issue, in this work we doped Y^{+3} atoms to substitute Bi^{+3} in $Bi_{25}VO_{40}$ to modify surface states. $Bi_{25}VO_{40}$ nano-grains had distinct emission peak centered at 460 nm according to the photoluminescence (PL) spectrum. The photocatalytic activity of $Y_{0.03}-Bi_{25}VO_{40}$ increased up to 1.6 folds as compared to pristine bismuth vanadium oxide for the degradation of aqueous methylene blue (MB) while photocurrent response in comparison to the pristine material was enhanced.

Key words: Photo-catalysis, water splitting, Methylene Blue, Hydrogen production

Table of Contents

Abstract	vii
List of Figures	xii
List of Tables.....	xiv
List of abbreviations.....	xv
Chapter 1	1
INTRODUCTION.....	1
1.1 The Need for Renewable Energy.....	1
1.2 Environmental Effect of Textile Effluents	2
1.3 Classification of Dyes.....	3
1.4 Waste water treatment strategies	4
1.4.1 Traditional physical techniques	4
1.4.2 Chemical process	4
1.4.3 Biological processes.....	4
1.4.4 Advanced oxidation process (AOPs)	4
1.5 Photo catalysis	5
1.6 Bismuth vanadium oxide as photo catalyst	7
1.6.1 Brief background of bismuth vanadium oxide.....	7
1.6.2 Structure of bismuth vanadium oxide.....	8
1.6.3 Photo physical properties	8
1.7 Bismuth Vanadium Oxide as Photo-anode for Photo-electrochemical water splitting	9
1.8 Problem statement	11
1.8.1 Doping.....	11
1.8.2 Bismuth vanadium oxide composites	12

1.9 Objectives	12
Summary of the chapter.....	13
References	14
Chapter 2	21
Litrature Review.....	21
2.1 Information from the literature on the photocatalytic degradation of dyes	21
2.2 Bi ₂₅ VO ₄₀ photo anode for production of hydrogen by PEC water splitting	24
2.2.1 Background	24
2.2.2 Literature data on based on synthesis techniques of different Bismuth based materials with their PEC response	25
Summary of the chapter.....	29
References	30
Chapter 3	34
Experimental Methods	34
3.1 Characterization Techniques	34
3.1.1 X-Ray Diffraction	34
3.1.2 Scanning Electron Microscopy	35
3.1.3 Energy Dispersive spectroscopy (EDS).....	37
3.1.4 UV-vis Spectroscopy	37
3.2 Solution based Synthesis techniques	38
3.2.1 Hydrothermal Synthesis of Nano/Micro Particles	38
3.2.2 Sol gel technique.....	39
3.2.3 Dip coating.....	40
3.2.4 Spin coating	40
3.2.5 Doctor Blading.....	41

3.2.6 Spray pyrolysis.....	41
3.2.7 Electrodeposition	42
3.3 Vacuum based deposition techniques.....	42
3.3.1 Physical vapor deposition.....	42
3.3.2 Chemical vapor deposition	44
Summary of the chapter.....	45
References	46
Chapter 4	48
Methods and Materials	48
4.1 Materials	49
4.2 Hydrothermal method.....	49
4.2.1 Synthesis of BiVO ₄ nanoparticles.....	49
4.2.2 Synthesis of Yttrium doped Bi ₂₅ VO ₄₀ nanoparticles	50
4.2.4 Synthesis of Y-Bi ₂₅ VO ₄₀ nano-grains.....	51
4.3 Photo anode Preparation.....	52
Summary of the chapter.....	54
References	55
CHAPTER 5.....	58
RESULTS AND DISCUSSION	58
5.1 Characterization.....	58
5.1.1 X-ray Diffraction	58
5.1.2 Scanning Electron Microscopy.....	58
5.1.3 EDS X-ray microanalysis using SEM.....	60
5.3.1 Uv-vis and Photolumiscence Spectroscopy	61
5.4 Photocatalytic testing.....	64

5.3.3 Bi ₂₅ VO ₄ photo anode for production of hydrogen by PEC water splitting.....	69
Summary of Results and Discussions.....	73
References	74
Chapter 6	78
Exchange Work.....	78
State of Charge (SOC) and State of Health (SOH) Estimation for Lead Acid Batteries .	78
6.1 Introduction	78
6.2 Material degradation of electrodes and grids	79
6.3 Purpose of Measuring SOC and SOH	79
6.4 Experiment	79
6.4.1 The charging and discharging behavior of single cell battery	81
6.4.2 Rate of Charge and discharge	83
6.4.3 Electrochemical Impedance spectroscopy (EIS)	84
Summary of chapter.....	87
References	88
Chapter 7	90
Conclusions and Future Recommendations	90
7.1 Conclusions	90
7.2 Future Recommendations.....	91
7.2.1 Employing use of different morphologies of Bismuth vanadium oxide	91
7.2.2 Optimization of Coating processes.....	91
7.2.3 Development of Technique to understand Chemical changes	92
7.3 Future Experimentation for better photocatalytic performance of Bismuth Vanadium oxide.....	92

List of Figures

Figure 1.1 Classification of Dyes	3
Figure 1.2 Photocatalytic water splitting mechanism	10
Fig 3.1 Probe beam and measuring particle in SEM.....	35
Fig.3.2 Schematic flow for sample preparation for SEM films	36
Figure 3.3 Probe beam and measuring particle	37
Figure 3.4 Schematic diagram of Ultraviolet visible spectrometry	38
Figure 3.4 Dip coater.....	40
Fig 4.1 Hydrothermal Synthesis process steps of BVO nanoparticles.....	50
Figure 4.2 Hydrothermal synthesis of BVO Nanograins	52
Figure 4.3 Photo anodes	53
Figure 5.1 a) XRD patters of Bismuth vanadium oxide $\text{Bi}_{25}\text{VO}_{40}$, and with yttrium doping $\text{Y}_{0.03}\text{Bi}_{25}\text{VO}_{40}$ and $\text{Y}_{0.05}\text{Bi}_{25}\text{VO}_{40}$ Figure 5.1 b) SEM images of a) $\text{Bi}_{25}\text{VO}_{40}$ b) $\text{Y}_{0.03}\text{Bi}_{25}\text{VO}_{40}$	59
Figure 5.2 a) Elemental analysis of $\text{Bi}_{25}\text{VO}_{40}$ b) yttrium doped $\text{Bi}_{25}\text{VO}_{40}$	60
Figure 5.3 a) UV-Vis absorbance spectra of $\text{Bi}_{25}\text{VO}_{40}$, $\text{Y}_{0.03}\text{Bi}_{25}\text{VO}_{40}$ & $\text{Y}_{0.05}\text{Bi}_{25}\text{VO}_{40}$ 62 b) Photoluminescence spectra of doped and undoped $\text{Bi}_{25}\text{VO}_{40}$	62
Figure 5.4 Kebulka-munk function band gap estimation of pristine $\text{Bi}_{25}\text{VO}_{40}$	63
Figure 5.5 Kebulka-munk function band gap estimation of $\text{Y}_{0.03}\text{Bi}_{25}\text{VO}_{40}$	64
Figure 5.6 Molecular structure of Methylene Blue.....	65
Figure 5.7 a) UV-Vis spectra of pristine BVO after specific time interval under solar simulator b) Peak analysis of UV-Vis spectra of MB.....	66
Figure 5.8 Rate of degradation of methylene blue dye	67
Figure 5.9 a) $-\ln C/C^0$ vs Wavelength (nm) b) Total oxygenated carbon %	68
Figure 5.10 Recyclability of methylene blue dye degradation rate for $\text{Y}_{0.03}\text{Bi}_{25}\text{VO}_{40}$	69
Figure 5.11 a) LSV of doped and undoped BVO b) LSV under chopped light.....	71

Figure 5.12 LSV of photo anodes in electrolyte with or without Na_2SO_3	72
Figure 6.1 Testing setup for battery pack (3 LA cells connected in series).....	80
Figure 6.2 Steps of input command for MITS pro schedule file.....	81
Figure 6.3 Schedule file window of MITS pro software.....	82
Figure 6.4 Charging curve (rate C/2 and C/5: upto 2.4 V) for single cell battery	83
Figure 6.5 Discharge curve (rate C/2 and C/5) for single cell battery after charging up to 2.4V	84

List of Tables

Table 2.1 Information from the literature on the photocatalytic degradation of dyes ...	211
Table 2.2 Literature data on based on synthesis techniques of different Bismuth based materials with their PEC response	254
Table 5.1 Summary of Results and Discussion.....	73

List of abbreviations

IPCC.....Intergovernmental Panel on Climate Change

GHG.....Green House Gas

AOPs.....Advanced oxidation process

BVO.....Bismuth vanadium oxide

XRD.....X-ray diffraction

SEM.....Scanning electron microscopy

CVD.....Chemical vapor deposition

PVD.....Physical vapor deposition

LUMO...Lowest Unoccupied Molecular Orbital

HOMO...Highest Occupied Molecular Orbital

EDTA.... Ethylenediaminetetraacetic acid

PL.....Photoluminescence

SOC.....State of charge

SOH.....State of health

LBT.....Laboratory battery testing

EIS..... Electrochemical Impedance spectroscopy

LSV.....Linear sweep voltammetry

SC.....Semiconductor

VB.....Valence band

CB.....Conduction band

Chapter 1

INTRODUCTION

1.1 The Need for Renewable Energy

For humanity, the oil crisis, drinking fresh water and climate change are the most dangerous problems nowadays. In order to reconcile the need for affordable energy with the urgent problem of climate change, we need to implement new policies that can use renewable energy sources other than fossil fuels to have sustainable solutions. In February 2007, the Intergovernmental Panel on Climate Change (IPCC) published a study on the rise in global concentrations of methane, nitrous oxide and carbon dioxide due to fossil fuel burning and other pollution-causing activities [1]. Carbon dioxide is the most influencing GHG (Green House Gas) which is mainly formed due to burning of coal. The increase in such gases cause an increase in temperatures, a phenomenon known as global warming. A rise of 0.13 °C per decade is caused by global warming. The study estimates that the world's average global temperature will experience a rise of 0.5 °C in the next ten decades [2]. This estimation will depend more on the quantity of GHGs produced by the atmosphere and the growth of the world's population. The gases created by the burning of fossil fuels also have other consequences than global warming, such as pollution that causes uncomfortable lives and badly affects health. As a result of global warming, in addition to rising temperatures, melting ice and glaciers posed threats to marine life and raised sea level at a rate of 1.88 mm/year in the years 1960-2005. It also raises the average ocean temperature. Acid rain is caused by nitrous and sulphurous oxides and is related to many respiratory and skin diseases [3]. These effects have been mild until now, but if the emission of gases causing such pollution continues along with a rapid population growth, the consequences will be serious. Our everyday lives and environmental processes will be affected by the affected atmosphere. Another problem with fossil fuel use is its rapid degradation, causing it to disappear. It takes millions of years for fossil fuels to develop and they are finite. 11 billion tons of oil is consumed annually and if we continue to use it at this pace, all known current oil reserves will end by 2050. We still have coal, but we

can only add a maximum of ten more years to our reserves by 2060. Huge coal deposits are present in the world, but if we continue using coal, its reserves would also end by 2090, to fill the oil and gas gap. One thing is to be kept in mind that the rate with which we are using fossil fuels today is slower than the rate with which we will be using in coming years due to population growth and industrialization. So fossil fuels will run out earlier than the estimated time [4]. The use of renewable energy options, such as solar photovoltaic technologies, solar thermal technologies, biofuels and clean coal technologies, should be used to meet current and potential energy needs and to generate clean energy. Sun powered is by all accounts an appealing clean elective fuel source among sustainable resources that can help increment our energy autonomy and lessen the ramifications of a worldwide temperature alteration. The sun is expected to shine for billions of years, well beyond the existence of Earth. One of the best ways of taking advantage of sufficient solar energy is decreasing the use of fossil fuels and, subsequently, reducing carbon emissions. While solar energy has a strong potential to reduce pollution and deliver significant amounts of energy to consumers, due to high capital costs, solar energy accounted for a very limited percentage of the total energy generated by alternative sources of energy. In 1 hour, more energy from the sun hits the planet (4.3×10^{20} J) than all the energy devoured by people in the entire year [5].

1.2 Environmental Effect of Textile Effluents

A key role played by dyes in many textile and dyeing industries. It is predicted that 100,000 different synthetic dyes are available commercially and widely used in dyeing industry. Dyes are derivative of two main sources, petroleum and coal tar which shows an annual total production of more than 7×10^5 tones [6-7].

Dyes with bright color as reactive and acidic dyes are soluble in water and hard to remove, the removal of such color dyes from waste water is a difficult and complex task [8]. Dyes known as the first recognized contamination present in industrial waste water due to their higher visibility at minimum concentration level (<1 ppm) [9]. Wastewater in the presence of dyes is a source for eutrophication and an unsightly contamination which can deliver by items through oxidation, hydrolysis or any other additional chemical process occurring in wastewater which are dangerous to both health and environment [10], other than these

harmful impacts of colors present in wastewater, the presence can lessen light infiltration and which in outcome decrease photosynthetic action, making O₂ inaccessible for biodegradation through microorganisms present in the water.

In addition to the textile industries, the tanning industries [11], the paper industries [12], the food industries [13], hair-dyes [14], photo electrochemical cells [15] and light harvesting matrices [16], further contribute the dyes presence in waste water. Mostly dyes used in different industries are proven toxic and carcinogenic, so they shows a serious danger to living organisms present both on earth and marine ecosystem [17]. Such effects of dyes give an increase to the study of impacts of dyes on ecosystem in recent years.

1.3 Classification of Dyes

There are following types of dyes, classified on the basis of natural and synthetic, characteristic colors are removed from plants and creatures while engineered colors are mostly Azo and non Azo dyes, further these are characterized into sub classes as demonstrated in Figure 1.1

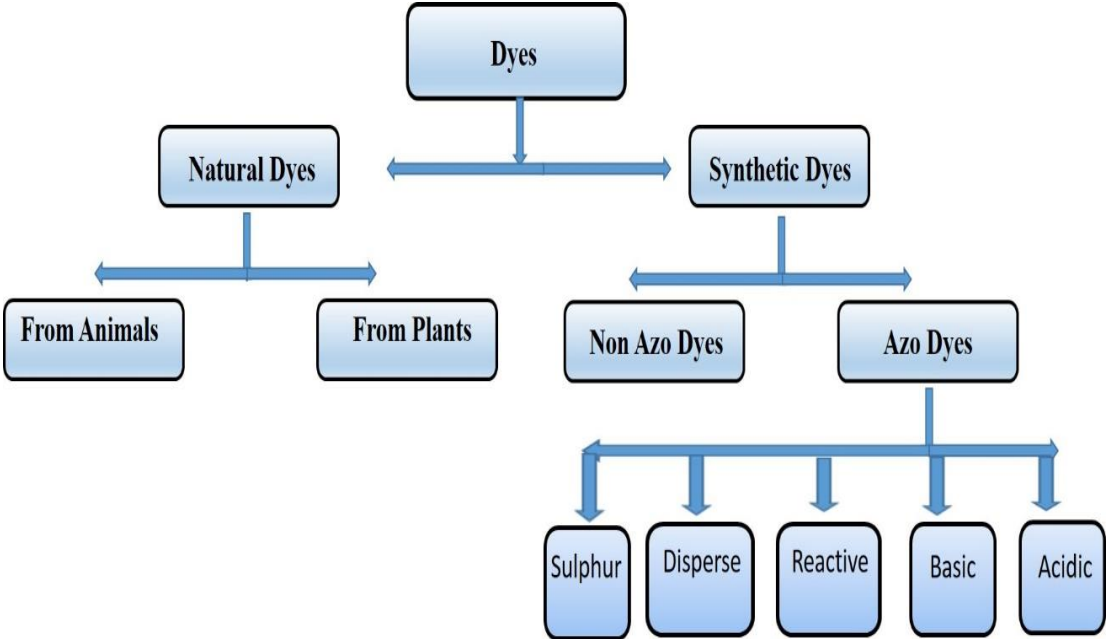


Figure 1.1 Classification of Dyes

1.4 Waste water treatment strategies

Apart from the physical irksome properties and toxicity, the increase in mass production of dyes due to the progress of industrial revolution has led to the prerequisite for effective treatment [18]. Therefore, a wide range of techniques have been studied and tested to address such obvious and challenging effluents and to reduce their amplified potential impact on the environment.

1.4.1 Traditional physical techniques

- Activated carbon.
- Adsorption
- Reverse osmosis
- Ultrafiltration

1.4.2 Chemical process

- Chlorination
- Ozonation
- Precipitation
- chemical oxidation processes

1.4.3 Biological processes

It involves enzymatic and microbiological degradation of dyes, Biological processes also used for removal of toxic dyes from waste waters [19].

1.4.4 Advanced oxidation process (AOPs)

Oxidants (for example ozone, hydrogen peroxide, oxygen) and/or fuel sources (bright light for instance) or impetuses (for example titanium dioxide, niobium pentoxide, thorium vanadate).

AOPs have capacity to rapidly oxidize defilements [20-21]. This depend on in-situ creation interaction of more receptive hydroxyl radical (OH[•]) which can oxidize practically all compound present in the wastewater, with dispersion controlled response speed. First radical that are delivered by or with the assistance [20] oxidants (for example ozone, hydrogen peroxide, oxygen) and/or fuel sources (bright light for instance) or

impetuses (for example titanium dioxide, niobium pentoxide and thorium vanadate) [22] molecules dye degradation by photo catalysts degraded both environmental (Atmosphere and aquatic organic) contaminants [23]. This process uses the sunlight in the presence of photo catalyst material for the destruction of these toxic molecules [24].

1.4.4.1 Photo-decolourization

This process is the involvement of both photo oxidation and photo reduction, which can restore the dye to its original condition by either reduction or oxidation process [25].

1.4.4.2 Photo degradation

This is the involvement of decomposition of stable forms of the dyes and is widely used and known photocatalytic dye treatment [26].

1.4.4.3 Photo mineralization

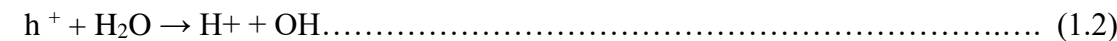
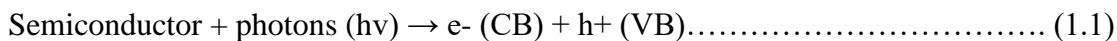
The process is regarded a complete decomposition of all the unwanted products such as CO₂, H₂O, N₂, NO³⁻ NO₂ [27- 28].

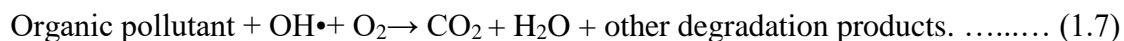
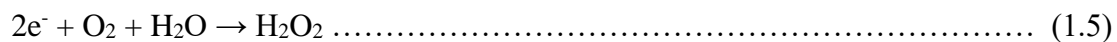
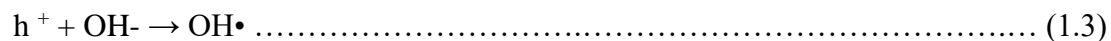
1.5 Photo catalysis

Heterogeneous photo catalysis for modern methods is widely used for dyes and stains for bleaching or degradation [29]. It uses the light of the sun in time of semiconductor photo catalysis, in the presence of an accelerated remediation of environmental contaminants and that it was for the destruction of highly toxic molecules [24].

Cycle for the most part includes the exchange of electrons in the conduction of the semiconductor surface band (generally oxides and sulphides) under the illumination of specific wavelength. The generated ions react with oxygen or water to produce superoxide positive ions and hydroxide radical ions. These kinds of species might have a high level of oxidizing molecules of numerous industrial dyes [30–32].

The radical species formed during the excitation process of semiconductor is mainly responsible for the dye degradation process. Steps involved in this process are following [33].





Semiconductors comprises of excited hole and electrons responsible for degradation of dye. Many semiconductors proved good for degradation and most of them used in Nano state to enhance the surface area for favorable conditions [34-35].

1.5.1 Difficulties in photo-catalysis and techniques for improving photocatalytic properties

Both metal oxides and sulfides among semiconductors photo catalysts are mostly used due to various properties like cheap, non-toxicity, stability and facileness in synthesis process and efficiency of these materials contrasted with different semiconductors those are proven toxic and less efficient like CdS and ZnO [36]. Furthermore, TiO₂ being a photoactive under UV region, shows about 5% of natural sunlight An enormous surface region, bountiful surface states, and various morphologies that are helpful for sun oriented photocatalytic response can be given by nanomaterials. But since of specific issues related with semiconductor metal oxide, the exhibition of the sun powered photo-catalyst is still lower. The photo-catalyst key issues are the confuse between the semiconductor and sunlight based range bandgap, wasteful confinement and transport of charges, and material insecurity [37-38].

1.5.1.1 Spectral mismatch

The sunlight based range comprises of UV (5%), noticeable (40%), and IR (55%) frequency, the greater part of the semiconductor photo-catalyst has high band-gap. Which can retain just UV part of sun based illumination, while most piece of sun oriented light is noticeable area. Tweak of the semiconductor photo-catalyst band-gap is a major issue. Moreover, researchers have examined for the improvement in TiO₂ by moving its photograph movement to the noticeable district, and towards the union of new photo-catalyst materials which are dynamic under obvious area [37].

1.5.1.2 Recombination of the photo generated charges

The recombination of photo produced electrons and openings is another central point of contention that impacts a semiconductor's photocatalytic movement. They relocate to the surface for oxidation and decrease measures after electron-openings are framed. Recombination of photo produced charge transporters can happen either in mass or on a superficial level during the movement stage by dispersing energy as light or warmth, consequently smothering photocatalytic action. There is an absence of main impetus for the division and transport of charges, so a little part of the charge transporter is isolated and takes an interest in the responses, while the remainder of the charge transporter is lost because of ineffective recombination. Debasements or imperfections in the gem encourage this recombination interaction. Thusly, the decrease of recombination is exceptionally basic for improving the activity.

1.5.1.3 Low surface area

Surface/interface chemistry also affects the photocatalytic activity, as surface energy plays a role in the photocatalytic reaction in the transmission of electrons between the reactant. The catalytic reaction at the surface or interface occurs in a heterogeneous catalyst.

Thus, efficiency depends on the catalyst's specific surface area, the higher the specific surface area the photocatalytic operation would be.

1.6 Bismuth vanadium oxide as photo catalyst

Bismuth vanadate is proven to be a serious candidate for photocatalytic activities. Number of works is carried out to investigate the properties of Bismuth vanadate and this work is increased significantly in last decade, especially with the focus on water oxidation [39-40].

1.6.1 Brief background of bismuth vanadium oxide

Bismuth vanadate meets a number of criteria needed for an ideal photo catalyst [41]. Non-toxicity, corrosion resistance and visible region light active are the most notable among them. For future applications in sustainable technology, the latter parameter is critical since the generated energy from Sun can be used to activate photocatalytic process.

1.6.2 Structure of bismuth vanadium oxide

Bismuth vanadium oxide happens in three polymorphs as for its primary attributes: monoclinic scheelite-like, tetragonal scheelite-like and tetragonal zircon-like constructions with E.g. 2.40, 2.34 and 2.90 eV separately [40–44].

There are $[\text{VO}_4]$ tetrahedra and $[\text{BiO}_8]$ polyhedra in the crystal structures, where V(V) and Bi(III) are in the center of the units. Every $[\text{BiO}_8]$ is surrounded by eight $[\text{VO}_4]$ in the scheelite phases, while Bi units are surrounded by only six $[\text{VO}_4]$ in the zircon structure [42].

The qualification among monoclinic and tetragonal scheelite structures is completely founded on the presence of neighborhood Bi and V setting, which in the monoclinic design is more sectarian [42]. Also, high temperature measure with alterable change to monoclinic scheelite at 255°C is the tetragonal construction [40,42]. In addition, the irreversible tetragon transformation. In the crystal structures, there are $[\text{VO}_4]$ tetrahedra and $[\text{BiO}_8]$ polyhedra, where V(V) and Bi(III) are in the Centre of the units. In the scheelite phases, each $[\text{BiO}_8]$ is surrounded by eight $[\text{VO}_4]$ while Bi units are surrounded by only six $[\text{VO}_4]$ in the zircon structure [42].

The separation among monoclinic and tetragonal scheelite structures depends on the presence of nearby Bi and V setting, which is more sectarian in the monoclinic framework. Besides, the tetragonal construction is a high temperature measure with alterable change to monoclinic scheelite at 255°C. The perpetual change of the tetragon, likewise. Contrasted with the tetragonal-zircon structure, this expanded light ingestion results from more modest E_g and more hardliner V and Bi units supporting charge transporter transport. There is an immediate band contrast between Bismuth vanadate and the upward of V [40-45].

1.6.3 Photo physical properties

Bismuth vanadate's photocatalytic activity relies strictly on its crystalline form, but also on the exposed facets of the crystal [41]. Undoubtedly by changing significant perspectives like particular adsorption of a reactant, the development of charge transporters and the desorption of materials [41,46], The crystal facets $\{0\ 1\ 0\}$ and $\{1\ 1\ 0\}$ distribute oxidation and reduction sites for monoclinic Bismuth vanadate, so these

facets having redox roles in which photo generated holes and electrons are available [47–50], however, found that monoclinic bismuth vanadate's photo oxidation properties are stronger for {0 1 0} dominant-BVO (facet with reduction sites). By rapid electron transfer to acceptor species, they clarified this fact.

1.7 Bismuth Vanadium Oxide as Photo-anode for Photo-electrochemical water splitting

It takes millions of years for fossil fuels to develop and they are finite. 11 billion tons of oil is consumed annually and if we continue to use it at this pace, all known current oil reserves will end by 2050. We still have coal, but we can only add a maximum of ten more years to our reserves by 2060. Huge coal deposits are present in the world, but if we continue using coal, its reserves would also end by 2090, to fill the oil and gas gap. One thing is to be kept in mind that the rate with which we are using fossil fuels today is slower than the rate with which we will be using in coming years due to population growth and industrialization. So fossil fuels will run out earlier than the estimated time. The use of renewable energy options, such as solar photovoltaic technologies, solar thermal technologies, biofuels and clean coal technologies, should be used to meet current and potential energy needs and to generate clean energy. Solar appears to be an appealing clean alternative energy source among renewable resources that can help us increase our energy independence while also reducing global warming's consequences. The sun is expected to shine for billions of years, well beyond the existence of Earth. One of the best ways of taking advantage of sufficient solar energy is decreasing the use of fossil fuels and, subsequently, reducing carbon emissions. While solar energy has a strong potential to reduce pollution and deliver significant amounts of energy to consumers. However solar suffers fluctuations so that need to be coupled with energy storage technologies. Solar energy can be stored in a variety of ways, including hydropower, solar-thermochemical storage, batteries, and chemical bonds. Among all these energy storage techniques, Energy storage in chemical bonds is most feasible and economical for solar energy storage. one of the attractive way to store electricity is to convert into storage fuels, such as hydrogen.

Hydrogen is a low-cost, zero-emission fuel that can be used in a range of applications, such as fuel cells, automobiles, and electric vehicles. The heat energy emitted by burning

1 kg of hydrogen is 147 MJ, which is higher than the energy yield of fossil fuels, which is 48 MJ/kg for gasoline and 44.8 MJ/kg for diesel.

Photo electrochemical water splitting is an alternate method of direct production of solar fuels, like hydrogen. The semiconductor is also used in this process. Photo electrodes are used to transform solar energy into chemical energy, allowing abundant yet abundant energy to be transformed into chemical energy. To harvest, store, and transform intermittent solar energy into a shape that can easily be stored. Several materials are used for effective and sustainable breakage of water into fuel (hydrogen and oxygen). Simultaneous compliance with the requirements is required: (1) ample photo voltage and sufficient water-breaking band alignment; (2) considerable absorption of the solar radiations spectrum, mainly visible light; (3) stable in addition easy transportation of charges through the semiconductor and the electrolyte solution and (4) cost-effectiveness and stability. Bottleneck of the process of use of photo anode TiO_2 and Platinum cathode in the presence of UV light is half reaction of oxidation of water. A variety of studies have been carried out to test suitable materials that can serve as successful to solve this bottleneck, photo anodes [40].

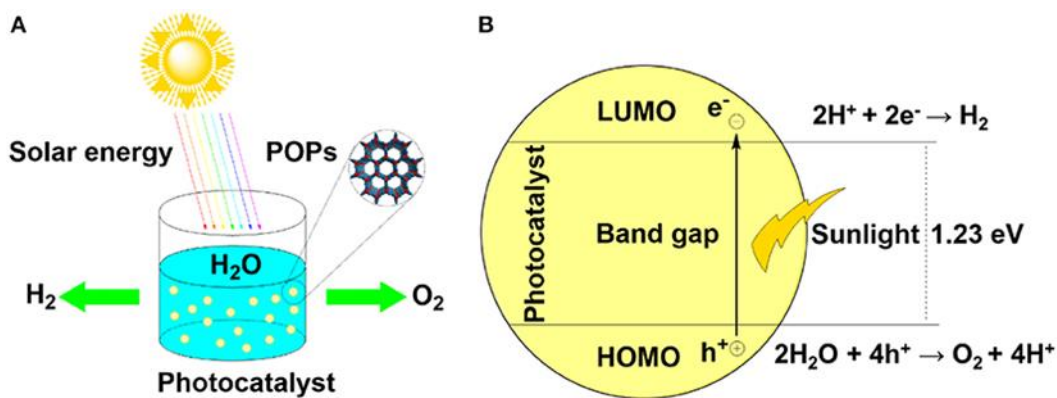


Figure 1.2 Photocatalytic water splitting mechanism

Bismuth based semiconductors (nanomaterials) are widely used as photo-catalyst material. Due to their small band gap and acceptable band locations, bismuth based nanomaterials have been regarded as possible candidates for PEC water splitting. This analysis focuses on the various bismuth-based materials used to date with extensive literature for solar water splitting applications.

1.8 Problem statement

Despite the benefits of Bismuth vanadium oxide many disadvantages are responsible for the poor performance of BVO photo catalysts [40,41], Secondly, bismuth vanadate has low electron mobility and elevated recombination of e^-/h^+ [41]. These key drawbacks are based on the structure of Bismuth vanadium oxide where $[VO_4]$ tetrahedral are not interconnected, as well as to the strong position of V 3d orbitals that make up the CB [41]. BVO also having a short diffusion length for holes which is around 70-100 nm that conciliations the optimization of harnessed light in compliance with the concept of optical penetration depth [40].

The following methods are used to increase Bismuth vanadate performance.

1.8.1 Doping

Since pure bismuth vanadate's photocatalytic efficiency is low, and only after long irradiation period leads to acceptable photo degradation rates, alteration of Bismuth vanadate is essential. The creation of altered BVO comprises the surface area improvement, the number of photocatalytic sites, the number of photons absorbed, the separation of the charge carrier and also the reduction of the E.g. energy band gap [51]. Doping is a method widely used to enhance BVO's photocatalytic efficiency. The theory of this approach is based on the insertion into the crystalline structure of Bismuth vanadate of electron acceptor or donor species (referred as n- and p type dopants). As a consequence, discrete amounts of electronic energy are incorporated into the semiconductor E_g . A surplus of both the electrons and holes population is available in the CB and VB at equilibrium dopant concentration. The useful effects usually found in a doped semiconductor photo catalyst are Tungsten (VI) and Molybdenum (VI) have been invent to be the most favorable n-type dopants among various evolution and rare earth metals for BVO, which is an n-type semiconductor [52–55]. The electronic properties of Bismuth vanadate, particularly for water oxidation are improved by Mo (VI) and W (VI) while other dopants, for example, Cu, Yb, Er, Nd and Sn particles are useful for Bismuth vanadate morphology and surface territory, and improved noticeable light ingestion.

1.8.2 Bismuth vanadium oxide composites

Composite processing is also an important way to enhance the photocatalytic process. $\text{Bi}_{25}\text{VO}_{40}$ properties [56]. Typically, a photo-catalyst for semiconductors including. It is possible to assemble bismuth vanadate with many types of materials, such as other Carbon materials (carbon nanotube, graphene oxide, etc.) can even be assembled with either $\text{Bi}_{25}\text{VO}_{40}$ [50–52]. Three forms are described according to the [53], structure of their electronic band [57]. In first type, both photo generated electron and holes are shifted from semiconductor (SC1). Semiconductor 2 (SC2) because of the location of E_{g2} within E_{g1} [56]. The photo-catalyst does not boost this form of heterojunction because all the charge carriers. In one semiconductor, they move and accumulate [56]. The CBM and VBM of semiconductor 1 is lower in energy than those of semiconductor 1 heterojunction and Semiconductor 2. As a consequence, when the photo generated electron moves from SC1 toward SC2, SC2 to SC1 photo generated holes travel [55–57]. Effective, if both semiconductors are in sufficient contact, during the photo activation process, charge carrier separation happens. The type III heterojunction, finally, it comprises of SC1 with an energy position of E_{g1} greater than SC2's E_{g2} . Accordingly, A recombination occurs between hole from SC1 VB and electron from SC2 CB [56] For the design of indirect Z-scheme, this form of heterojunction may be important Device with an effective mediator of electrons [56]. The majority of this is in the form II semiconductor heterojunction will be addressed in this section, as it is the easiest way to restrict electron and hole recombination of pairs that extend the lifespan of charge carriers, to achieve efficient effectiveness.

1.9 Objectives

- To synthesize BiVO_4 photo-catalysts using simple hydrothermal method
- To dope Yttrium in BiVO_4 to minimize the recombination for improved photocatalysis
- To characterize (morphological and structural, optical) of the synthesized materials
- To evaluate photocatalytic HER and dye degradation potential of Y- BiVO_4

Summary of the chapter

In this chapter an introduction to the solar photocatalytic water splitting and waste water treatment technology, its need and its importance has been discussed. There is a need for development of green energy generation systems which are alternative to conventional generation systems like using coal fired or oil fired power plants. The use of conventional energy resources is causing their depletion and may become extinct in coming years if we kept on using them. The pollutants caused by burning of such fossil fuels are responsible for global warming and other environment related bad impacts. Solar photo catalysis technology is a green option to replace the conventional Hydrogen production and waste water treatment technology. Scientists have been working to develop efficient and economical systems for their active commercialization. Scientists have developed different non-Nobel, non-toxic and environment friendly photo-catalyst systems. This research has been made to study Bismuth vanadium oxide system as a potential photo catalyst different factors to increase its photocatalytic performance in applications of hydrogen production and dye degradation.

References

- [1] Z. C. Meehl, G.A.; Stocker, T. F.; Collins, W. D.; Friedlingstein, P.; Gaye, T.; Gregory, J. M.; Kitoh, A.; Knutti, R.; Murphy, J. M.; Noda, A.; Raper, S. C. B.; Watterson, I. G.; Weaver, A. J.; Zhao, “IPCC, 2007: Climate Change 2007: the physical science basis. contribution of Working Group I to the Fourth Assessment Report of the Intergovernmental Panel on Climate Change,” *Cambridge Univ. Press*, pp. 747–846, 2007.
- [2] L. Authors *et al.*, “Chapter 1 : Historical Overview of Climate Change Science,” pp. 1–41.
- [3] M. Kampa and E. Castanas, “Human health effects of air pollution,” *Environ. Pollut.*, vol. 151, no. 2, pp. 362–367, 2008, doi: 10.1016/j.envpol.2007.06.012.
- [4] “All data from <https://www.cia.gov/library/publications/the-worldfactbook/geos/xx.html>.”
- [5] J. Tsao, N. Lewis, and G. Crabtree, “Solar FAQs,” *US Dep. Energy*, pp. 1–24, 2006, [Online]. Available: [http://www.sandia.gov/~jytsao/Solar FAQs.pdf](http://www.sandia.gov/~jytsao/Solar%20FAQs.pdf).
- [6] N. Bensalah, M. A. Q. Alfaro, and C. A. Martínez-Huitle, “Electrochemical treatment of synthetic wastewaters containing Alphazurine A dye,” *Chem. Eng. J.*, vol. 149, no. 1–3, pp. 348–352, 2009, doi: 10.1016/j.cej.2008.11.031.
- [7] F. Gosetti, V. Gianotti, S. Angioi, S. Polati, E. Marengo, and M. C. Gennaro, “Oxidative degradation of food dye E133 Brilliant Blue FCF: Liquid chromatography-electrospray mass spectrometry identification of the degradation pathway,” *J. Chromatogr. A*, vol. 1054, no. 1–2, pp. 379–387, 2004, doi: 10.1016/j.chroma.2004.07.106.
- [8] “Carliell et al. 1996 (anaerobic).pdf.” .
- [9] S. V. Mohan, Y. V. Bhaskar, and J. Karthikeyan, “Biological decolourisation of simulated azo dye in aqueous phase by algae *Spirogyra* species,” *Int. J. Environ. Pollut.*, vol. 21, no. 3, pp. 211–222, 2004, doi: 10.1504/IJEP.2004.004190.

- [10] A. G. S. Prado and L. L. Costa, "Photocatalytic decoloration of malachite green dye by application of TiO₂ nanotubes," *J. Hazard. Mater.*, vol. 169, no. 1–3, pp. 297–301, 2009, doi: 10.1016/j.jhazmat.2009.03.076.
- [11] A. Cassano, R. Molinari, M. Romano, and E. Drioli, "Treatment of aqueous effluents of the leather industry by membrane processes: A review," *J. Memb. Sci.*, vol. 181, no. 1, pp. 111–126, 2001, doi: 10.1016/S0376-7388(00)00399-9.
- [12] G. Crini, "Non-conventional low-cost adsorbents for dye removal: A review," *Bioresour. Technol.*, vol. 97, no. 9, pp. 1061–1085, 2006, doi: 10.1016/j.biortech.2005.05.001.
- [13] M. Pérez-Urquiza and J. L. Beltrán, "Determination of dyes in foodstuffs by capillary zone electrophoresis," *J. Chromatogr. A*, vol. 898, no. 2, pp. 271–275, 2000, doi: 10.1016/S0021-9673(00)00841-4.
- [14] A. Ajmal, I. Majeed, R. N. Malik, H. Idriss, and M. A. Nadeem, "Principles and mechanisms of photocatalytic dye degradation on TiO₂ based photocatalysts: A comparative overview," *RSC Adv.*, vol. 4, no. 70, pp. 37003–37026, 2014, doi: 10.1039/c4ra06658h.
- [15] D. Wróbel, A. Boguta, and R. M. Ion, "Mixtures of synthetic organic dyes in a photoelectrochemical cell," *J. Photochem. Photobiol. A Chem.*, vol. 138, no. 1, pp. 7–22, 2001, doi: 10.1016/S1010-6030(00)00377-4.
- [16] L. Yang, Y. Lin, J. Jia, X. Xiao, X. Li, and X. Zhou, "Light harvesting enhancement for dye-sensitized solar cells by novel anode containing cauliflower-like TiO₂ spheres," *J. Power Sources*, vol. 182, no. 1, pp. 370–376, 2008, doi: 10.1016/j.jpowsour.2008.03.013.
- [17] R. Nilsson, R. Nordlinder, U. Wass, B. Meding, and L. Belin, "Asthma, rhinitis, and dermatitis in workers exposed to reactive dyes," *Br. J. Ind. Med.*, vol. 50, no. 1, pp. 65–70, 1993, doi: 10.1136/oem.50.1.65.
- [18] W. Z. Tang and Huren An, "UV/TiO₂ photocatalytic oxidation of commercial dyes in aqueous solutions," *Chemosphere*, vol. 31, no. 9, pp. 4157–4170, 1995, doi:

10.1016/0045-6535(95)80015-D.

- [19] O. J. Hao, H. Kim, and P. C. Chiang, "Decolorization of wastewater," *Crit. Rev. Environ. Sci. Technol.*, vol. 30, no. 4, pp. 449–505, 2000, doi: 10.1080/10643380091184237.
- [20] M. Sleiman, D. Vildoza, C. Ferronato, and J. M. Chovelon, "Photocatalytic degradation of azo dye Metanil Yellow: Optimization and kinetic modeling using a chemometric approach," *Appl. Catal. B Environ.*, vol. 77, no. 1–2, pp. 1–11, 2007, doi: 10.1016/j.apcatb.2007.06.015.
- [21] S. Chakrabarti and B. K. Dutta, "Photocatalytic degradation of model textile dyes in wastewater using ZnO as semiconductor catalyst," *J. Hazard. Mater.*, vol. 112, no. 3, pp. 269–278, 2004, doi: 10.1016/j.jhazmat.2004.05.013.
- [22] J. Madhavan, P. Maruthamuthu, S. Murugesan, and S. Anandan, "Kinetic studies on visible light-assisted degradation of acid red 88 in presence of metal-ion coupled oxone reagent," *Appl. Catal. B Environ.*, vol. 83, no. 1–2, pp. 8–14, 2008, doi: 10.1016/j.apcatb.2008.01.021.
- [23] P. Pizarro, C. Guillard, N. Perol, and J. M. Herrmann, "Photocatalytic degradation of imazapyr in water: Comparison of activities of different supported and unsupported TiO₂-based catalysts," *Catal. Today*, vol. 101, no. 3-4 SPEC. ISS., pp. 211–218, 2005, doi: 10.1016/j.cattod.2005.03.008.
- [24] H. M. Yates, M. G. Nolan, D. W. Sheel, and M. E. Pemble, "The role of nitrogen doping on the development of visible light-induced photocatalytic activity in thin TiO₂ films grown on glass by chemical vapour deposition," *J. Photochem. Photobiol. A Chem.*, vol. 179, no. 1–2, pp. 213–223, 2006, doi: 10.1016/j.jphotochem.2005.08.018.
- [25] L. C. Chen and T. C. Chou, "Photodecolorization of Methyl Orange Using Silver Ion Modified TiO₂ as Photocatalyst," *Ind. Eng. Chem. Res.*, vol. 33, no. 6, pp. 1436–1443, 1994, doi: 10.1021/ie00030a002.
- [26] K. Vinodgopal and P. V. Kamat, "Enhanced Rates of Photocatalytic Degradation

- of an Azo Dye Using SnO₂/TiO₂ Coupled Semiconductor Thin Films,” *Environ. Sci. Technol.*, vol. 29, no. 3, pp. 841–845, 1995, doi: 10.1021/es00003a037.
- [27] Y. Wang, “Solar photocatalytic degradation of eight commercial dyes in TiO₂ suspension,” *Chinese J. Catal.*, vol. 21, no. 4, pp. 327–331, 2000.
- [28] A. Wang, J. Qu, H. Liu, and J. Ru, “Mineralization of an azo dye Acid Red 14 by photoelectro-Fenton process using an activated carbon fiber cathode,” *Appl. Catal. B Environ.*, vol. 84, no. 3–4, pp. 393–399, 2008, doi: 10.1016/j.apcatb.2008.04.016.
- [29] V. U. Pandit *et al.*, “Solar light driven dye degradation using novel organo-inorganic (6,13-pentacenequinone/TiO₂) nanocomposite,” *RSC Adv.*, vol. 5, no. 14, pp. 10326–10331, 2015, doi: 10.1039/c4ra11920g.
- [30] T. M. Elmorsi, Y. M. Riyad, Z. H. Mohamed, and H. M. H. Abd El Bary, “Decolorization of Mordant red 73 azo dye in water using H₂O₂/UV and photo-Fenton treatment,” *J. Hazard. Mater.*, vol. 174, no. 1–3, pp. 352–358, 2010, doi: 10.1016/j.jhazmat.2009.09.057.
- [31] Ş. Gül and Ö. Özcan-Yildirim, “Degradation of Reactive Red 194 and Reactive Yellow 145 azo dyes by O₃ and H₂O₂/UV-C processes,” *Chem. Eng. J.*, vol. 155, no. 3, pp. 684–690, 2009, doi: 10.1016/j.cej.2009.08.029.
- [32] F. H. AlHamedi, M. A. Rauf, and S. S. Ashraf, “Degradation studies of Rhodamine B in the presence of UV/H₂O₂,” *Desalination*, vol. 239, no. 1–3, pp. 159–166, 2009, doi: 10.1016/j.desal.2008.03.016.
- [33] C. Cameselle, M. A. Sanromán, and M. M. Pazos, “Journal of Environmental Science and Health - Part A Toxic/Hazardous Substances and Environmental Engineering: Foreword,” *J. Environ. Sci. Heal. - Part A Toxic/Hazardous Subst. Environ. Eng.*, vol. 43, no. 8, pp. 793–794, 2008, doi: 10.1080/10934520801973899.
- [34] J. C. Colmenares, R. Luque, J. M. Campelo, F. Colmenares, Z. Karpiński, and A. A. Romero, “Nanostructured photocatalysts and their applications in the photocatalytic transformation of lignocellulosic biomass: An overview,” *Materials*

- (*Basel*), vol. 2, no. 4, pp. 2228–2258, 2009, doi: 10.3390/ma2042228.
- [35] M. Ye *et al.*, “Magnetically Recoverable Core-Shell Nanocomposites with Enhanced Photocatalytic Activity,” *Chem. - A Eur. J.*, vol. 16, no. 21, pp. 6243–6250, 2010, doi: 10.1002/chem.200903516.
- [36] U. I. Gaya, “Heterogeneous photocatalysis using inorganic semiconductor solids,” *Heterog. Photocatal. Using Inorg. Semicond. Solids*, vol. 9789400777, pp. 1–213, 2014, doi: 10.1007/978-94-007-7775-0.
- [37] K. Hashimoto, H. Irie, and A. Fujishima, “TiO₂ photocatalysis: A historical overview and future prospects,” *Japanese J. Appl. Physics, Part 1 Regul. Pap. Short Notes Rev. Pap.*, vol. 44, no. 12, pp. 8269–8285, 2005, doi: 10.1143/JJAP.44.8269.
- [38] M. C. Leu and W. Zhang, “Interactive sketch-based digital prototyping by using the level-set method,” *ASME Int. Mech. Eng. Congr. Expo. Proc.*, vol. 3, pp. 257–264, 2007, doi: 10.1115/IMECE200743738.
- [39] S. S. M. Bhat and H. W. Jang, “Recent Advances in Bismuth-Based Nanomaterials for Photoelectrochemical Water Splitting,” *ChemSusChem*, vol. 10, no. 15, pp. 3001–3018, 2017, doi: 10.1002/cssc.201700633.
- [40] P. Lianos, “Review of recent trends in photoelectrocatalytic conversion of solar energy to electricity and hydrogen,” *Appl. Catal. B Environ.*, vol. 210, pp. 235–254, 2017, doi: 10.1016/j.apcatb.2017.03.067.
- [41] J. Gan, X. Lu, and Y. Tong, “Towards highly efficient photoanodes: boosting sunlight-driven semiconductor nanomaterials for water oxidation,” pp. 7142–7164, 2014, doi: 10.1039/c4nr01181c.
- [42] Y. Park, K. J. Mc Donald, and K. S. Choi, “Progress in bismuth vanadate photoanodes for use in solar water oxidation,” *Chem. Soc. Rev.*, vol. 42, no. 6, pp. 2321–2337, 2013, doi: 10.1039/c2cs35260e.
- [43] Y. H. Xu, C. J. Liu, M. J. Chen, and Y. Q. Liu, “A review in visible-light-driven BiVO₄ photocatalysts,” *Int. J. Nanoparticles*, vol. 4, no. 2–3, pp. 268–283, 2011, doi: 10.1504/IJNP.2011.040513.

- [44] X. Xu, Q. Zou, Y. Yuan, F. Ji, Z. Fan, and B. Zhou, "Preparation of BiVO₄-graphene nanocomposites and their photocatalytic activity," *J. Nanomater.*, vol. 2014, 2014, doi: 10.1155/2014/401697.
- [45] S. Tokunaga, H. Kato, and A. Kudo, "Selective preparation of monoclinic and tetragonal BiVO₄ with scheelite structure and their photocatalytic properties," *Chem. Mater.*, vol. 13, no. 12, pp. 4624–4628, 2001, doi: 10.1021/cm0103390.
- [46] W. Y. Teoh, J. A. Scott, and R. Amal, "Progress in heterogeneous photocatalysis: From classical radical chemistry to engineering nanomaterials and solar reactors," *J. Phys. Chem. Lett.*, vol. 3, no. 5, pp. 629–639, 2012, doi: 10.1021/jz3000646.
- [47] S. M. Thalluri, M. Hussain, G. Saracco, J. Barber, and N. Russo, "Green-synthesized BiVO₄ oriented along {040} facets for visible-light-driven ethylene degradation," *Ind. Eng. Chem. Res.*, vol. 53, no. 7, pp. 2640–2646, 2014, doi: 10.1021/ie403999g.
- [48] T. Tachikawa, T. Ochi, and Y. Kobori, "Crystal-Face-Dependent Charge Dynamics on a BiVO₄ Photocatalyst Revealed by Single-Particle Spectroelectrochemistry," *ACS Catal.*, vol. 6, no. 4, pp. 2250–2256, 2016, doi: 10.1021/acscatal.6b00234.
- [49] H. L. Tan, X. Wen, R. Amal, and Y. H. Ng, "BiVO₄ {010} and {110} Relative Exposure Extent: Governing Factor of Surface Charge Population and Photocatalytic Activity," *J. Phys. Chem. Lett.*, vol. 7, no. 7, pp. 1400–1405, 2016, doi: 10.1021/acs.jpcclett.6b00428.
- [50] G. Xi and J. Ye, "Synthesis of bismuth vanadate nanoplates with exposed {001} facets and enhanced visible-light photocatalytic properties," *Chem. Commun.*, vol. 46, no. 11, pp. 1893–1895, 2010, doi: 10.1039/b923435g.
- [51] A. O. Ibadon and P. Fitzpatrick, "Heterogeneous photocatalysis: Recent advances and applications," *Catalysts*, vol. 3, no. 1, pp. 189–218, 2013, doi: 10.3390/catal3010189.
- [52] W. Luo *et al.*, "Solar hydrogen generation from seawater with a modified BiVO₄ photoanode," *Energy Environ. Sci.*, vol. 4, no. 10, pp. 4046–4051, 2011, doi:

10.1039/c1ee01812d.

- [53] Z. F. Huang, L. Pan, J. J. Zou, X. Zhang, and L. Wang, “Nanostructured bismuth vanadate-based materials for solar-energy-driven water oxidation: A review on recent progress,” *Nanoscale*, vol. 6, no. 23, pp. 14044–14063, 2014, doi: 10.1039/c4nr05245e.
- [54] S. P. Berglund, A. J. E. Rettie, S. Hoang, and C. B. Mullins, “Incorporation of Mo and W into nanostructured BiVO₄ films for efficient photoelectrochemical water oxidation,” *Phys. Chem. Chem. Phys.*, vol. 14, no. 19, pp. 7065–7075, 2012, doi: 10.1039/c2cp40807d.
- [55] J. Huang, G. Tan, L. Zhang, H. Ren, A. Xia, and C. Zhao, “Enhanced photocatalytic activity of tetragonal BiVO₄: Influenced by rare earth ion Yb³⁺,” *Mater. Lett.*, vol. 133, pp. 20–23, 2014, doi: 10.1016/j.matlet.2014.06.123.
- [56] M. Reza Gholipour, C. T. Dinh, F. Béland, and T. O. Do, “Nanocomposite heterojunctions as sunlight-driven photocatalysts for hydrogen production from water splitting,” *Nanoscale*, vol. 7, no. 18, pp. 8187–8208, 2015, doi: 10.1039/c4nr07224c.
- [57] S. J. A. Moniz, S. A. Shevlin, D. J. Martin, Z. X. Guo, and J. Tang, “Visible-light driven heterojunction photocatalysts for water splitting—a critical review,” *Energy Environ. Sci.*, vol. 8, no. 3, pp. 731–759, 2015, doi: 10.1039/c4ee03271c.
- [58] Z. Zhu, Q. Han, D. Yu, J. Sun, and B. Liu, “A novel p-n heterojunction of BiVO₄/TiO₂/GO composite for enhanced visible-light-driven photocatalytic activity,” *Mater. Lett.*, vol. 209, no. 3, pp. 379–383, 2017, doi: 10.1016/j.matlet.2017.08.045.

Chapter 2

Literature Review

2.1 Information from the literature on the photocatalytic degradation of dyes

Table 2.1 Information from the literature on the photocatalytic degradation of dyes

Catalyst systems studied	Dyes Employed	Comments	Refs
Graphene-gold Nano composites	Rhodamine B Methylene blue Orange H	The debasement pace of methylene blue color is more noteworthy than Rhodamine B within the sight of noticeable light despite the fact that the redox potential is most elevated among these three colors. Adsorption of the color on a superficial level recognized as the purpose behind the photo activity	[1]
TiO ₂ , ZnO, SnO ₂	Crystal violet Methyl Red	ZnO shows preferred photo-activity over Degussa P-25 and silver stored ZnO expands the photocatalytic action by 20%	[2]
TiO ₂	Methyl Orange	The photocatalytic movement is discovered to be more	[3]

	Methylene Blue	noteworthy within the sight of sun powered light than in UV	
Mg ₂ -TiO ₂	Methyl orange	The catalyst has preferred photo-activity over the undoped TiO ₂ -Dye sensitization and infusion of the energized electron is considered as cause	[4]
TiO ₂	Indigo Indigo carmine	Complete mineralization of the dyes	[5]
Nanostructured TiO ₂	Categories of indigoid, anthraquinone triaryl methane and xanthene dyes	Degradation relies upon the chemical structure of the color (dye), the nature of functional group. Mono-azo colors corrupt quicker than anthraquinone colors. The presence of nitrite bunch advances the debasement action.	[6]
High surface area TiO ₂	Methylene blue Congo Red	Sol gel preparation method of TiO ₂ is suitable for degradation of Dyes	[7]
ZnO and TiO ₂	Rhodamine B Methylene Blue Acridine Orange	ZnO breaks down as Zn(OH) ₂ and henceforth shows lower movement when contrasted with TiO ₂	[8]
TiO ₂ (UV/Solar/pH)	Procion Yellow	TiO ₂ in the presence of solar irradiation gives better degradation	[9]

ZnO photocatalyst	Methylene Blue	The basic solution is better for the degradation reaction	[10]
Carbon doped TiO ₂	Amido Black-10B	Dynamic oxygenated species is liable for decolourization	[11]
Undoped and Fe doped CeO ₂	Methyl Orange	1.5 % doping of Fe ³⁺ was optimal	
La-Y/TiO ₂	Methylene Blue	Optimum catalyst dose 4 g/L	[12]

Titanium dioxide as a photo catalyst has been studied mostly for photocatalytic degradation of dyes. It has band gap of 3.2 eV so it only lies in UV region which is major disadvantage of Titania. The photon energizes an electron from the valence band to the conduction band and free electron in the conduction band and opening in the valence band, produce revolutionary species answerable for the debasement of natural colors to carbon dioxide and water and different types of degradation. For effective dye degradation, large surface area is required. Dye degradation kinetics can be understood by influence of adsorption that may precede degradation. Dye degradation has major place among numerous waste water treatment processes. The deterioration of dyes in the effluent water of the textile dyeing and finishing industry has been the most important because of environmental concerns. Semiconductors like TiO₂, ZnO are synthesized as nanospheres, nanorods, thin porous films, nanofibers and nanowires, Such systems are highly active, low-cost, and environmentally appropriate [13]. Other than these numerous other systems like CdS, Nb₂O₅, WO₃, have been used for photocatalytic dye degradation. These systems are included in Table, Drawback of most of these systems like Titania is higher value of band gap, due to which they only require UV light source to degrade waste water.

2.2 Bi₂₅VO₄₀ photo anode for production of hydrogen by PEC water splitting

2.2.1 Background

Photo electrochemical water splitting is an alternate method of direct production of solar fuels, like hydrogen. The semiconductor is also used in this process. Photo electrodes are used to transform solar energy into chemical energy, allowing abundant yet abundant energy to be transformed into chemical energy [14]. To harvest, store, and transform intermittent solar energy into a shape that can easily be stored. Several materials are used to effective and sustainable breakage of water into fuel (hydrogen and oxygen) [15]. Simultaneous compliance with the requirements is required: (1) ample photo voltage and sufficient water-breaking band alignment; (2) considerable absorption of the solar radiations spectrum, mainly visible light; (3) stable in addition easy transportation of charges through the semiconductor and the electrolyte solution and (4) cost-effectiveness and stability. Bottleneck of the process of use of photo anode TiO₂ and Platinum cathode in the presence of UV light is half reaction of oxidation of water. A variety of studies have been carried out to test suitable materials that can serve as successful to solve this bottleneck, photo anodes [16].

Bismuth based semiconductors (nanomaterials) are widely used as photo-catalyst material. Due to their small band gap and acceptable band locations, bismuth based nanomaterials have been regarded as possible candidates for PEC water splitting. This analysis focuses on the various bismuth-based materials used to date with extensive literature for solar water splitting applications. Since pure bismuth vanadate's photocatalytic efficiency is low, and only after long irradiation period leads to acceptable water splitting, alteration of Bismuth vanadate is essential The useful effects usually found in a doped semiconductor photo catalyst are Tungsten (VI) and Molybdenum (VI) have been invent to be the most favorable n-type dopants among various evolution and rare earth metals for BVO, which is an n-type semiconductors.

2.2.2 Literature data on based on synthesis techniques of different Bismuth based materials with their PEC response

Table 2.2 Literature data on based on synthesis techniques of different Bismuth based materials with their PEC response

Materials	Synthesis method	Heterojunction / co-catalyst	Electrolyte	Photocurrent density	Ref
BiOCl	Hydrothermal + Sol-gel + Chemical solution method	TiO ₂	0.5M Na ₂ SO ₄	10 ⁻³ mA Cm ⁻² at 1.2 V vs RHE	[17]
BiOBr	Aerosol-assisted chemical vapor deposition	None	0.5M Na pH 6.5M H ₂ SO ₄	0.38 mA Cm ⁻² at 1.2 V vs RHE	[18]
BiOI	Solvothermal/Hydr othermal method	TiO ₂	0.1M Na ₂ SO ₄	0.38 mA Cm ⁻² at 0.46 V vs. Ag/AgCl	[19]
BiVO ₄ ultrathin film	Modified sol-gel method	Sn polydimethylsil oxane O ₂ /Au on	0.5 M buffer phosp hate	1.37 mA Cm ⁻² at 1.23 V vs RHE	[20]
BiVO ₄ film	Modified metal organic decomposition method	SnO ₂	0.5M phosphate buffer	0.95 mA Cm ⁻² at 1.23 V vs. RHE	[21]
BiVO ₄	Spray pyrolysis	Co-Pi and W	0.5 M K ₂ SO ₄	2.3 mA Cm ⁻²	[22]

film		doping	in	at	
			phosphate buffer	1.23 V vs. RHE	
BiVO ₄ island	Spin coating	WO ₃ and TiO ₂	0.1 M Na ₂ SO ₄	4.2 mA Cm ⁻² at 1.23 V vs. RHE	[23]
BiVO ₄ island	Co-magnetron sputtering	Mo	0.5 M Na ₂ SO ₄ With 0.1M phosphate buffer	1.2 mA Cm ⁻² at 1.23 V vs. RHE	[24]
BiVO ₄ shell	Drop casting	SnO ₂ :Sb	Phosphate Buffer with 1M Na ₂ SO ₄	3.9 mA cm ⁻² at 0.6 V vs. RHE	[25]
Bi ₂ WO ₆ agglomerated nano- porous particles	Electrochemical method followed by coating and thermal annealing	none	0.1 M borate buffer (pH 9)	0.1 mA cm ⁻² at 0.99 V vs. RHE	[26]
Bi ₂ WO ₆	Hydrothermal method	Co-Pi	0.5 M Na ₂ SO ₄	30 μA Cm ⁻² at 1.23 V vs. RHE	[27]
Bi ₂ WO ₆ 2D arrays	Self-assembly method	None	1M NaOH	6 x 10 ⁻⁵ Cm ⁻² at 0.4 V vs. Ag/AgCl	[28]

Bi ₂ MoO ₆ nanosheet	Microwave assisted ultrasonic separation process	WO ₃	0.1M Na ₂ SO ₄	2.2 mA Cm ⁻² at 0.8 V vs SCE	[29]
Bi ₂ MoO ₆ nanorod array	Hydrothermal method	BiVO ₄	0.1M Na ₂ SO ₄	250 μA Cm ⁻² at 0.8 V vs SCE	[30]
BiFeO ₃ nano- particles	Low pressure CVD	Ni-B	1M potassium borate	0.72 mA Cm ⁻² at 1 V vs. Ag/AgCl	[31]

Bismuth based semiconductors (nanomaterials) are widely used as photocatalyst material. Due to their small band gap and acceptable band locations, bismuth based nanomaterials have been regarded as possible candidates for PEC water splitting. This analysis focuses on the various bismuth-based materials used to date with extensive literature for solar water splitting applications. This literature data also summarizes the performance of bismuth containing PEC water splitting materials. The bismuth-based materials most commonly studied include oxyhalides, Aurivillius phase oxides such as Bi₂WO₆ and Bi₂MoO₆, other mixed metal oxides such as BiVO₄, BiFeO₃, BiPO₄, Bi₂O₃, CuBi₂O₄, etc. Most of these materials have one common factor: visible light is absorbed by them. Quick charge recombination and photocorrosion are the critical problems associated with bismuth based materials for the PEC system. The new attempts to deal with these problems are discussed in depth. BVO was found to be promising for water splitting, particularly as a photoanode, among all the bismuth-based materials published. Therefore, tremendous effort has been spent on BVO to boost the efficiency of PEC compared to other bismuth-based materials. Conversion efficiency, however, is far from the expected performance, which is due to weak electron transport and slow water oxidation kinetics. To address the aforementioned limitations of bismuth-based semiconductor photo electrodes, several approaches have been adopted. Nanostructure synthesis involves facet and morphology

control due to large surface area and directional flow of charges. Different doping is done to improve intrinsic properties and to increase the charge separation, other than doping, heterojunctions are also an effective technique to reduce charge recombination rate of charge carriers and photo corrosion.

Summary of the chapter

In this chapter details on working principle of Photo electrochemical water splitting and organic pollutant degradation, factors effecting performance of PEC and available materials for photocatalytic water splitting and dye degradation have been summarized. The excitation of electron and generation of electron hole pair at surface of semiconductor surface when exposed to photons exhibit water splitting and pollutant degradation. Pool of semiconductors are available for photocatalytic applications but Semiconductor should have bandgap range in visible light active region and less recombination of electron hole pair. Material used for water splitting are based on noble metals (Pt, Ir, Ru, Pd, Au etc.). Titania is most potential photocatalyst but it has high band gap ranges in ultraviolet region. Bismuth vanadium oxide is potential non Nobel photo catalyst which is chemically stable, easily scalable, non-toxic, environmental friendly and low bandgap. It is active in visible region. In water oxidation reaction (water splitting), the kinetics of the reaction is low and require careful tuning to fully realize its photocatalytic potential. so Yttrium is doped in Bismuth vanadium oxide to minimize the recombination for improved photo catalysis.

References

- [1] S. Di Mo and W. Y. Ching, “Electronic and optical properties of three phases of titanium dioxide: Rutile, anatase, and brookite,” *Phys. Rev. B*, vol. 51, no. 19, pp. 13023–13032, 1995, doi: 10.1103/PhysRevB.51.13023.
- [2] D. V. Bavykin, J. M. Friedrich, and F. C. Walsh, “Protonated titanates and TiO₂ nanostructured materials: Synthesis, properties, and applications,” *Adv. Mater.*, vol. 18, no. 21, pp. 2807–2824, 2006, doi: 10.1002/adma.200502696.
- [3] S. Bakardjieva, J. Šubrt, V. Štengl, M. J. Dianez, and M. J. Sayagues, “Photoactivity of anatase-rutile TiO₂ nanocrystalline mixtures obtained by heat treatment of homogeneously precipitated anatase,” *Appl. Catal. B Environ.*, vol. 58, no. 3–4, pp. 193–202, 2005, doi: 10.1016/j.apcatb.2004.06.019.
- [4] M. Koelsch, S. Cassaignon, J. F. Guillemoles, and J. P. Jolivet, “Comparison of optical and electrochemical properties of anatase and brookite TiO₂ synthesized by the sol-gel method,” *Thin Solid Films*, vol. 403–404, pp. 312–319, 2002, doi: 10.1016/S0040-6090(01)01509-7.
- [5] B. Ohtani, Y. Ogawa, and S. Nishimoto, “JPysChemB,101,(1997)3746(アモルファスTiO2).pdf,” *J. Phys. Chem. B*, vol. 5647, no. 101, pp. 3746–3752, 1997.
- [6] A. R. Khataee and M. B. Kasiri, “Photocatalytic degradation of organic dyes in the presence of nanostructured titanium dioxide: Influence of the chemical structure of dyes,” *J. Mol. Catal. A Chem.*, vol. 328, no. 1–2, pp. 8–26, 2010, doi: 10.1016/j.molcata.2010.05.023.
- [7] M. Z. Bin Mukhlis, F. Najnin, M. M. Rahman, and M. J. Uddin, “Photocatalytic Degradation of Different Dyes Using TiO₂ with High Surface Area: A Kinetic Study,” *J. Sci. Res.*, vol. 5, no. 2, pp. 301–314, 2013, doi: 10.3329/jsr.v5i2.11641.
- [8] I. Bsu, “Весці нацыянальнай акадэміі навук беларусі № 2 2016,” pp. 57–67, 2016.
- [9] M. D. Hernández-Alonso, F. Fresno, S. Suárez, and J. M. Coronado, “Development

- of alternative photocatalysts to TiO₂: Challenges and opportunities,” *Energy Environ. Sci.*, vol. 2, no. 12, pp. 1231–1257, 2009, doi: 10.1039/b907933e.
- [10] H. Y. He, Y. Yan, J. F. Huang, and J. Lu, “Rapid photodegradation of methyl blue on magnetic Zn_{1-x}CoxFe₂O₄ nanoparticles synthesized by hydrothermal process,” *Sep. Purif. Technol.*, vol. 136, pp. 36–41, 2014, doi: 10.1016/j.seppur.2014.08.028.
- [11] W. Z. Tang and Huren An, “UV/TiO₂ photocatalytic oxidation of commercial dyes in aqueous solutions,” *Chemosphere*, vol. 31, no. 9, pp. 4157–4170, 1995, doi: 10.1016/0045-6535(95)80015-D.
- [12] B. Viswanathan, “Photocatalytic Degradation of Dyes: An Overview,” *Curr. Catal.*, vol. 7, no. 2, pp. 99–121, 2017, doi: 10.2174/2211544707666171219161846.
- [13] K. Mondal and A. Sharma, “Photocatalytic Oxidation of Pollutant Dyes in Wastewater by TiO₂ and ZnO nano-materials – A Mini-review,” *indian Inst. Technol.*, no. January 2015, pp. 36–72, 2016.
- [14] X. Chen, S. Shen, L. Guo, and S. S. Mao, “Semiconductor-based photocatalytic hydrogen generation,” *Chem. Rev.*, vol. 110, no. 11, pp. 6503–6570, 2010, doi: 10.1021/cr1001645.
- [15] S. P. Berglund, A. J. E. Rettie, S. Hoang, and C. B. Mullins, “Incorporation of Mo and W into nanostructured BiVO₄ films for efficient photoelectrochemical water oxidation,” *Phys. Chem. Chem. Phys.*, vol. 14, no. 19, pp. 7065–7075, 2012, doi: 10.1039/c2cp40807d.
- [16] Y. Zhu, M. W. Shah, and C. Wang, “Insight into the role of Ti³⁺ in photocatalytic performance of shuriken-shaped BiVO₄/TiO_{2-x} heterojunction,” *Appl. Catal. B Environ.*, vol. 203, pp. 526–532, 2017, doi: 10.1016/j.apcatb.2016.10.056.
- [17] W. Q. Fan *et al.*, “Fabrication of TiO₂-BiOCl double-layer nanostructure arrays for photoelectrochemical water splitting,” *CrystEngComm*, vol. 16, no. 5, pp. 820–825, 2014, doi: 10.1039/c3ce42001a.
- [18] M. Serhan *et al.*, “Total iron measurement in human serum with a smartphone,”

AIChE Annu. Meet. Conf. Proc., vol. 2019-Novem, 2019, doi: 10.1039/x0xx00000x.

- [19] L. Wang and W. A. Daoud, “BiOI/TiO₂ -nanorod array heterojunction solar cell: Growth, charge transport kinetics and photoelectrochemical properties,” *Appl. Surf. Sci.*, vol. 324, pp. 532–537, 2015, doi: 10.1016/j.apsusc.2014.10.110.
- [20] J. Zhao *et al.*, “High-Performance Ultrathin BiVO₄ Photoanode on Textured Polydimethylsiloxane Substrates for Solar Water Splitting,” *ACS Energy Lett.*, vol. 1, no. 1, pp. 68–75, 2016, doi: 10.1021/acsenergylett.6b00032.
- [21] S. Byun, B. Kim, S. Jeon, and B. Shin, “Effects of a SnO₂ hole blocking layer in a BiVO₄-based photoanode on photoelectrocatalytic water oxidation,” *J. Mater. Chem. A*, vol. 5, no. 15, pp. 6905–6913, 2017, doi: 10.1039/c7ta00806f.
- [22] F. F. Abdi, N. Firet, and R. vandeKrol, “Efficient BiVO₄ Thin Film Photoanodes Modified with Cobalt Phosphate Catalyst and W-doping,” *ChemCatChem*, vol. 5, no. 2, pp. 490–496, 2013, doi: 10.1002/cctc.201200472.
- [23] S. S. Kalanur, I. H. Yoo, J. Park, and H. Seo, “Insights into the electronic bands of WO₃/BiVO₄/TiO₂, revealing high solar water splitting efficiency,” *J. Mater. Chem. A*, vol. 5, no. 4, pp. 1455–1461, 2017, doi: 10.1039/c6ta07592d.
- [24] S. Byun *et al.*, “Compositional engineering of solution-processed BiVO₄ photoanodes toward highly efficient photoelectrochemical water oxidation,” *Nano Energy*, vol. 43, no. August 2017, pp. 244–252, 2018, doi: 10.1016/j.nanoen.2017.11.034.
- [25] L. Zhou *et al.*, “High Light Absorption and Charge Separation Efficiency at Low Applied Voltage from Sb-Doped SnO₂/BiVO₄ Core/Shell Nanorod-Array Photoanodes,” *Nano Lett.*, vol. 16, no. 6, pp. 3463–3474, 2016, doi: 10.1021/acs.nanolett.5b05200.
- [26] J. C. Hill and K. S. Choi, “Synthesis and characterization of high surface area CuWO₄ and Bi₂WO₆ electrodes for use as photoanodes for solar water oxidation,” *J. Mater. Chem. A*, vol. 1, no. 16, pp. 5006–5014, 2013, doi: 10.1039/c3ta10245a.

- [27] S. Y. Chae, E. S. Lee, H. Jung, Y. J. Hwang, and O. S. Joo, "Synthesis of Bi_2WO_6 photoanode on transparent conducting oxide substrate with low onset potential for solar water splitting," *RSC Adv.*, vol. 4, no. 46, pp. 24032–24037, 2014, doi: 10.1039/c4ra02868f.
- [28] L. Zhang and D. Bahnemann, "Synthesis of nanovoid Bi_2WO_6 2D ordered arrays as photoanodes for photoelectrochemical water splitting," *ChemSusChem*, vol. 6, no. 2, pp. 283–290, 2013, doi: 10.1002/cssc.201200708.
- [29] Y. Ma, Y. Jia, L. Wang, M. Yang, Y. Bi, and Y. Qi, "Exfoliated thin Bi_2MoO_6 nanosheets supported on WO_3 electrode for enhanced photoelectrochemical water splitting," *Appl. Surf. Sci.*, vol. 390, pp. 399–405, 2016, doi: 10.1016/j.apsusc.2016.08.116.
- [30] Y. Ma, Y. Jia, L. Wang, M. Yang, Y. Bi, and Y. Qi, " $\text{Bi}_2\text{MoO}_6/\text{BiVO}_4$ heterojunction electrode with enhanced photoelectrochemical properties," *Phys. Chem. Chem. Phys.*, vol. 18, no. 7, pp. 5091–5094, 2016, doi: 10.1039/c5cp07784b.
- [31] S. J. A. Moniz, C. S. Blackman, P. Southern, P. M. Weaver, J. Tang, and C. J. Carmalt, "Visible-light driven water splitting over BiFeO_3 photoanodes grown via the LPCVD reaction of $[\text{Bi}(\text{OtBu})_3]$ and $[\text{Fe}(\text{OtBu})_3]_2$ and enhanced with a surface nickel oxygen evolution catalyst," *Nanoscale*, vol. 7, no. 39, pp. 16343–16353, 2015, doi: 10.1039/c5nr04804d.

Chapter 3

Experimental Methods

3.1 Characterization Techniques

External techniques used in material science to probe the properties and internal structure of the materials under study are characterization techniques. It is possible to use characterization methods for structural analysis, thermal analysis, composition analysis, etc. Some of the strategies are explained below.

3.1.1 X-Ray Diffraction

X-Ray diffraction is an amazing procedure for portrayal and investigation of crystalline materials. As 95% of strong components in earth covering are crystalline shape. It gives data of structural phases, crystal orientations, and different boundaries identified with structure like normal grain size, crystallinity, strain, crystalloid defects, size of molecules and compound bond length and so on [1].

3.1.1.1 Working principle

XRD provide the peak by constructive interference of single monochromatic beam of X-rays which are scattered at different angles and each set of lattice plane of sample. Peak intensities determined by the position of atoms within lattice planes. Furthermore, XRD patterns are the fingerprints of atomic arrangements of the material. When X-ray interacts with matter, three type of phenomenon may occur, florescence, ionization and diffraction. In XRD when X-ray interact with atoms, the electrons starts vibrations with same frequency as X-rays, usually destructive interface occurs [1].

But in few directions constructive interface occurs. And determines by Bragg's law.

$$n\lambda = 2d\sin\theta \dots\dots\dots (Eq. 3.1)$$

θ is episode point between occurrence beam and dissipating planes, d is dividing between planes, λ is wavelength if the X-rays and n is integer value. These diffracted X-rays can

be detected by detector to make a diffractogram. Graph is plotted between 2θ on x-axis and intensity on y-axis [2].

3.1.2 Scanning Electron Microscopy

SEM is a technique used to provide the information related to the surface structure and topography of the synthesized material. It uses a high energy beam of electron to scan pattern of material topography. It provides magnification up to 300,000X and have effective probing length of 10nm to 1 μm [3].

3.1.2.1 Working principle

Primary electron beam is produced under vacuum and scanned across the surface. On striking electron with the specimen, secondary electron beam and back scattered electrons came out creating variation in signals that provide image of the surface.

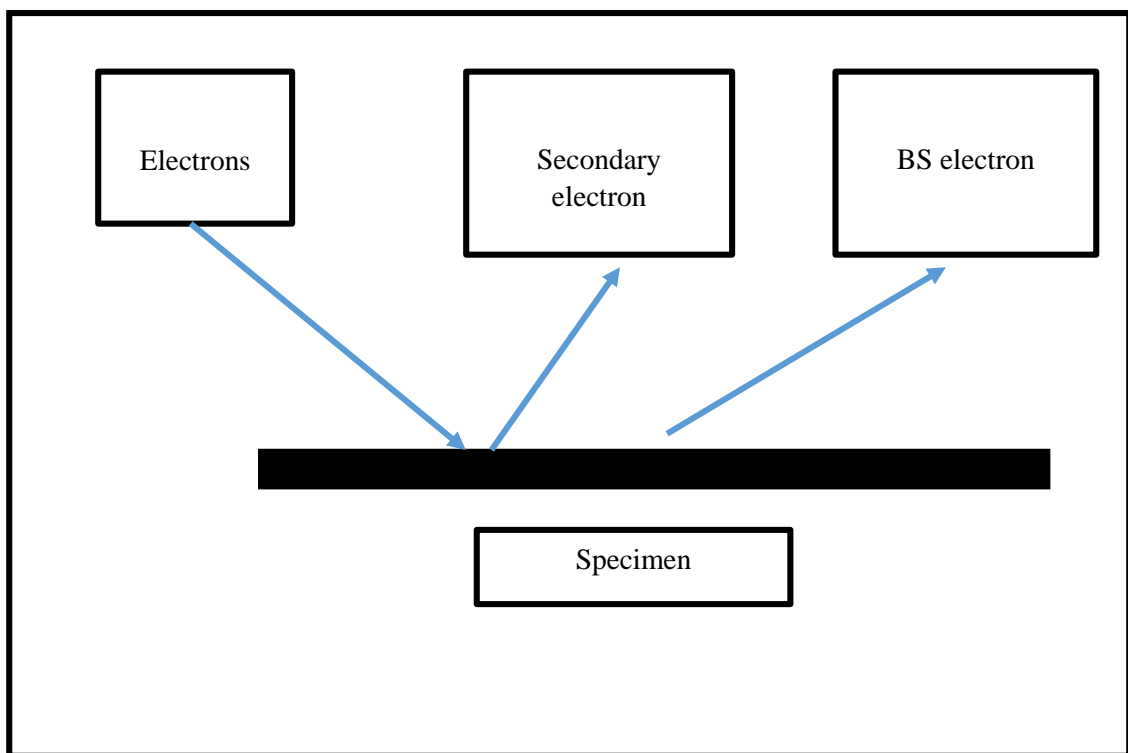


Fig 3.1 Probe beam and measuring particle in SEM

Electrons are accelerated toward the sample, released from a heated filament. As gas molecules can cause interference with electron beams and backscattered or secondary electrons, a high vacuum is needed. The electrons interact with the sample atoms and can

generate secondary electrons, characteristic X-rays, and electrons that are dispersed backwards. The primary beam of the second electromagnetic lens is de-magnified by the first electromagnetic lens. A detector detects these signals. Many electron scanning microscopes only have secondary electron detectors, though a few may also include X-rays or other detectors. Due to elastic distribution, back-scattered electrons are produced [3], The detector produces the micrograph image along with the cathode ray tube [4].

3.1.2.2 Sample preparation

Sample preparation is important step for proper imaging in SEM. If sample is in powder form then it simply put on stub, coated with conductor if an insulator and an image is obtained. if films are under examination then substrates are properly prepared. The preparation steps are explained in Figure 3.2 [5].

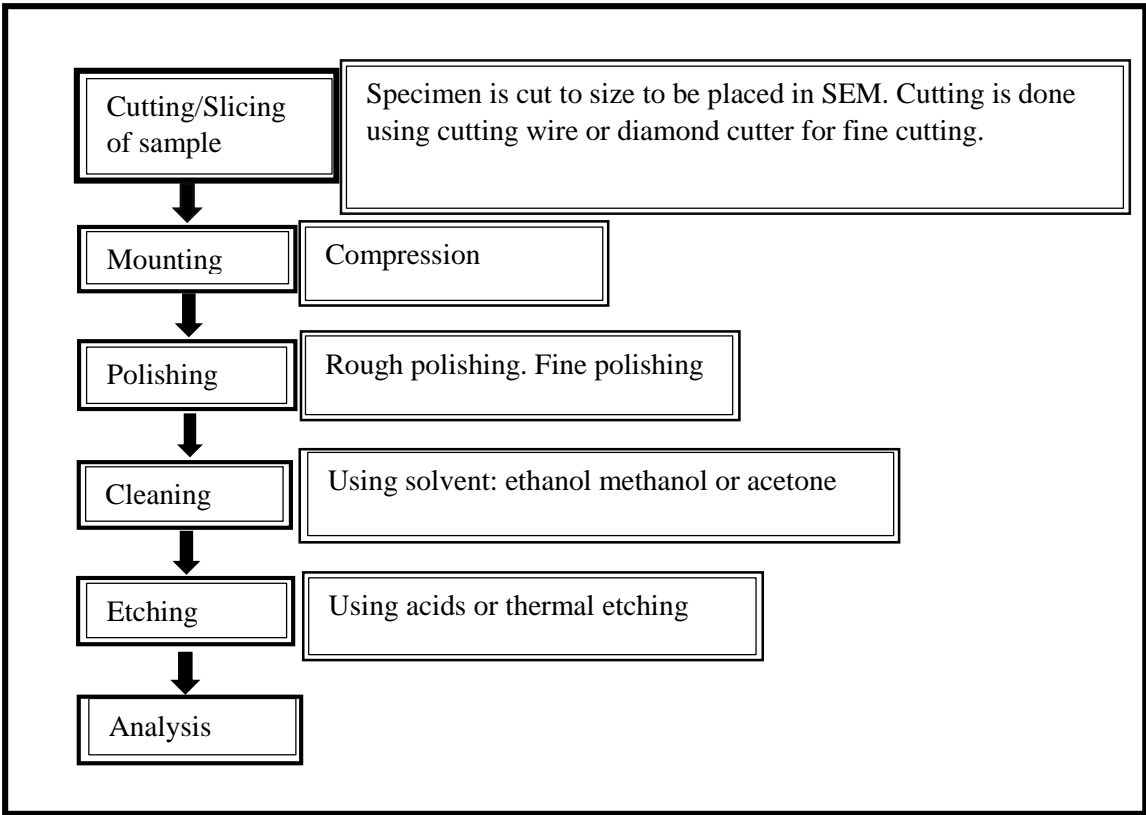


Fig.3.2 Schematic flow for sample preparation for SEM films

3.1.3 Energy Dispersive spectroscopy (EDS)

EDS or EDX is compositional elemental analysis technique for chemical characterization of specimen. EDS pattern is the result of absorption of X-rays by the semiconductors, this absorbance excite the crystal electrons which move to the conduction band, results in electric pulse is produced that is corresponding to the energy of X-beams which are included and coordinated in a multichannel analyzer, and an introduction of solidarity of the sign against its energy give the needed range [3].

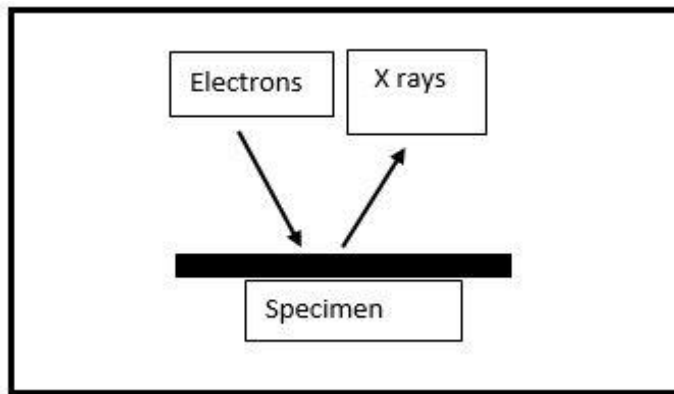


Figure 3.3 Probe beam and measuring particle

When electrons strike the specimen, the electrons contained in specimen are excited creating vacant places in the atomic shells. Electrons in the higher shells fill these vacancies. The energy is released in this process in form of X-rays. All elements emit X rays with characteristic energy values. Each element in periodic table has its specific energy value which makes elemental analysis through EDS possible. $K\alpha$ X-rays are emitted when an electron from L shell fills the vacancy in K shell of the atom. Letters K, L, M represents the shell from where electrons are emitted and α , β , γ represents the shell where they are substituted. Sample preparation is same as for SEM. In principle, all elements in periodic table from beryllium to uranium (atomic number 4 to 92) can be detected by EDS

3.1.4 UV-vis Spectroscopy

UV-Visible is a spectroscopy technique based on transmittance or absorption of UV light or visible light visible (400-800) nm and ultraviolet (190-400) nm regions of electromagnetic spectrum to obtain information about organic molecules, this technique

is based on the interaction of light and material. When material absorb the falling light, excitation of electron occurs and during de excitation, a spectrum is produced.

3.1.4.1 Working principle

As UV-Vis light is irradiated by molecules that have non-bonding or π electrons, the electrons are excited to higher anti-bonding orbitals. The smaller the energy difference between a material's HOMO and LUMO, the smoother the excitation of electrons by longer radiation wavelengths is. Electrons are bumped from HOMO to LUMO when a molecule with an energy difference between HOMO-LUMO equal to ΔE is exposed to radiation with a wavelength equivalent to ΔE . This is known as the move to $\sigma - \sigma^*$. The plot between the x-axis wavelength and the y-axis absorbance is obtained and analyzed.

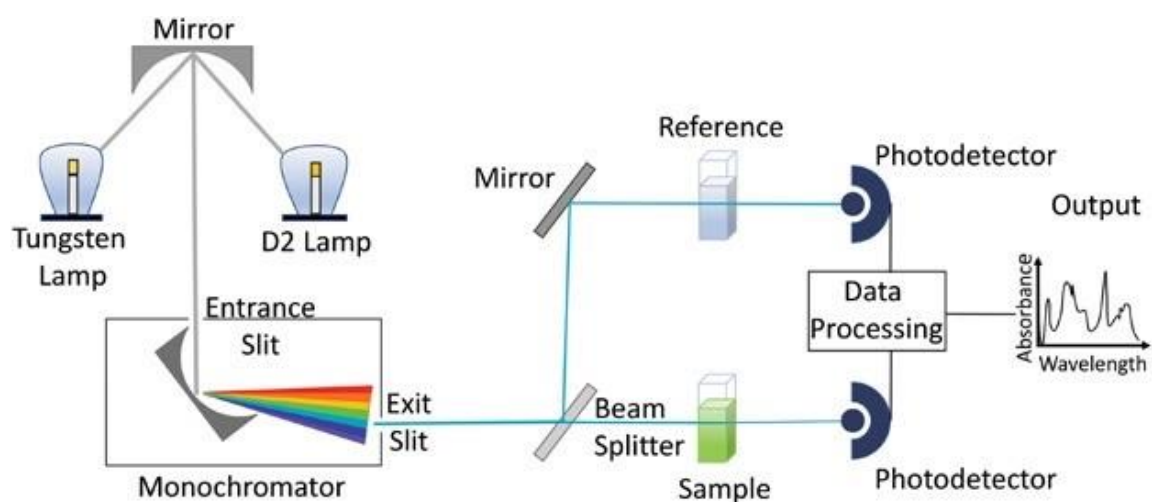


Figure 3.4 Schematic diagram of Ultraviolet visible spectrometry

3.2 Solution based Synthesis techniques

3.2.1 Hydrothermal Synthesis of Nano/Micro Particles

Hydrothermal or solvothermal synthesis is low cost, environmental friendly technique for producing many functional nanomaterials of transition metal compounds. Synthesis conditions depends on precursor solubility in water, temperature and pressure. Initial material is poured in autoclave. which is a pressure vessel lined internally with Teflon and made up of steel. Operating conditions are optimized to get required shapes of Nano or micro particle crystals. This method gives controllable growth of desired shapes and structures [6].

3.2.2 Sol gel technique

One of the most common methods for nanoparticle synthesis is sol-gel synthesis. The colloid suspension of solid particles in liquid can be described as Sol. The synthesis of sol-gel can include a metal-organic approach in which metal alkoxides are dissolved in organic solvents or a metal-inorganic approach in which metal salts are used as precursors in water, such as nitrates, chlorides, oxychlorides, etc. The metal-inorganic approach to particle synthesis is much cheaper than the former, but the reactions are fast and difficult to monitor [7].

Metal alkoxides $M(OR)_y$ belong to the metal-organic compound family, where M is a metal (Ti, Si, Al, Ce, Zr, etc.), OR is an alkoxy group or organic ligand attached to the metal atom, and y is the state of metal oxidation. Hydrolysis and condensation of metal alkoxides leading to polymerization are the main reactions in the organic metal pathway. The first step is alkoxy group hydrolysis.



The polycondensation reaction is the next step. The formation of polymers and oligomers based on the metal Oxo skeleton is the result of this reaction. In this process, reactive alkoxy and hydroxo groups are the residual. The reaction to polycondensation takes place in two stages. First, oxygen bridge formation, known as oxalation, and secondly, hydroxo bridge formation, known as olation.



Where X represents H or R, depending upon the hydrolysis ratio (H_2O/M). The kinetics of oxalation is slower than the kinetics of olation.



Metal-Oxo-macromolecular networks are formed after polycondensation. A sol is formed where the polymerized structures have not reached macroscopic scale. As the bushy structures are formed due to the recombination of metal Oxo polymers, a gel is formed. The structure of these Oxo polymers depends on the temperature, the hydrolysis ratio, the type of solvents and catalysts, the use of nucleophilic reagents and ligands, etc [7].

3.2.3 Dip coating

Dip coating is also low cost solution based technique for film deposition from 25nm to 60 μ m. The coating content is in liquid form in the dip coating deposition phase, typically a solution or a sol and the substrate to be coated is submerged, remained in solution for some time and then removed at a well-optimized speed. Under controlled atmospheric and controlled temperature conditions, the coating process takes place [7-8].

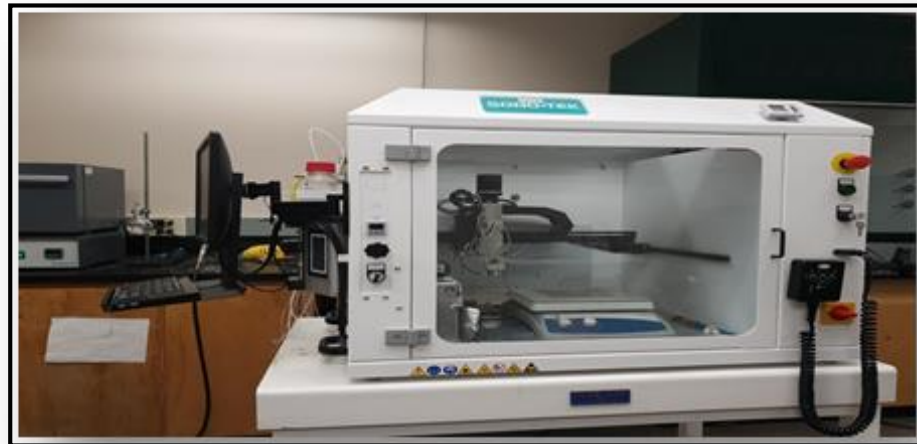


Figure 3.4 Dip coater

It can easily control the thickness of the coating. It depends on the solution's viscosity, the speed of removal, and the solid content of the solution. The thicker the substrate is extracted, the denser the coating is and the solution is viscous, the thicker the film.

The unregulated uniformity of the film is a downside of using such a deposition method. On one edge of the substrate, the film can be thicker and thinner [9].

3.2.4 Spin coating

Spin coating is a technique of deposition that requires the use of centrifugal force to deposit thin films uniformly on substrates. The spin-coater is called the deposition unit. A colloid in liquid or semi liquid form, but finer than paste, is a coating material. It usually requires volatile solvents. Tiny quantities of this colloid are put in the center of the substrate to be coated and added to the non-coating side of the substrate to be connected

to the stub of the spin coater that retains the substrate using vacuum or double tape. After retaining the substrate, the coater spins the substrate by spinning at the appropriate rpm and the colloid is distributed uniformly on the substrate by centripetal acceleration. The substrate is dried and, depending on the desired thickness, the process can or may not be repeated. The thickness of the film can easily be managed. Thickness depends on rotating angular velocity, colloid viscosity, colloid solid material quantity, and rate of drying. The thinner the deposited film is, the higher the speed [9].

3.2.5 Doctor Blading

The easiest and cheapest process for coating films on substrates is the Doctor blade coating. Using a sharp edged metal applicator, it is a quick diffusion of a paste. Precursors, a surfactant, and a volatile solvent are used to make the slurry or paste. To change thickness from a few nanometers to the micrometer scale, the Doctor blade comes with screws. Substrates are fixed using tape on a flat table, and only part of the substrate to be coated is exposed. Tape protects the rest. A large volume of slurry is mounted on one end of the substrate and the doctor's blade screws are modified according to the thickness necessary. The doctor's blade glides manually over the substrate in one go. They then dry the coated films. The thickness of the film depends on the paste viscosity, the surface tension and the velocity of the coating (moving speed of the hand).

3.2.6 Spray pyrolysis

Another solution-based wet chemistry path to deposit thin films on substrates is spray pyrolysis, also known as chemical deposition spray pyrolysis. Pyrolysis is a process in which, in the absence of oxygen at a high temperature, thermo-chemical decomposition of organic materials occurs. The deposition method consists of an atomizer, a liquid source, and heated substrates. A solution containing the coating precursors is sprayed onto the heated surface in the deposition process, where they react to form the desired material coating. In other words, on the surface of substrates forming the desired and undesirable products, chemical reaction occurs [10], The precursors are selected so that the reaction by-products are reactive and do not remain together with the coating on the substrate. For the deposition of various oxides, this process is specifically used [11].

3.2.7 Electrodeposition

Another strategy for forming thin films on a piece of work is electrodeposition. As this is an old procedure, it has as of late been embraced for use in IC assembling, particularly for saving the copper films that are supplanting aluminum films in most exceptional incorporated circuits. The source and work piece are both lowered in a fluid electrolyte during electrodeposition and are likewise associated by an outside electrical circuit. As a voltage is applied between the source and the work piece, particles of the source material disintegrate in the electrolyte, float towards the work piece affected by the field, and tie on its surface synthetically. A thin film is along these lines saved after some time. An outer electric field may not be required in specific conditions; this is called electroless affidavit. Electrodeposition and electroless affidavit are frequently alluded to as "plating," and regularly it is said that the stored film is "plated out" on the work object.

3.3 Vacuum based deposition techniques

3.3.1 Physical vapor deposition

Physical vapor deposition (PVD) is one of the most important thin-film growth methods for substrates that need an ultra-high pressure deposition environment.

3.3.1.1 Sputtering

Sputtering is an example of the physical vapor deposition process in which the bombardment of the target material with energetic particles causes source atoms to be expelled from the target material. Only if the kinetic energy of the bombarded particles is very high (about 1 eV) will the atoms be expelled. Prolonged bombardment of highly energetic particles may be counterproductive as it contributes to significant material erosion. It is also used, however, for the deposition of thin films, analytical techniques and the method of etching. It is also the one that the most significant PVD process for producing integrated circuits. The interconnections that hold electrical signals on an IC chip from one electronic system to another were usually made of aluminum alloys that were deposited by sputter. To deposit both conducting and insulating materials, sputtering can be used.

Collisions that cause the momentum exchange between the atoms and ions in the materials drive the sputtering process "Argon or different particles in a gas are first ionized in a sputtering chamber and afterward quickened by an electric field to a source material to be stored, called a "target". In a faltering chamber, argon or different molecules in a gas are first ionized and afterward quickened by an electric field to a source material to be kept, called a "target. It is conceivable to falter store films that are a few microns thick relying upon how long the cycle goes on [9].

3.3.1.2 Evaporation and electron beam evaporation

Evaporation takes place in a vacuum chamber, and a low-pressure vapor of the substance to be deposited is produced by one means or another. Any of this vapor on the work piece will condense and therefore begin to deposit as a thin film. Simply melting a substance in a vacuum may often create a useful material deposit, depending on its vapor pressure. Selenides, sulfides, and certain other oxides are rapidly evaporated by sublimation furnaces. The evaporative materials are sintered and pressed to form pellets which are then exposed to the source of radiant heat. Graphite, pyrolytic BN and refractory materials are the most common examples of this type of evaporative material. Metals, most of which are produced by hot pressing of powder to form pallets. The heating is typically achieved by external heating elements of the tungsten wire resistance.

Heating by the resistive heating portion of the evaporant source (in traditional heating elements). Disadvantages such as contamination caused by the supporting components, crucibles, and heaters that obstruct the deposition of pure films include the evaporation process. The downside of evaporating high melting point materials at high rates is also included.

Electron beam evaporation overcomes these limits and is thus a better evaporative film deposition technique based on vacuum. The benefit of evaporating a wide variety of materials at practical rates is this technique. By putting the evaporative content in the water-cooled crucible or copper hearth, the technique works. A small fraction of sublimates or melts of evaporant that ensure the purity of evaporative content as the crucible is cooled by water that hinders its melting and contamination with the evaporant source.

The technique of electron beam deposition usually has a configuration that works by emitting electrons from heated filaments isolated from both the substrate and the evaporative source's direct line of sight. This method removes the film contamination generated by cathode heated filament. The cathode is skewed negatively.

3.3.2 Chemical vapor deposition

Another set of techniques that are commonly used for deposition is chemical vapor deposition (CVD). The various forms of chemical vapor deposition process are LPCVD, APCVD, and PECVD. In CVD, in gaseous form, the source of the material to be stored remains. In a heated vacuum chamber, the source gas and other gases are added into a chemical reaction that produces the desired material as a product.

This item condenses on the work piece, forming a layer of material over time. The chemical reaction can take place preferentially on the work piece itself in some CVD procedures.

The CVD methods were very old and were used to deposit tungsten coatings on the filaments of incandescent bulbs as a protective layer to extend their lifespan. High-temperature, high-quality CVD methods for the development of thin film and coating epitaxial growth are now primarily used in a wide range of applications, including the manufacture of solid-state electronic devices, cutting tools and ball bearings, the manufacture of nuclear reactor parts, and rocket engines. As part of IC processing, thin films of polycrystalline silicon, tungsten, and titanium nitride are typically deposited by CVD. The growth of Nanowire also often proceeds through CVD [9,12].

Summary of the chapter

In this chapter a review on the experimental techniques including the methods of preparation of Nano-grains and methods of deposition of thin films on substrates has been presented. Details on the working of different characterization techniques like XRD, SEM/EDX, UV-Vis and PL etc. has also been summarized. The most common method of preparation of Bismuth vanadium oxide Nano-grains is through hydrothermal process which includes one step facile hydrothermal treatment. Hydrothermal synthesis method is low-cost technique for particle synthesis. Thin films can be coated on number of substrates using low-cost solution based techniques like dip coating, spin coating, spray pyrolysis etc. or the comparatively expensive vacuum based techniques like PVD, CVD etc. They require high and ultra-high vacuum for the deposition process. Among the techniques the expensive techniques like evaporation, electron beam evaporation, CVD etc. offer homogenous and fine coating allowing easy control over the film formation and thickness. Whereas solution based wet chemistry routes are cheap and can be done with simple apparatus. No high vacuum is required and can be done in low or no vacuum. After the synthesis of particles and deposition of thin films, it is required to characterize the particles and films. Different material characterization techniques like XRD, SEM/EDX, UV-Vis spectroscopy etc. can be employed to study the samples. Structural and compositional analysis of films and particles can be done using XRD, SEM, AFM, EDX, PL, UV-Vis spectroscopy etc., thermal analysis techniques like TG-DTA, dilatometry etc. can be employed to check thermal stability and reactions occurring with increasing temperature and electrical analysis can be done using four probe method for IV measurements or C-V measurements etc. structural analysis is performed to check the morphology, shape, size etc. of the films and particles and compositional analysis is done to analyze the presence of phases, amounts of phases, bonds, elements, amount of elements etc.

The information obtained from these characterization data are utilized to optimize better conditions and to check the functioning of particles and films.

References

- [1] S. A. Speakman, “Estimating Crystallite Size Using XRD, MIT Center for Materials Science and Engineering,” 2008.
- [2] R. Shiraki and B. A. Holmén, “Airborne respirable silica near a sand and gravel facility in Central California: XRD and elemental analysis to distinguish source and background quartz,” *Environ. Sci. Technol.*, vol. 36, no. 23, pp. 4956–4961, 2002, doi: 10.1021/es0257265.
- [3] T. N. Angelidis and S. A. Sklavounos, “A SEM-EDS study of new and used automotive catalysts,” *Appl. Catal. A, Gen.*, vol. 133, no. 1, pp. 121–132, 1995, doi: 10.1016/0926-860X(95)00165-4.
- [4] K. D. Parry V, “Microscopy : An introduction,” *III-Vs Rev.*, vol. 13, no. 4, pp. 40–44, 2000.
- [5] R. L. Folk and F. L. Lynch, “The possible role of nannobacteria (dwarf bacteria) in clay-mineral diagenesis and the importance of careful sample preparation in high-magnification SEM study,” *Journal of Sedimentary Research*, vol. 67, no. 3. pp. 583–589, 1997, doi: 10.1306/d42685db-2b26-11d7-8648000102c1865d.
- [6] Yan Y. Xi, Yan F. Hsu, and Wai K. Chan, “Hydrothermal Synthesis of Nanostructures,” *Recent Pat. Nanotechnol.*, vol. 1, no. 2, pp. 121–128, 2008, doi: 10.2174/187221007780859591.
- [7] E. Yilmaz and M. Soylak, *Functionalized nanomaterials for sample preparation methods*. Elsevier Inc., 2019.
- [8] S. K. Sahoo, B. Manoharan, and N. Sivakumar, *Introduction: Why perovskite and perovskite solar cells?* Elsevier Inc., 2018.
- [9] A. Behera, P. Mallick, and S. S. Mohapatra, “Nanocoatings for anticorrosion,” *Corros. Prot. Nanoscale*, pp. 227–243, 2020, doi: 10.1016/b978-0-12-819359-

4.00013-1.

- [10] D. Perednis and L. J. Gauckler, “Thin film deposition using spray pyrolysis,” *J. Electroceramics*, vol. 14, no. 2, pp. 103–111, 2005, doi: 10.1007/s10832-005-0870-x.
- [11] J. B. Mooney and S. B. Radding, “Spray Pyrolysis Processing,” *Annu. Rev. Mater. Sci.*, vol. 12, pp. 81–101, 1982, doi: 10.1146/annurev.ms.12.080182.000501.
- [12] C. S. Law, L. F. Marsal, and A. Santos, “Electrochemically engineered nanoporous photonic crystal structures for optical sensing and biosensing,” *Handb. Nanomater. Anal. Chem. Mod. Trends Anal.*, pp. 201–226, 2019, doi: 10.1016/B978-0-12-816699-4.00009-8.

Chapter 4

Methods and Materials

Bismuth vanadium oxide preparation is critical to the growth of Bismuth vanadium oxide [1]. Many parameters, including phase formation, morphology, crystal facets, surface area, and surface defects, are directly dependent on the synthesis process. As a result, the synthesis has a major impact on e-/h+ transport and interfacial Kinetics [1], Bismuth in Solid state [2] and melting reactions were first synthesized by vanadate in 1963 [3]. To date, the synthesis methods most widely used.

Metal organic decomposition of BVO in the form of film and powder [4] , Precipitation and hydrothermal methods (MOD), precipitation and hydrothermal methods [5]. Other methods such as electrochemical and sol-gel processes can also be used, But they are l, they It is less frequent [6]. Most of these methods of preparation allow the use of dopants and/or to change the chemical composition and to regulate the surfactants in the reactive mixture [7].

The morphology of materials from Bismuth vanadium oxide [5]. A surfactant, sometimes referred to as the structure. A polymer that influence the micro- and Nano-structure of a material is also the steering agent. Adjustment of its morphology, surface area, porosity, crystallinity and formation of crystal phases [8].

Ethylene-diamnetetraacetic acid (EDTA) is a chelating agent and surfactant, $\text{Bi}_{25}\text{VO}_{40}$ spheres are synthesized in the presence of Ethylene-diamnetetraacetic acid (EDTA). The amount of EDTA applied had a big impact on the shape of the samples. Addition of EDTA plays vital role in to assist crystal growth [9].

The importance of hydrothermal time and temperature in deciding BVO morphologies cannot be overstated [10].

4.1 Materials

Following materials are used in synthesis of different Nano and micro particles of Bismuth vanadate.

- ✓ Bismuth nitrate pentahydrate ($\text{Bi}(\text{NO}_3)_3 \cdot 5\text{H}_2\text{O}$) crystal
- ✓ Nitric acid (HNO_3)
- ✓ Sodium hydroxide (NaOH) granule
- ✓ Vanadium (III) acetylacetonate ($\text{C}_{10}\text{H}_{14}\text{O}_5\text{V}$) crystal
- ✓ Methylene blue dye powder
- ✓ Ethylenediaminetetraacetates (EDTA)
- ✓ Titanium isopropoxide ($\text{Ti}(\text{OiPr})_4$)
- ✓ Ultrapure water was used in all experiments

All synthetic substances were insightful evaluation and utilized as gotten, minus any additional cleaning.

4.2 Hydrothermal method

4.2.1 Synthesis of BiVO_4 nanoparticles

Nano grains of BVO (bismuth vanadium oxide) were synthesized using a hydrothermal method (no template) at 70°C for 24 hours. 0.84 g $\text{Bi}(\text{NO}_3)_3 \cdot 5\text{H}_2\text{O}$ and 0.054 g vanadium acetylacetonate ($\text{C}_{10}\text{H}_{14}\text{O}_5\text{V}$) dissolved in 20 mL HNO_3 at a 4 mol L^{-1} concentration. It was filled with ultra-pure until it reached a final volume of 100mL. The solution was magnetically stirred until it became transparent and light blue. After that, sodium hydroxide was added to bring the pH of the solution to 12 (NaOH). The color of the prepared solution shifts from light blue to bluish precipitate and then brownish precipitate, indicating a pH change from acidic to neutral to alkaline. After that, the suspension was placed in an autoclave at 70°C for 24 hours without stirring. The yellow precipitates is centrifuged and washed with ethanol and DI water several times. Then it was calcined at 500°C in a muffle furnace [11].

The yellow precipitates are centrifuged and washed with ethanol and DI water several times. Then it was calcined at 500°C in a muffle furnace [11].

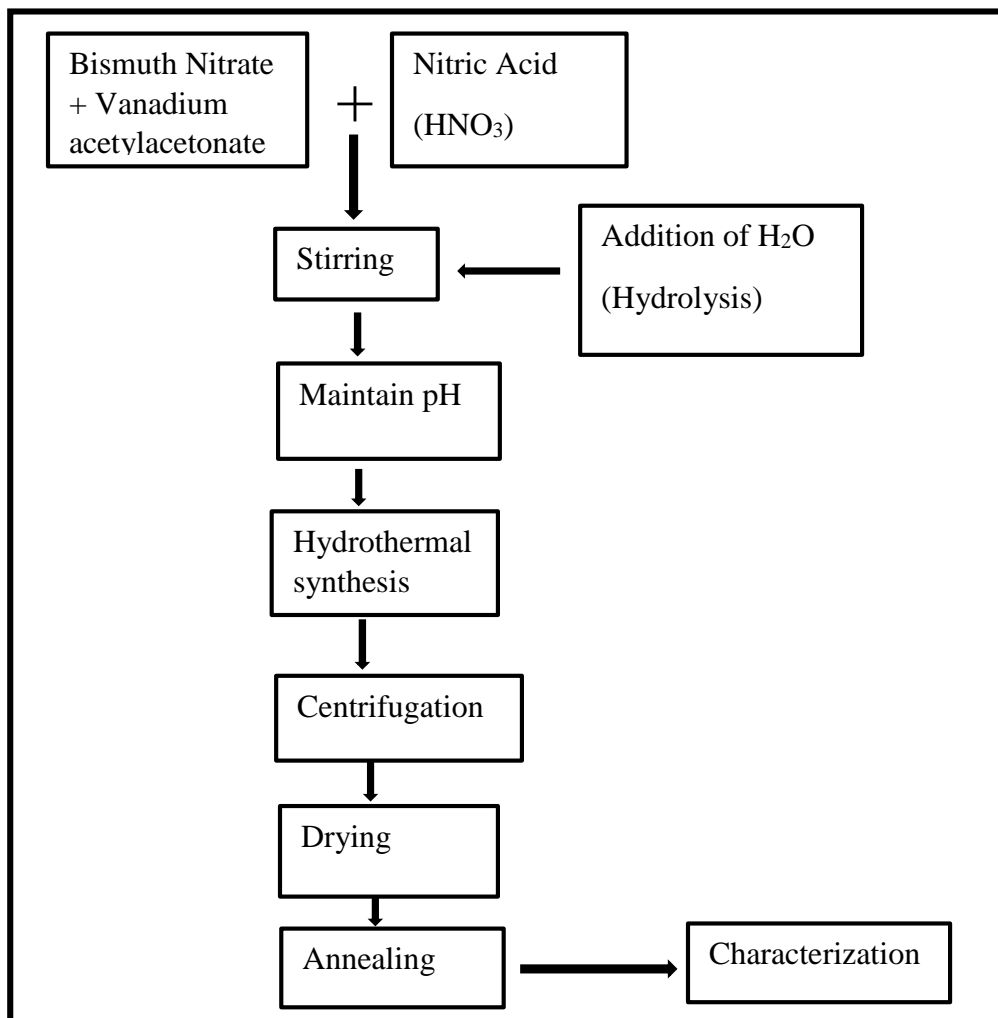


Fig 4.1 Hydrothermal Synthesis process steps of BVO

4.2.2 Synthesis of Yttrium doped $\text{Bi}_{25}\text{VO}_{40}$ nanoparticles

$\text{Y-Bi}_{25}\text{VO}_{40}$ microspheres were synthesized by a simple hydrothermal method at 70°C for 24 h according to following Yttrium doped (1,3 and 5%) $\text{Bi}_{25}\text{VO}_{40}$ $\text{Bi}_{10.99}\text{Y}_{0.01}\text{VO}_{40}$, $\text{Bi}_{10.97}\text{Y}_{0.03}\text{VO}_{40}$, $\text{Bi}_{10.95}\text{Y}_{0.05}\text{VO}_{40}$ by following similar procedure.

0.84-x g of $\text{Bi}(\text{NO}_3)_3 \cdot 5\text{H}_2\text{O}$, Y_x and 0.054 g of vanadium acetylacetonate ($\text{C}_{10}\text{H}_{14}\text{O}_5\text{V}$) were dissolved in 20 mL of HNO_3 at a concentration of 4 mol L^{-1} . It was filled with ultra-pure until it reached a final volume of 100mL. The solution was magnetically stirred until it became transparent and light blue. After that, sodium hydroxide was added to bring the pH of the solution to 12 (NaOH). The color of the prepared solution shifts from light blue to bluish precipitate and then brownish precipitate, indicating a pH change from acidic to neutral to alkaline. After that, the suspension was placed in an autoclave at 70°C for 24

hours without stirring. The yellow precipitates are centrifuged and washed with ethanol and DI water several times. Then it was calcined at 500°C in a muffle furnace [12].

4.2.4 Synthesis of Y-Bi₂₅VO₄₀ nano-grains

According to this empirical formula, 3% doping is performed in Bi₂₅VO₄₀. By following the above-mentioned method, Bi_{0.97}Y_{0.03}VO₄₀ can be obtained. 2.34 g of Bi(NO₃).3H₂O and 0.0726 g Yttrium nitrate were dissolved in 2 mL of nitric acid and then added to 7.5 mL of ultrapure water to form a white solution A. Second, 0.58 g of NH₄VO₃ was dissolved in 10 mL of 4 M NaOH solution, followed by the addition of 1.00 g of HTMA when stirring to form the white solution B [14]. Third, solution B was dissolved drop by drop into solution A to make a yellow suspension solution. The pH of the prepared mixture suspension was changed to 7 by slowly adding 2 M of NaOH solution. The resulting mixture was then sealed in a 50 mL Teflon-lined stainless-steel autoclave [15]. The autoclave was heated to 180°C for 24 hours and held at that temperature for another 24 hours before being allowed to cool to room temperature. After centrifugation, a yellow powder was collected, washed several times with water, and then dried at 70°C in a vacuum oven [12].

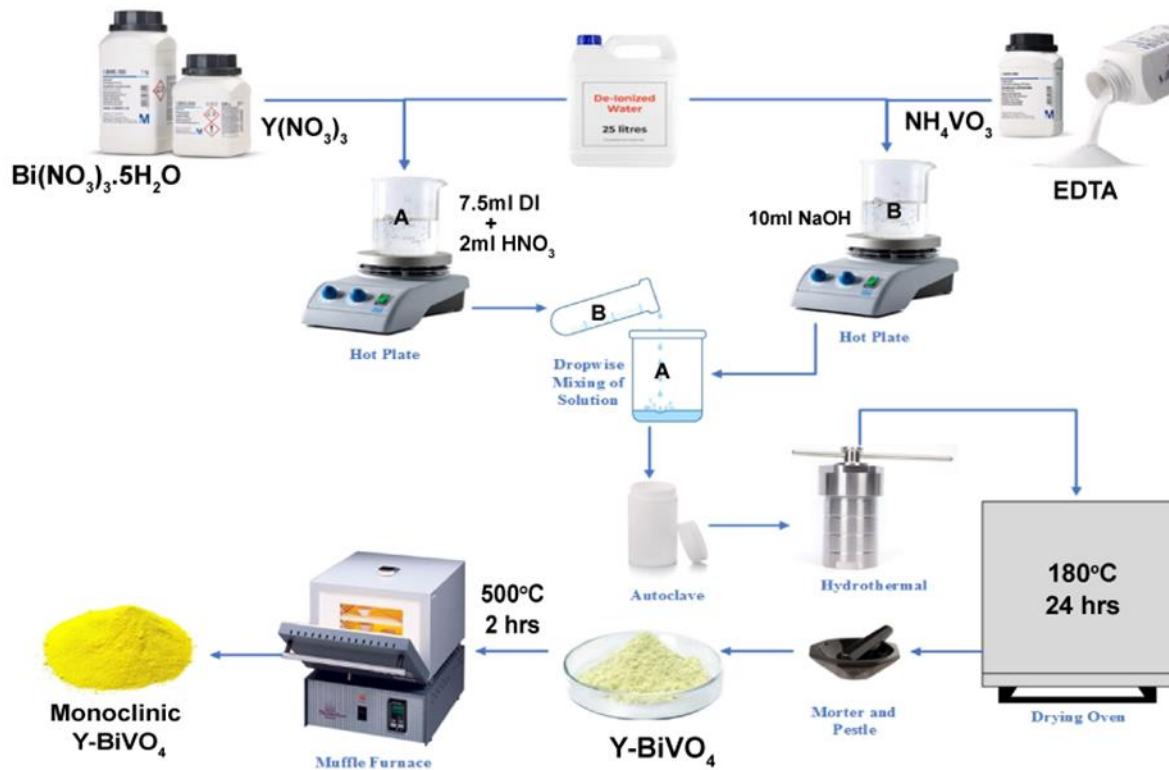


Figure 4.2 Hydrothermal synthesis of BVO Nanograins

4.3 Photo anode Preparation

- FTO, 2.3 mm thick. coated glass substrates are cleaned by acetone.
- To produce a 10 ml precursor solution, 3M ammonium metavanadate, 3M bismuth nitrate pentahydrate, and 6M nitric acid were dissolved in water.
- Thin films with foot print of 1cm^2 of doped and undoped Bismuth vanadate samples were prepared by dip coating technique [10].
- The FTO glass slide was soaked in the precursor solution for 5 seconds, vacuum dried at 70°C for 5 minutes, and heat treated in air for 10 minutes at 500°C .
- The process was repeated to coat several layers before being calcined in air for 2 hours at 500°C .
- 3 layered films were prepared as previous study showed maximum performance
- Prepared precursor solution of Lithium nitrate in DI water. 0.6834g of anhydrous lithium nitrate is dissolved in DI water by magnetic stirring. Lithium nitrate precursor is used to flow all the inert gasses. Put Bismuth vanadate sample and DI lithium nitrate solution in tube furnace for half hour.



Figure 4.3 Photo anodes

- Then started making electrodes, tilted heads of copper wires twice and then arranged copper wires on sample FTOs and then dip these curved heads in silver conductivity paste and attached these on FTOs [17].

Summary of the chapter

In this chapter all the experimentation, experimentation techniques have been employed in the research has been explained. Undoped and doped Bismuth vanadium oxide nano-grains were synthesized using hydrothermal synthesis method and characterized using XRD, SEM/EDX, PL and UV-Vis analysis. Thin films on FTO was deposited by dip coating. Annealing at 500°C temperature were done using muffle furnace. The Photo electrochemical setup was set using platinum as counter electrode in electrolyte 0.2 M NaSO₃ under simulated AM 1.5 visible and IV characteristics were measured.

References

- [1] J. Gan, X. Lu, and Y. Tong, "Towards highly efficient photoanodes: boosting sunlight-driven semiconductor nanomaterials for water oxidation," pp. 7142–7164, 2014, doi: 10.1039/c4nr01181c.
- [2] Y. H. Xu, C. J. Liu, M. J. Chen, and Y. Q. Liu, "A review in visible-light-driven BiVO₄ photocatalysts," *Int. J. Nanoparticles*, vol. 4, no. 2–3, pp. 268–283, 2011, doi: 10.1504/IJNP.2011.040513.
- [3] X. Chen, S. Shen, L. Guo, and S. S. Mao, "Semiconductor-based photocatalytic hydrogen generation," *Chem. Rev.*, vol. 110, no. 11, pp. 6503–6570, 2010, doi: 10.1021/cr1001645.
- [4] A. Galembeck and O. L. Alves, "BiVO₄ thin film preparation by metalorganic decomposition," *Thin Solid Films*, vol. 365, no. 1, pp. 90–93, 2000, doi: 10.1016/S0040-6090(99)01079-2.
- [5] Y. Park, K. J. McDonald, and K. S. Choi, "Progress in bismuth vanadate photoanodes for use in solar water oxidation," *Chem. Soc. Rev.*, vol. 42, no. 6, pp. 2321–2337, 2013, doi: 10.1039/c2cs35260e.
- [6] J. A. Seabold and K. S. Choi, "Efficient and stable photo-oxidation of water by a bismuth vanadate photoanode coupled with an iron oxyhydroxide oxygen evolution catalyst," *J. Am. Chem. Soc.*, vol. 134, no. 4, pp. 2186–2192, 2012, doi: 10.1021/ja209001d.
- [7] B. O. Orimolade and O. A. Arotiba, "Bismuth vanadate in photoelectrocatalytic water treatment systems for the degradation of organics: A review on recent trends," *J. Electroanal. Chem.*, vol. 878, p. 114724, 2020, doi: 10.1016/j.jelechem.2020.114724.
- [8] Y. Lin, C. Lu, and C. Wei, "Microstructure and photocatalytic performance of BiVO₄ prepared by hydrothermal method," *J. Alloys Compd.*, vol. 781, pp. 56–63, 2019, doi: 10.1016/j.jallcom.2018.12.071.
- [9] Z. Zhu, J. Du, J. Li, Y. Zhang, and D. Liu, "An EDTA-assisted hydrothermal

- synthesis of BiVO₄ hollow microspheres and their evolution into nanocages,” *Ceram. Int.*, vol. 38, no. 6, pp. 4827–4834, 2012, doi: 10.1016/j.ceramint.2012.02.071.
- [10] S. Obregón, A. Caballero, and G. Colón, “Hydrothermal synthesis of BiVO₄: Structural and morphological influence on the photocatalytic activity,” *Appl. Catal. B Environ.*, vol. 117–118, pp. 59–66, 2012, doi: 10.1016/j.apcatb.2011.12.037.
- [11] A. N. Zulkifili, A. Fujiki, and S. Kimijima, “Flower-like BiVO₄ microspheres and their visible light-driven photocatalytic activity,” *Appl. Sci.*, vol. 8, no. 2, 2018, doi: 10.3390/app8020216.
- [12] W. Wang *et al.*, “Preparation of p-n junction Cu₂O/BiVO₄ heterogeneous nanostructures with enhanced visible-light photocatalytic activity,” *Appl. Catal. B Environ.*, vol. 134–135, no. February 2018, pp. 293–301, 2013, doi: 10.1016/j.apcatb.2013.01.013.
- [13] Z. Guo *et al.*, “One-dimensional spindle-like BiVO₄/TiO₂ nanofibers heterojunction nanocomposites with enhanced visible light photocatalytic activity,” *Ceram. Int.*, vol. 42, no. 3, pp. 4517–4525, 2016, doi: 10.1016/j.ceramint.2015.11.142.
- [14] W. Zheng, X. Liu, J. Guo, L. Wu, and D. Liao, “Preparation and crystal structure of two novel cadmium (II)-trimesates, Cd(HTMA)(NC₅H₅)₂·0.5CH₃OH·0.5DMF and Cd(HTMA)·2H₂O,” *Inorganica Chim. Acta*, vol. 357, no. 5, pp. 1571–1578, 2004, doi: 10.1016/j.ica.2003.11.039.
- [15] I. Khan, S. Ali, M. Mansha, and A. Qurashi, “Sonochemical assisted hydrothermal synthesis of pseudo-flower shaped Bismuth vanadate (BiVO₄) and their solar-driven water splitting application,” *Ultrason. Sonochem.*, vol. 36, pp. 386–392, 2017, doi: 10.1016/j.ultsonch.2016.12.014.
- [16] Y. Hu *et al.*, “Hydrothermal synthesis of BiVO₄ /TiO₂ composites and their application for degradation of gaseous benzene under visible light irradiation,” *Appl. Surf. Sci.*, vol. 436, pp. 319–326, 2018, doi: 10.1016/j.apsusc.2017.12.054.
- [17] U. Prasad, J. Prakash, B. Azeredo, and A. Kannan, “Stoichiometric and non-

stoichiometric tungsten doping effect in bismuth vanadate based photoactive material for photoelectrochemical water splitting,” *Electrochim. Acta*, vol. 299, pp. 262–272, 2019, doi: 10.1016/j.electacta.2019.01.013.

CHAPTER 5

RESULTS AND DISCUSSION

5.1 Characterization

5.1.1 X-ray Diffraction

The successful synthesis of bismuth vanadium oxide (vanadate), was confirmed by its structural characterizations employing XRD. **Figure 5.1 (a)** show XRD patterns of synthesized sample where diffraction peaks with 2θ values at 24.570, 27.520, 30.210, 32.700, 50.30, 52.20 and 53.60 corresponds to (220), (3 1 0), (222), (3 2 1), (4 4 0), (5 3 0), and (6 0 0) crystallographic planes perfectly match with the PDF # 46-0419 representing $\text{Bi}_{25}\text{VO}_{40}$ phase isostructural to sillenites [26]. The phase is pure, with body centered cubic cell (space group I23) and unit cell parameters are $a=10.2373 \text{ \AA}$ $\alpha= 900$ $V=1072.9\text{\AA}$. While with the doping of 3% yttrium, no new peaks are noticed. This is likely due to lower yttrium concentration in the structure which are below the detection limit of the instrument. Whereas the doping of 5% yttrium resulted in peak broadening of all major peaks inferring the loss of crystallinity and disruption of pure $\text{Bi}_{25}\text{VO}_{40}$. crystal structure. Moreover, the crystallite size analysis with Scherrer equation real the particle size of average 57 nm.

5.1.2 Scanning Electron Microscopy

To collect the information about the morphology of bismuth vanadium oxide SEM was performed. It can be seen that the pristine $\text{Bi}_{25}\text{VO}_{40}$ have the granular structure with fairly uniformed size distribution of the particle, **Figure 5.1 (b)**, that with the doping of yttrium are transformed into flake like morphology. In addition, elemental composition analysis revealed presence of expected O, V and Bi, elements, confirming the doping of yttrium. Moreover, the concentration of the yttrium was found to be 1.84%, which is below the detection limit of XRD instrument further confirming which is why no yttrium peak with 3% doping was observed.

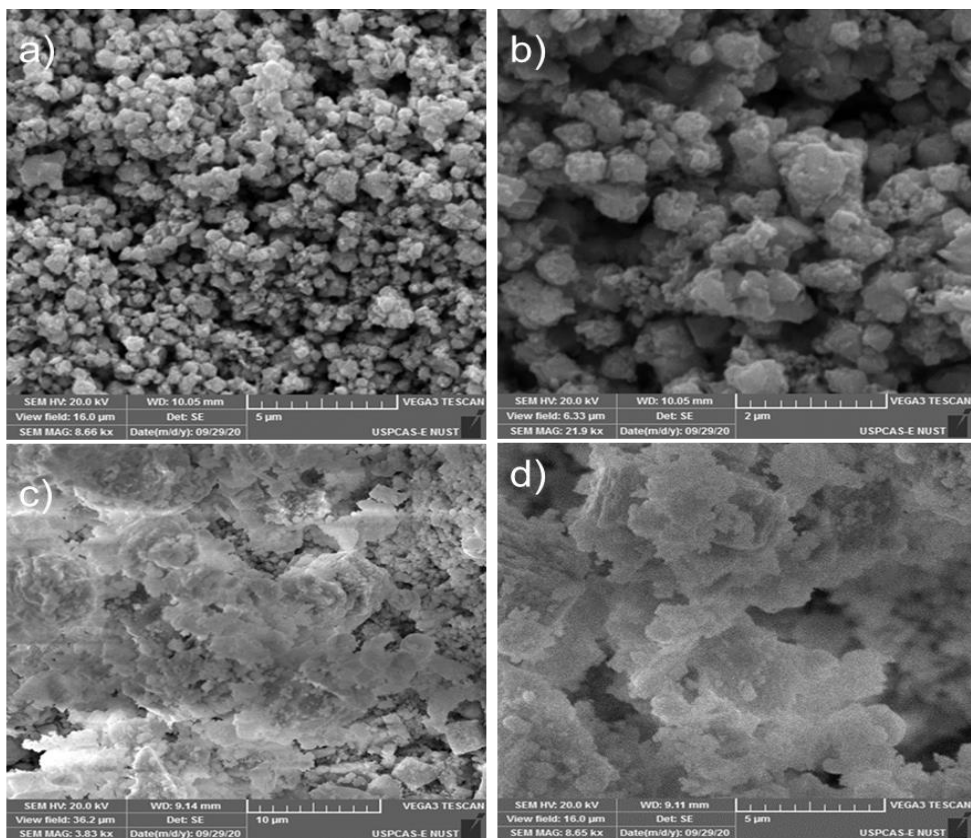
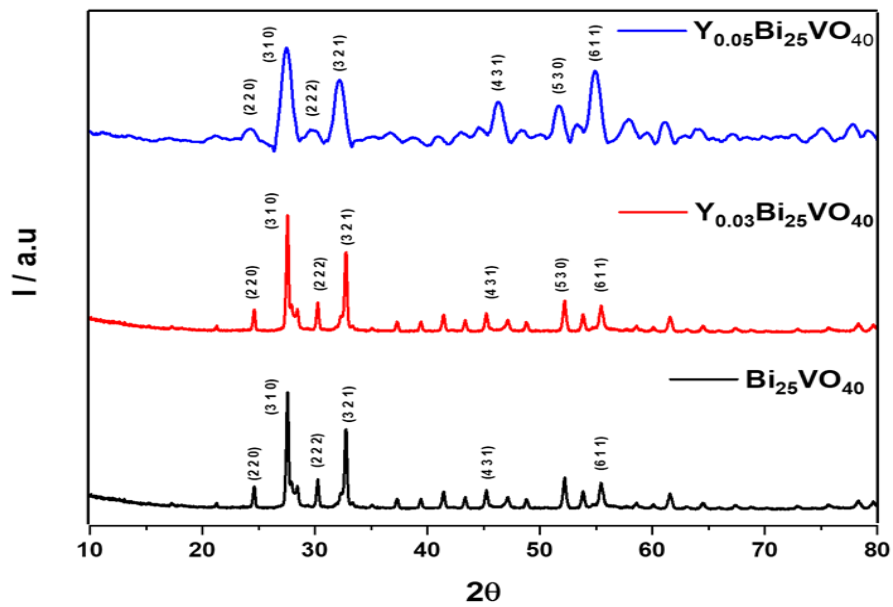


Figure 5.1 a) XRD patterns of Bismuth vanadium oxide $\text{Bi}_{25}\text{VO}_{40}$, and with yttrium doping $\text{Y}_{0.03}\text{Bi}_{25}\text{VO}_{40}$ and $\text{Y}_{0.05}\text{Bi}_{25}\text{VO}_{40}$ Figure 5.1 b) SEM images of a) $\text{Bi}_{25}\text{VO}_{40}$ b) $\text{Y}_{0.03}\text{Bi}_{25}\text{VO}_{40}$

5.1.3 EDS X-ray microanalysis using SEM

Qualitative microanalysis means that, from their characteristic X-ray peaks, the elements present in the sample are known, but their abundances are not determined. Quantitative EDS is used to analysis mass fractions and weight percent of elements present in the sample. EDS of pristine BVO showed Bi 80.36, V 1.57 and O 18.07 by weight percentages. and Bi 24.90, V 1.99, O 73.11 by atomic percentage. And no impurity is seen. Similarly, EDS pattern of Yttrium doped BVO showed Bi 77.57, V 2.73, Y 1.58 and O 18.63 by weight percentages. and Bi 23.24, V 2.73, Y 1.12 and O 72.91 by atomic percentage. No impurity has been seen.

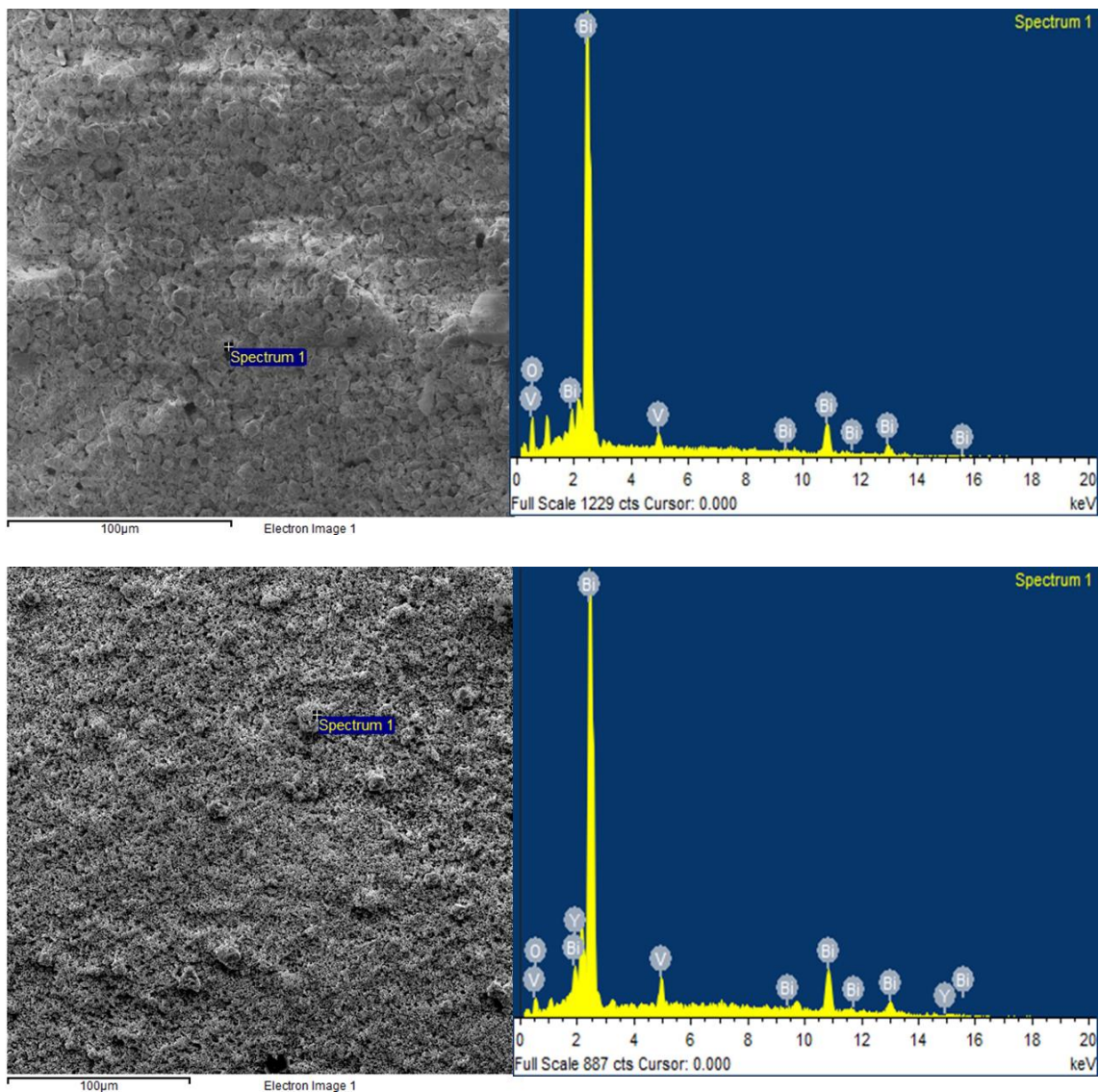


Figure 5.2 a) Elemental analysis of Bi₂₅VO₄₀ b) yttrium doped Bi₂₅VO₄₀

EDS microanalysis of Undoped BVO shows presence of Bi 80.36%, V 1.57% and O 18.07% and EDS pattern of doped BVO shows presence of Bi 85.47%, Y 1.84%, V 3.77% all by weight % and no impurities are observed.

5.3 Optical Testing

5.3.1 Uv-vis and Photoluminescence Spectroscopy

To analyse the optical behaviour of the sample, UV-Vis absorption spectra of pristine $\text{Bi}_{25}\text{VO}_{40}$ and yttrium doped $\text{Bi}_{25}\text{VO}_{40}$ are measured and compared. As shown in **Figure 5.3 (a)**, a strong absorption peak between (450-460) nm, is observed for pristine sample. The doping of yttrium in bismuth vanadium oxide resulted in strong absorption red shift, where absorption edge around 460 nm, probably due to well-known charge transfer process happening in VO_4^{3-} groups where transitions from O^{2-} to V^{5+} ions occur, and absorption tail is extended to the 490 nm is a likely result of intrinsic defect within the crystal structure. The band gap analysis of materials shows that 3 % yttrium doped photocatalyst has a band gap of 2.46 eV while pure material showed 2.61 eV and a yellowish coloured powder. These result show that materials are active under visible light. Furthermore, to have insight into the recombination process of the photo-generated electron-holes carrier's photoluminescence (PL) spectra were recorded. The higher the fluorescence intensity, the higher the rate of electron-hole pair recombination [14]. **Figure 5.3 (b)** presents the PL spectra of the pure and yttrium doped bismuth vanadium oxide materials, showing both doped and undoped $\text{Bi}_{25}\text{VO}_{40}$ exhibit a strong peak centred at around 450 nm. The strong emission is caused by the recombination of holes formed by the hybrid orbitals of Bi 6s and O 2p, as well as electrons produced by V 3d orbitals. Intriguingly, a very small blue shift in the emission band of doped $\text{Bi}_{25}\text{VO}_{40}$ material is seen along with low peak different inter-band transitions between defects (VO) and different luminescence canters may be the source of the emitted energy where the emission is thought to come from various inter-band transitions between defects (VO) and luminescence canters (Bi^{3+} and VO_4^{3-}) [19]. These features make materials interesting for photocatalytic application studies

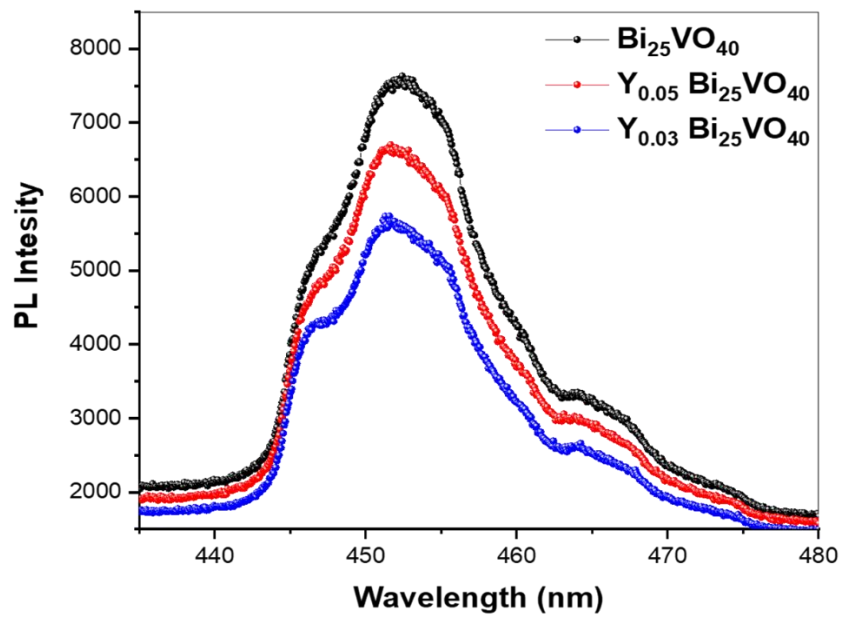
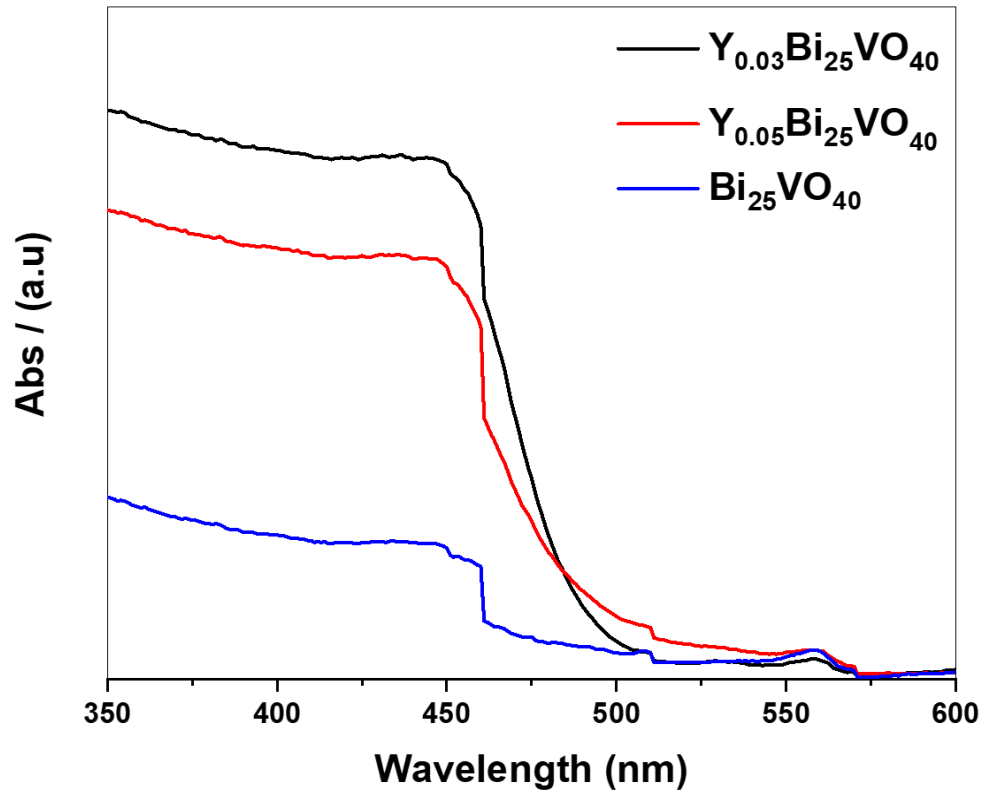


Figure 5.3 a) UV-Vis absorbance spectra of $\text{Bi}_{25}\text{VO}_{40}$, $\text{Y}_{0.03}\text{Bi}_{25}\text{VO}_{40}$ & $\text{Y}_{0.05}\text{Bi}_{25}\text{VO}_{40}$
 b) Photoluminescence spectra of doped and undoped $\text{Bi}_{25}\text{VO}_{40}$.

The band gap analysis of materials shows that 3 % yttrium doped photo-catalyst has a band gap of 2.46 eV while pure material showed 2.61 eV and a yellowish coloured powder. These result show that materials are active under visible light. Band gap was estimated by kebulka munk function. Kabulka Munk Function equation was used to calculate band gap of prepared composites. UV-Vis absorbance data is used in the equation for calculation. Equation is as follows:

$$FR \cdot hv = B(hv - E_g)$$

Where FR is Kebulka Munk Function, hv is Energy of photon and its value can be calculated by $1240/\lambda$. E_g is band gap of sample that can be calculated from above equation

Plotting value of hv on X-axis and $(FR \cdot hv)^2$ on Y-axis a peak is obtained as in figure. A projection is drawn to calculate exact bandgap.

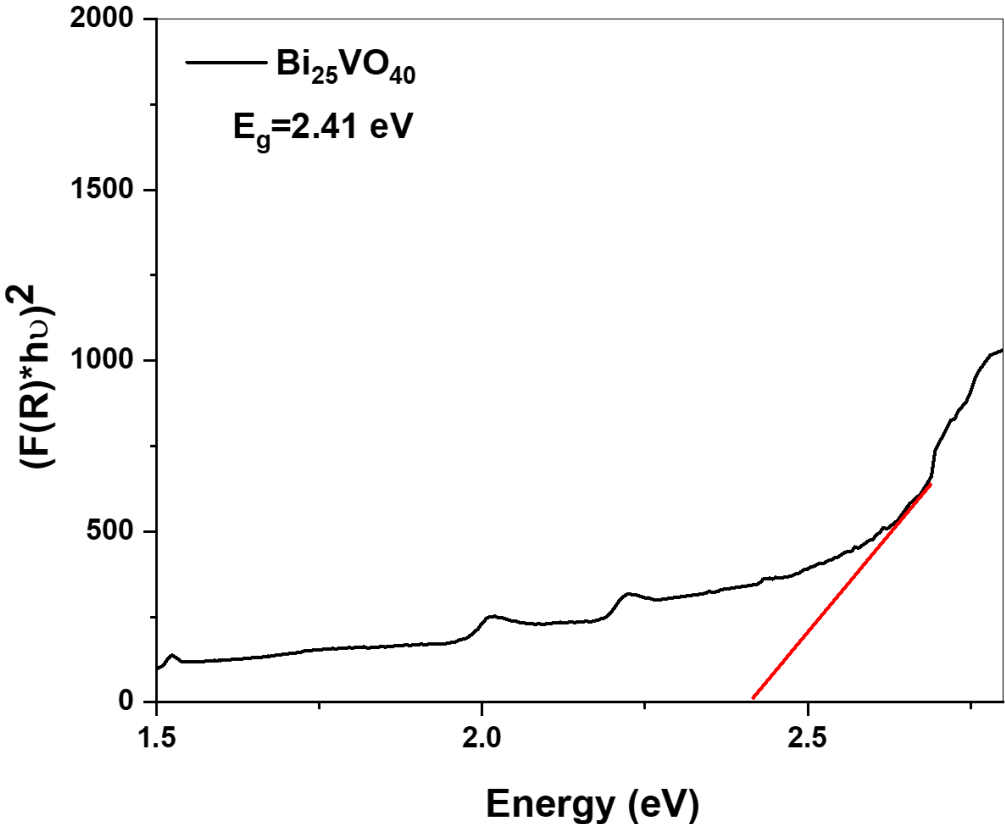


Figure 5.4 Kebulka-munk function band gap estimation of pristine Bi₂₅VO₄₀

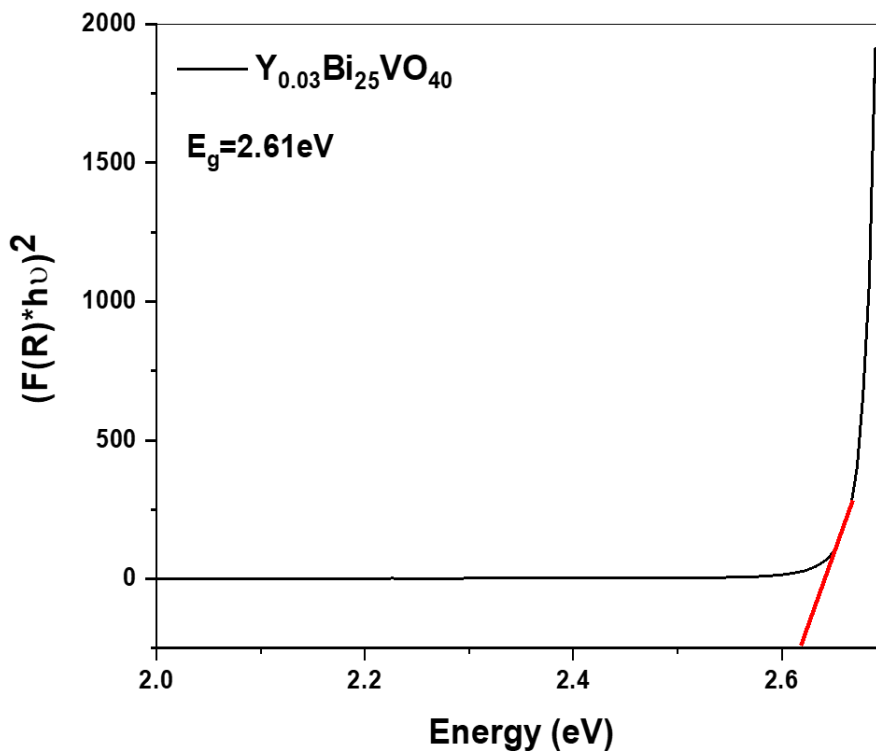


Figure 5.5 Kebulka-munk function band gap estimation of $Y_{0.03}Bi_{25}VO_{40}$

5.4 Photocatalytic testing

Methylene blue Dye (MB) is used for testing photo activity of BVO nanoparticles. Methylene blue is frequently used as a textile dye. Chemical is $C_{16}H_{18}N_3SCl$ Blue Homogenous blue mixture 4 ml methylene blue solution at concentration of 0.3mg/100ml and 96 ml DI water was prepared in vessel. Then 0.3 g of BVO fine powder added in to the solution [14]. Solution was magnetically stirred as well as stirred by harsh stirrer.

Uv-vis spectroscopy is used to measure photoactivity of doped and undoped Bismuth vanadate, Absorbance spectra is carried out of degradation of methylene blue dye. Samples were collected from round bottom flask after every 15 mints with 3mL syringe and then placed inside UV-Vis spectrometer to measure maximum absorption of wavelength for that specific dye and rate of decolourization. Percentage degradation is calculated by following formula $\{1 - (C/C_0)\} * 100\%$. C_0 is the initial concentration of the dye solution and C is the concentration of dye after every 15 mints interval.

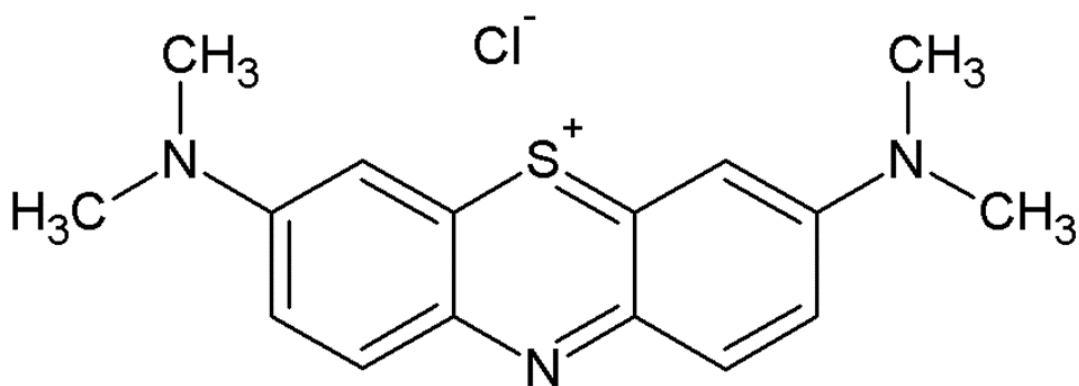


Figure 5.6 Molecular structure of Methylene Blue [15].

Degradation products should be nontoxic towards material that are dyed as well as living organisms. Parameters for dyeing are not purely safe so optimization of parameters and identifying suitable photocatalyst is necessary for successful and safe implementation of this process of waste water treatment.

Bismuth based semiconductors (nanomaterials) are widely used as photocatalyst material. Due to their small band gap and acceptable band locations, bismuth based nanomaterials have been regarded as possible candidates for dye degradation.

Quick charge recombination and photocorrosion are the critical problems associated with bismuth based materials for the dye decolorization. The new attempts to deal with these problems are discussed in depth. $\text{Bi}_{25}\text{VO}_{40}$ was found to be promising for dye degradation, among all the bismuth-based materials published. Several efforts have been done to boost BVO efficiency. In this study yttrium is doped in BVO to reduce charge recombination and enhance charge separation's.

Results showed that pristine bismuth vanadate degraded less amount of dye as compare to doped. Peak analysis is studied in Origin. All peaks are at 665 nm wavelength.

Samples were collected with syringe after 15 mints and then after 30 mints under solar simulator and continuous stirring 3% doped bismuth vanadate degraded more dye in less time, C/C_0 graph is shown below **Figure 5.8** and results of doped and un doped BVO nanoparticles are shown in term of % degradation after 180 mints under solar simulator. Comparison is shown is **Figure 5.9**.

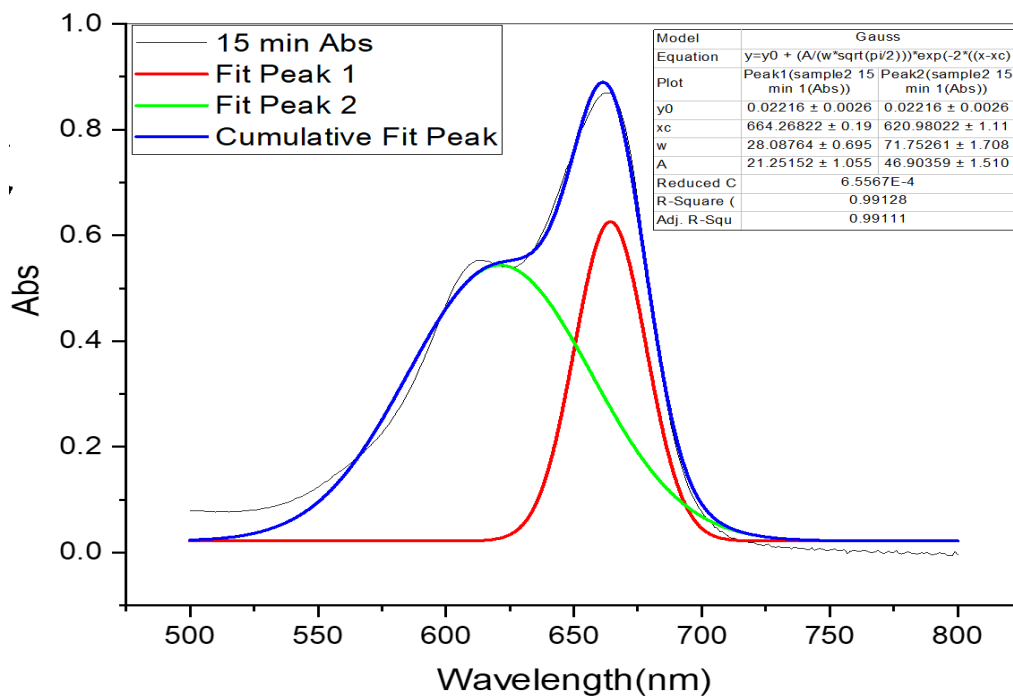
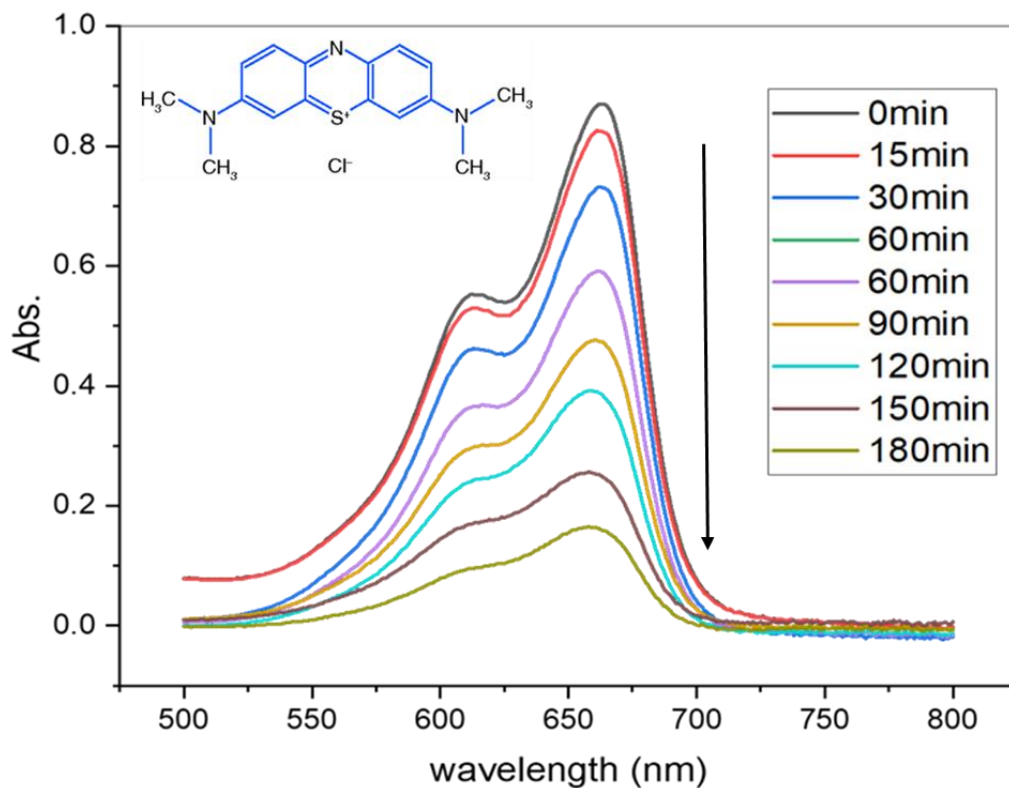


Figure 5.7 a) UV-Vis spectra of pristine BVO after specific time interval under solar simulator b) Peak analysis of UV-Vis spectra of MB

Absorption of methylene blue aqueous solution under visible light solar irradiation are shown in Fig. By peak analysis as shown in Fig absorption at 664nm wavelength is used for dye decolorizing rate process. After 180 mints Y doped BVO nanoparticles degraded 84.2% methylene blue as compared to pristine BVO nanoparticles which degraded 66% dye after 180 mints under Solar simulator. These results show yttrium doped BVO nanoparticles have more photocatalytic activity.

The stability of $Y_{0.03}\text{-Bi}_{25}\text{VO}_{40}$ was also examined by operating the photocatalytic properties test of this photo-catalyst was performed (Figure 5.10). After four cycles of operation, we discovered that this substance has strong stability, as it only dropped from 84.2 % to 76 %. It has decent stability and recyclability, so it's a good option

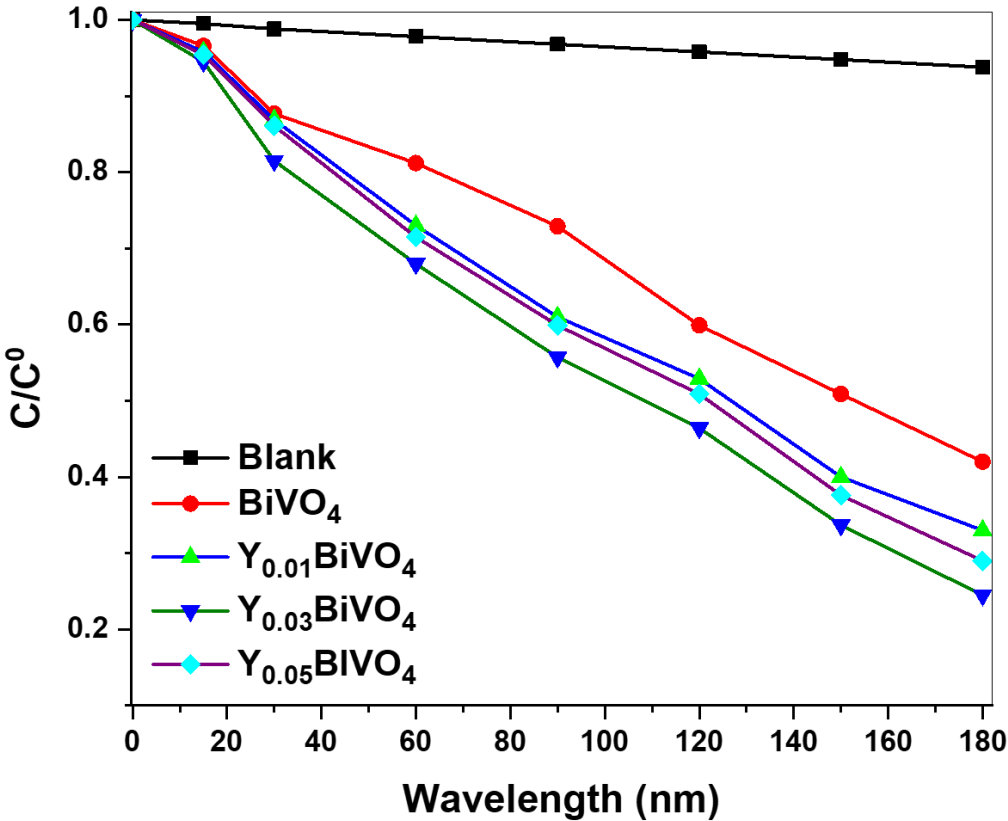


Figure 5.8 Rate of degradation of methylene blue dye

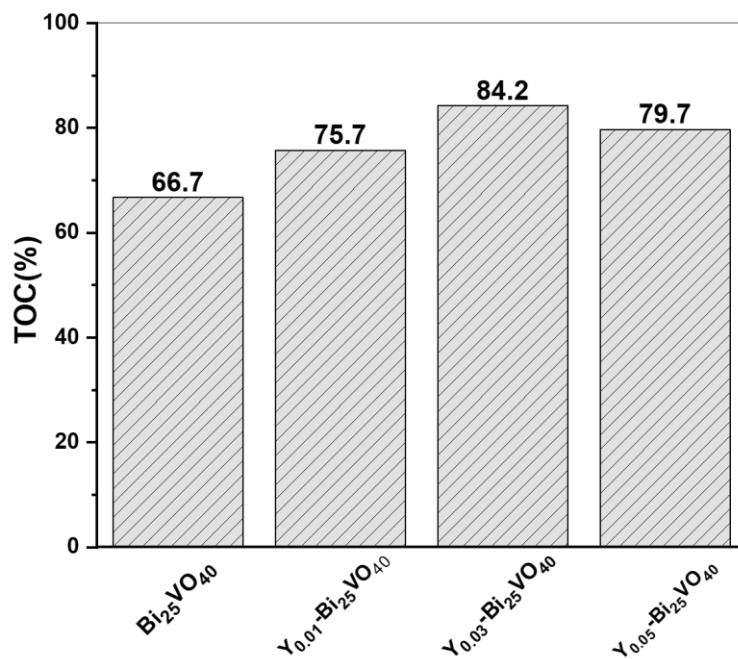
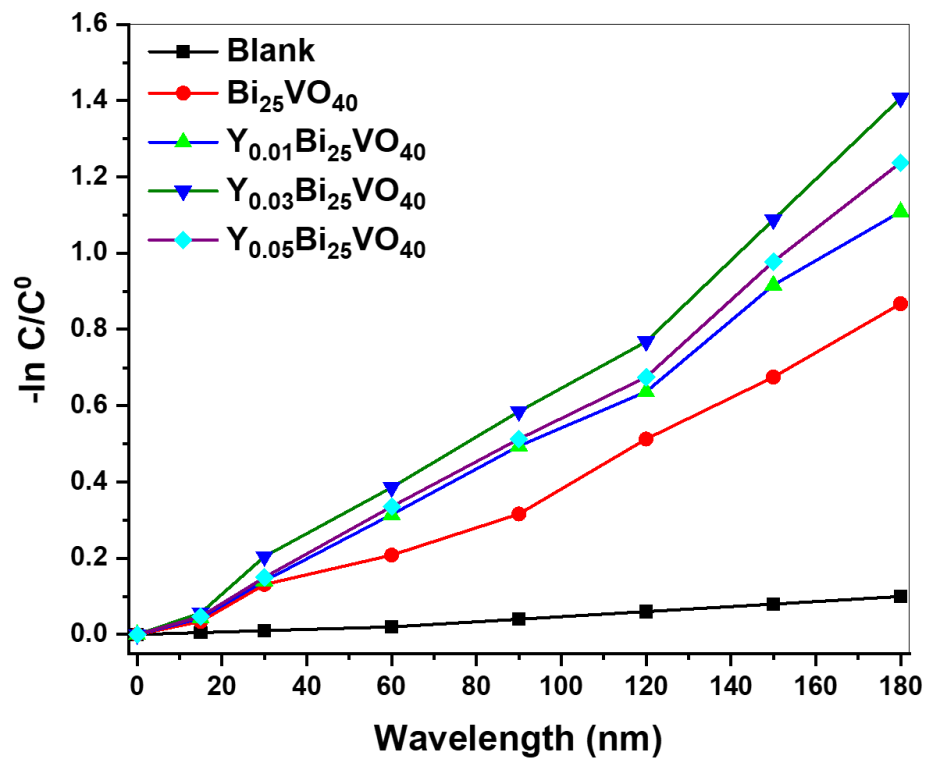


Figure 5.9 a) $-\ln C/C^0$ vs Wavelength (nm) b) Total oxygenated carbon %

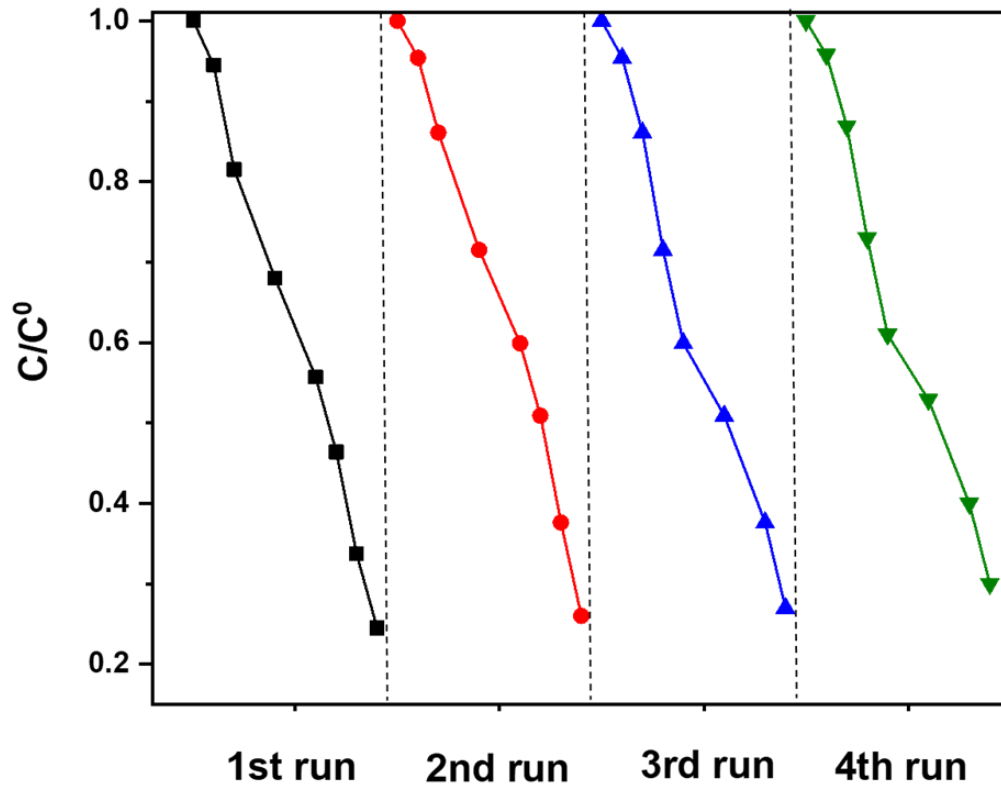


Figure 5.10 Recyclability of methylene blue dye degradation rate for $Y_{0.03}Bi_{25}VO_{40}$

5.3.3 Bi₂₅VO₄ photo anode for production of hydrogen by PEC water splitting

5.3.3.1 Background

Photo electrochemical water splitting is an alternate method of direct production of solar fuels, like hydrogen. The semiconductor is also used in this process.

Photo electrodes are used to transform solar energy into chemical energy, allowing abundant yet abundant energy to be transformed into chemical energy [16].

To harvest, store, and transform intermittent solar energy into a shape that can easily be stored. Several materials are used to effective and sustainable breakage of water into fuel (hydrogen and oxygen) [17].

Simultaneous compliance with the requirements is required: (1) ample photo voltage and sufficient water-breaking band alignment; (2) considerable absorption of the solar

radiations spectrum, mainly visible light; (3) stable in addition easy transportation of charges through the semiconductor and the electrolyte solution and (4) cost-effectiveness and stability.

Bottleneck of the process of use of photo anode TiO_2 and Platinum cathode in the presence of UV light is half reaction of oxidation of water. A variety of studies have been carried out to test suitable materials that can serve as successful to solve this bottleneck, photo anodes [18].

5.3.2.3 PEC performance calculation

- It is carried under room temperature, in 0.1M K_2HPO_4 electrolyte (at PH 8,7) with addition and without addition of 1M Na_2SO_3 (hole scavenger).
- Platinum wire utilized as counter anode and standard calomel cathode is utilized as reference terminal.
- Solar simulator (new port 69907) with 1.5 AM, 300 Wm^2 Xenon light was utilized as a light source (calibrated to 100 mWCm^{-2} one sun).
- Partstat-2273 Potentiostat is used is used for electrochemical measurement,
- PEC performance was calculated by LSV (linear sweep voltammetry) with scan rate of 20 mVs^{-1} .
- PEC evaluation was also measured under chopped light.
- In all electrochemical measurement, electrode surface area is kept 1cm^2 .

5.3.2.4 PEC performance under chopped light

PEC water splitting performance of prepared photo anodes were analyzed under chopped light. After every 3 s light coming from solar simulator has been chopped with the help of a card, in order to notice performance of photo anode without light (dark).

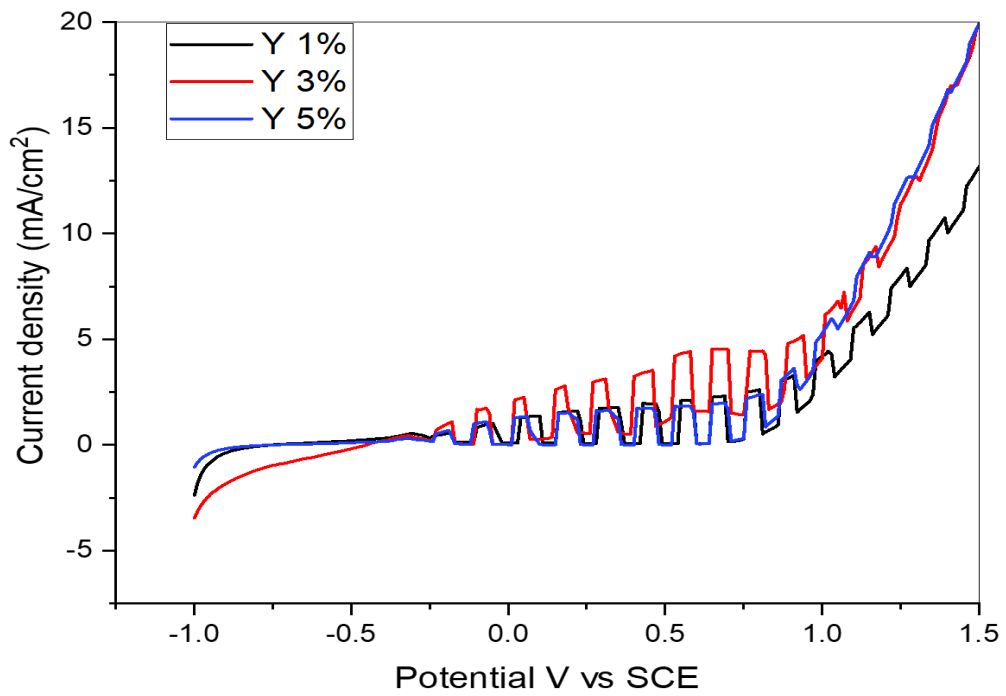
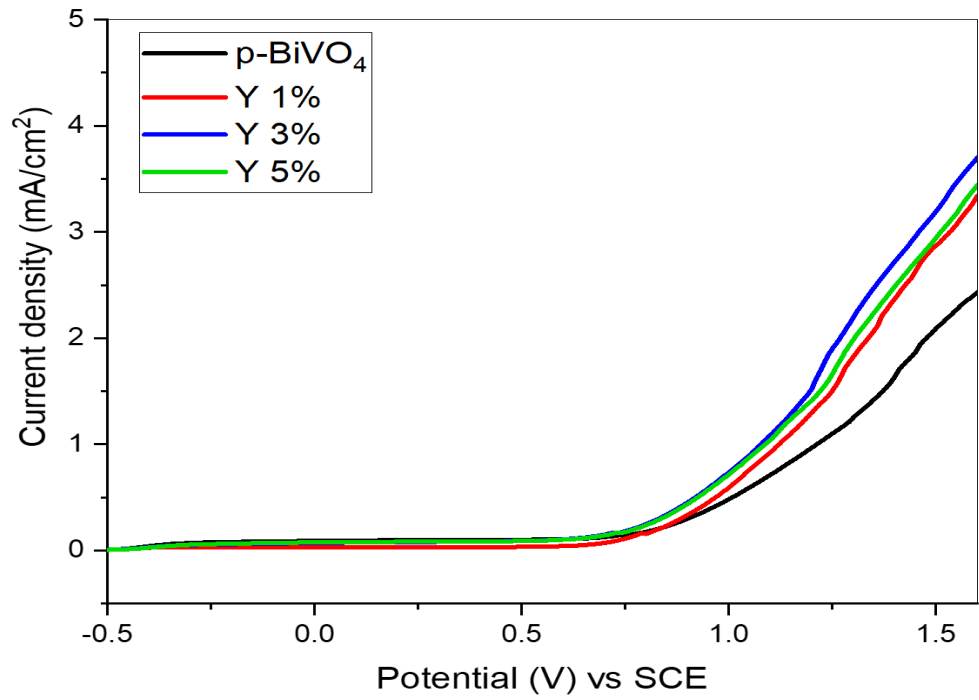


Figure 5.11 a) LSV of doped and undoped BVO b) LSV under chopped light

PEC performance is also compared without hole scavenger Na_2SO_3 . It is observed that Photo electrochemical response was increased with addition of hole scavenger (sacrificial agent) in reference to the KOH solution.

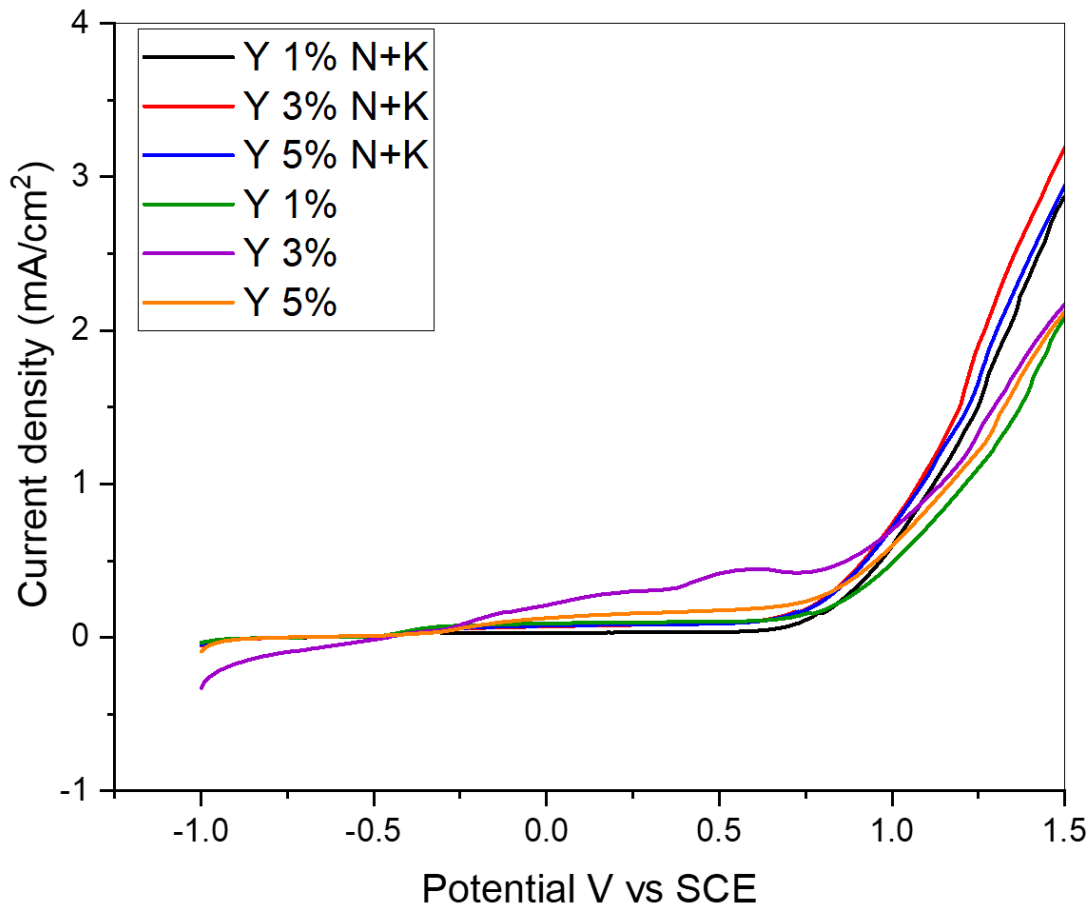


Figure 5.12 LSV of photo anodes in electrolyte with or without Na_2SO_3

The optimal 3% Y+3 doping showed significantly improved photocurrent response in comparison to the pristine material. It is important to note that no change in phase and morphology yet a noticeable change in absorption behavior and reduction in recombination rate with yttrium doping in $\text{Bi}_{25}\text{VO}_{40}$ was noted, that in turns leads to better photocurrent density for water splitting

Summary of Results and Discussions

Table 5.1 Summary of Results

Catalyst	J*	% Degradation	E _g	K [min ⁻¹]	Adj. R-Square
Bi ₂₅ VO ₄₀	2.09	58	2.68	0.00475 ± 2.75 *10 ⁻⁴	0.9798
Y _{0.1} Bi ₂₅ VO ₄₀	2.87	67	2.70	0.00621 ± 2.2 *10 ⁻⁴	0.99123
Y _{0.3} Bi ₂₅ VO ₄₀	3.19	75.5	2.70	0.0076 ± 3.54 *10 ⁻⁴	0.98494
Y _{0.5} Bi ₂₅ VO ₄₀	2.94	71	2.70	0.0068 ± 3.11 *10 ⁻⁴	0.98545

* (Current density in mA/Cm⁻² vs Ag/AgCl)

References

- [1] S. Di Mo and W. Y. Ching, “Electronic and optical properties of three phases of titanium dioxide: Rutile, anatase, and brookite,” *Phys. Rev. B*, vol. 51, no. 19, pp. 13023–13032, 1995, doi: 10.1103/PhysRevB.51.13023.
- [2] D. V. Bavykin, J. M. Friedrich, and F. C. Walsh, “Protonated titanates and TiO₂ nanostructured materials: Synthesis, properties, and applications,” *Adv. Mater.*, vol. 18, no. 21, pp. 2807–2824, 2006, doi: 10.1002/adma.200502696.
- [3] S. Bakardjieva, J. Šubrt, V. Štengl, M. J. Dianez, and M. J. Sayagues, “Photoactivity of anatase-rutile TiO₂ nanocrystalline mixtures obtained by heat treatment of homogeneously precipitated anatase,” *Appl. Catal. B Environ.*, vol. 58, no. 3–4, pp. 193–202, 2005, doi: 10.1016/j.apcatb.2004.06.019.
- [4] M. Koelsch, S. Cassaignon, J. F. Guillemoles, and J. P. Jolivet, “Comparison of optical and electrochemical properties of anatase and brookite TiO₂ synthesized by the sol-gel method,” *Thin Solid Films*, vol. 403–404, pp. 312–319, 2002, doi: 10.1016/S0040-6090(01)01509-7.
- [5] B. Ohtani, Y. Ogawa, and S. Nishimoto, “JPysChemB,101,(1997)3746(アモルファスTiO₂).pdf,” *J. Phys. Chem. B*, vol. 5647, no. 101, pp. 3746–3752, 1997.
- [6] A. R. Khataee and M. B. Kasiri, “Photocatalytic degradation of organic dyes in the presence of nanostructured titanium dioxide: Influence of the chemical structure of dyes,” *J. Mol. Catal. A Chem.*, vol. 328, no. 1–2, pp. 8–26, 2010, doi: 10.1016/j.molcata.2010.05.023.
- [7] M. Z. Bin Mukhlish, F. Najnin, M. M. Rahman, and M. J. Uddin, “Photocatalytic Degradation of Different Dyes Using TiO₂ with High Surface Area: A Kinetic Study,” *J. Sci. Res.*, vol. 5, no. 2, pp. 301–314, 2013, doi: 10.3329/jsr.v5i2.11641.
- [8] I. Bsu, “Весці нацыянальнай акадэміі навук беларусі № 2 2016,” pp. 57–67, 2016.
- [9] M. D. Hernández-Alonso, F. Fresno, S. Suárez, and J. M. Coronado, “Development

- of alternative photocatalysts to TiO₂: Challenges and opportunities,” *Energy Environ. Sci.*, vol. 2, no. 12, pp. 1231–1257, 2009, doi: 10.1039/b907933e.
- [10] H. Y. He, Y. Yan, J. F. Huang, and J. Lu, “Rapid photodegradation of methyl blue on magnetic Zn_{1-x}CoxFe₂O₄ nanoparticles synthesized by hydrothermal process,” *Sep. Purif. Technol.*, vol. 136, pp. 36–41, 2014, doi: 10.1016/j.seppur.2014.08.028.
- [11] W. Z. Tang and Huren An, “UV/TiO₂ photocatalytic oxidation of commercial dyes in aqueous solutions,” *Chemosphere*, vol. 31, no. 9, pp. 4157–4170, 1995, doi: 10.1016/0045-6535(95)80015-D.
- [12] B. Viswanathan, “Photocatalytic Degradation of Dyes: An Overview,” *Curr. Catal.*, vol. 7, no. 2, pp. 99–121, 2017, doi: 10.2174/2211544707666171219161846.
- [13] K. Mondal and A. Sharma, “Photocatalytic Oxidation of Pollutant Dyes in Wastewater by TiO₂ and ZnO nano-materials – A Mini-review,” *indian Inst. Technol.*, no. January 2015, pp. 36–72, 2016.
- [14] A. N. Zulkifili, A. Fujiki, and S. Kimijima, “Flower-like BiVO₄ microspheres and their visible light-driven photocatalytic activity,” *Appl. Sci.*, vol. 8, no. 2, 2018, doi: 10.3390/app8020216.
- [15] T. S. Hui and M. A. A. Zaini, “Isotherm studies of methylene blue adsorption onto potassium salts-modified textile sludge,” *J. Teknol.*, vol. 74, no. 7, pp. 57–63, 2015, doi: 10.11113/jt.v74.4699.
- [16] X. Chen, S. Shen, L. Guo, and S. S. Mao, “Semiconductor-based photocatalytic hydrogen generation,” *Chem. Rev.*, vol. 110, no. 11, pp. 6503–6570, 2010, doi: 10.1021/cr1001645.
- [17] S. P. Berglund, A. J. E. Rettie, S. Hoang, and C. B. Mullins, “Incorporation of Mo and W into nanostructured BiVO₄ films for efficient photoelectrochemical water oxidation,” *Phys. Chem. Chem. Phys.*, vol. 14, no. 19, pp. 7065–7075, 2012, doi: 10.1039/c2cp40807d.
- [18] Y. Zhu, M. W. Shah, and C. Wang, “Insight into the role of Ti³⁺ in photocatalytic

- performance of shuriken-shaped BiVO₄/TiO_{2-x} heterojunction,” *Appl. Catal. B Environ.*, vol. 203, pp. 526–532, 2017, doi: 10.1016/j.apcatb.2016.10.056.
- [19] W. Q. Fan *et al.*, “Fabrication of TiO₂-BiOCl double-layer nanostructure arrays for photoelectrochemical water splitting,” *CrystEngComm*, vol. 16, no. 5, pp. 820–825, 2014, doi: 10.1039/c3ce42001a.
- [20] M. Serhan *et al.*, “Total iron measurement in human serum with a smartphone,” *AIChE Annu. Meet. Conf. Proc.*, vol. 2019-Novem, 2019, doi: 10.1039/x0xx00000x.
- [21] L. Wang and W. A. Daoud, “BiOI/TiO₂ -nanorod array heterojunction solar cell: Growth, charge transport kinetics and photoelectrochemical properties,” *Appl. Surf. Sci.*, vol. 324, pp. 532–537, 2015, doi: 10.1016/j.apsusc.2014.10.110.
- [22] J. Zhao *et al.*, “High-Performance Ultrathin BiVO₄ Photoanode on Textured Polydimethylsiloxane Substrates for Solar Water Splitting,” *ACS Energy Lett.*, vol. 1, no. 1, pp. 68–75, 2016, doi: 10.1021/acseenergylett.6b00032.
- [23] S. Byun, B. Kim, S. Jeon, and B. Shin, “Effects of a SnO₂ hole blocking layer in a BiVO₄-based photoanode on photoelectrocatalytic water oxidation,” *J. Mater. Chem. A*, vol. 5, no. 15, pp. 6905–6913, 2017, doi: 10.1039/c7ta00806f.
- [24] F. F. Abdi, N. Firet, and R. vandeKrol, “Efficient BiVO₄ Thin Film Photoanodes Modified with Cobalt Phosphate Catalyst and W-doping,” *ChemCatChem*, vol. 5, no. 2, pp. 490–496, 2013, doi: 10.1002/cctc.201200472.
- [25] S. S. Kalanur, I. H. Yoo, J. Park, and H. Seo, “Insights into the electronic bands of WO₃/BiVO₄/TiO₂, revealing high solar water splitting efficiency,” *J. Mater. Chem. A*, vol. 5, no. 4, pp. 1455–1461, 2017, doi: 10.1039/c6ta07592d.
- [26] S. Byun *et al.*, “Compositional engineering of solution-processed BiVO₄ photoanodes toward highly efficient photoelectrochemical water oxidation,” *Nano Energy*, vol. 43, no. August 2017, pp. 244–252, 2018, doi: 10.1016/j.nanoen.2017.11.034.
- [27] L. Zhou *et al.*, “High Light Absorption and Charge Separation Efficiency at Low

- Applied Voltage from Sb-Doped SnO₂/BiVO₄ Core/Shell Nanorod-Array Photoanodes,” *Nano Lett.*, vol. 16, no. 6, pp. 3463–3474, 2016, doi: 10.1021/acs.nanolett.5b05200.
- [28] J. C. Hill and K. S. Choi, “Synthesis and characterization of high surface area CuWO₄ and Bi₂WO₆ electrodes for use as photoanodes for solar water oxidation,” *J. Mater. Chem. A*, vol. 1, no. 16, pp. 5006–5014, 2013, doi: 10.1039/c3ta10245a.
- [29] S. Y. Chae, E. S. Lee, H. Jung, Y. J. Hwang, and O. S. Joo, “Synthesis of Bi₂WO₆ photoanode on transparent conducting oxide substrate with low onset potential for solar water splitting,” *RSC Adv.*, vol. 4, no. 46, pp. 24032–24037, 2014, doi: 10.1039/c4ra02868f.
- [30] L. Zhang and D. Bahnemann, “Synthesis of nanovoid Bi₂WO₆ 2D ordered arrays as photoanodes for photoelectrochemical water splitting,” *ChemSusChem*, vol. 6, no. 2, pp. 283–290, 2013, doi: 10.1002/cssc.201200708.
- [31] Y. Ma, Y. Jia, L. Wang, M. Yang, Y. Bi, and Y. Qi, “Exfoliated thin Bi₂MoO₆ nanosheets supported on WO₃ electrode for enhanced photoelectrochemical water splitting,” *Appl. Surf. Sci.*, vol. 390, pp. 399–405, 2016, doi: 10.1016/j.apsusc.2016.08.116.
- [32] Y. Ma, Y. Jia, L. Wang, M. Yang, Y. Bi, and Y. Qi, “Bi₂MoO₆/BiVO₄ heterojunction electrode with enhanced photoelectrochemical properties,” *Phys. Chem. Chem. Phys.*, vol. 18, no. 7, pp. 5091–5094, 2016, doi: 10.1039/c5cp07784b.
- [33] S. J. A. Moniz, C. S. Blackman, P. Southern, P. M. Weaver, J. Tang, and C. J. Carmalt, “Visible-light driven water splitting over BiFeO₃ photoanodes grown via the LPCVD reaction of [Bi(OtBu)₃] and [Fe(OtBu)₃]₂ and enhanced with a surface nickel oxygen evolution catalyst,” *Nanoscale*, vol. 7, no. 39, pp. 16343–16353, 2015, doi: 10.1039/c5nr04804d.

Chapter 6

Exchange Work

State of Charge (SOC) and State of Health (SOH)

Estimation for Lead Acid Batteries

6.1 Introduction

Battery heaps of lead destructive batteries (LAB) are used in various applications like Electric vehicles, Hybrid electric vehicles, off-system Photovoltaics, grid strength, top shaving, and energy amassing of other boundless resources [1]. For all of these applications State of charge (SOC) of each cell is basic to evaluate. SOC described in Ampere hour (Ah) and conveyed in degree of evaluated limit. The SOC limit can be viewed as a thermodynamic sum engaging one to overview the conceivable energy of a battery. SOC of a battery is described as extent of its current breaking point $Q(t)$ as far as possible (Q_n). Q_n is the best proportion of charge that can be taken care of in a battery. This rating of battery is given by maker [2].

$$\text{SOC (T)} = \frac{Q(t)}{Q_n}$$

With change of SOC of battery, resistance and temperature varies during charge discharge cycles so these parameters are useful for measuring SOC.

SOC = 100% → fully charged battery

It is additionally imperative to gauge the state of health (SOH) of a battery, which addresses a proportion of the battery's capacity to store and convey electrical energy, contrasted and another battery. SOH is significant marker of batteries life [3].

Cycle life is influenced by:

- ✓ Charge/Discharge rate
- ✓ Depth of discharge

- ✓ Level of overcharge
- ✓ Ambient temperature

6.2 Material degradation of electrodes and grids

Truth be told, the oxidation and decrease rates at both Pb anode and PbO₂ cathode, separately increment essentially prompting higher release limit at raised temperatures [4].

Reduction causes:

- ✓ Reduce life cycle
- ✓ Self-discharge
- ✓ Loss of electrolyte
- ✓ Active material shedding
- ✓ Grid corrosion
- ✓ Mechanical power of the +ve electrode deteriorates

6.3 Purpose of Measuring SOC and SOH

1. To evade unpredicted framework interference and keep the batteries from being over charged and over released in various climate condition
2. To measure the battery's capacity to store and convey electrical energy
3. Correlate the exhibition estimations to assess cycle life by high recurrence Impedance examination

6.4 Experiment

Programmable Arbin Battery Cycling unit is used for conducting charge/discharge tests and also to record discharge profiles for these cells. In present study, the SOC and SOH estimation [5] was carried out through EIS, 6 Lead-acid (LA) cells (2V, 5Ah) has been procured as batteries accomplish the ideal working voltage by associating a few cells in arrangement specifically in electric vehicles, the operating high voltage is achieved by connecting batteries in series. For this particular purpose we have planned to test cells connected in series as shown below in Fig. using programmable Arbin Battery Cycling unit. Performance measured at room temperature (27°C) [6].

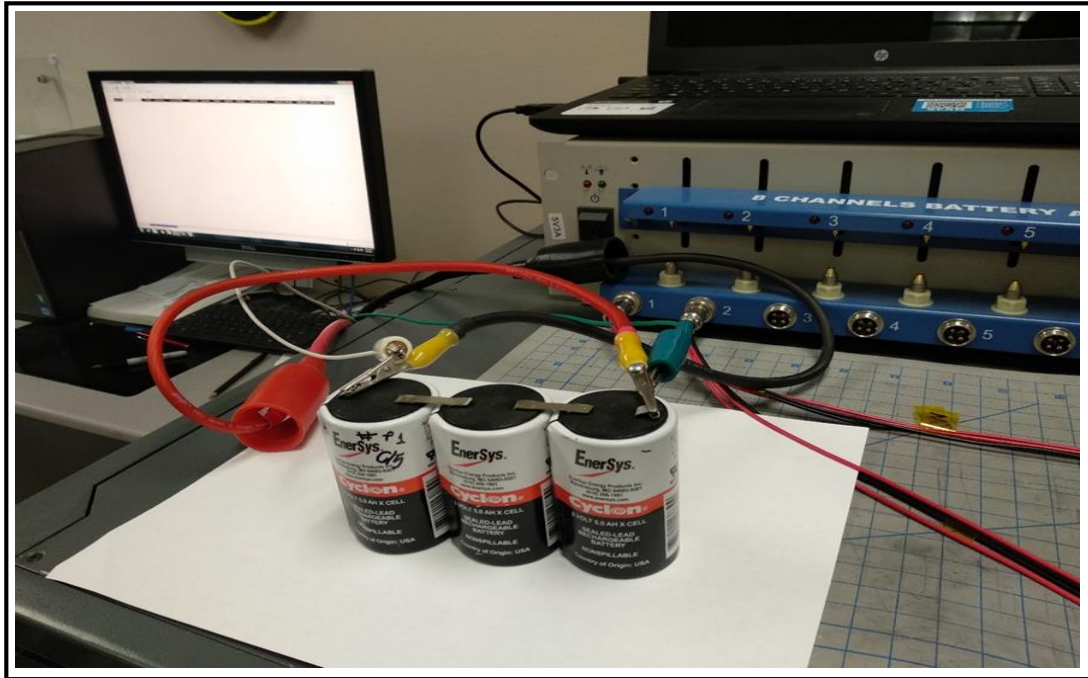


Figure 6.1 Testing setup for battery pack (3 LA cells connected in series)

Conducted first cycle performance evaluation at room temperature (25°C) by measuring current and potential and discharge profiles. Preliminary test of charging discharging (10 cycle) of single cell battery was carried out under following experimental condition.

- ✓ Charging condition (2.5 V): current – 2.5 A and 1 A
- ✓ Discharging condition (1.5 V): current – 2.5 A and 1 A

MITS pro software is used to give command to Arbin battery cycling unit. MITS pro schedule file window is shown in Fig. input command is given by following above mentioned steps. Charging of cells at 105% of charge input of previous discharge discharge capacity values for all the cells using DC regulated power supply [7].

Arbin laboratory battery testing (LBT) systems is commercialized high precision testing system having independent charge/discharge channels used for testing battery or super capacitor modules and other energy storage devices. It gives safe and high precision data measurement and fast data sampling. It comes with MITS pro and data watcher software for real time data monitoring.

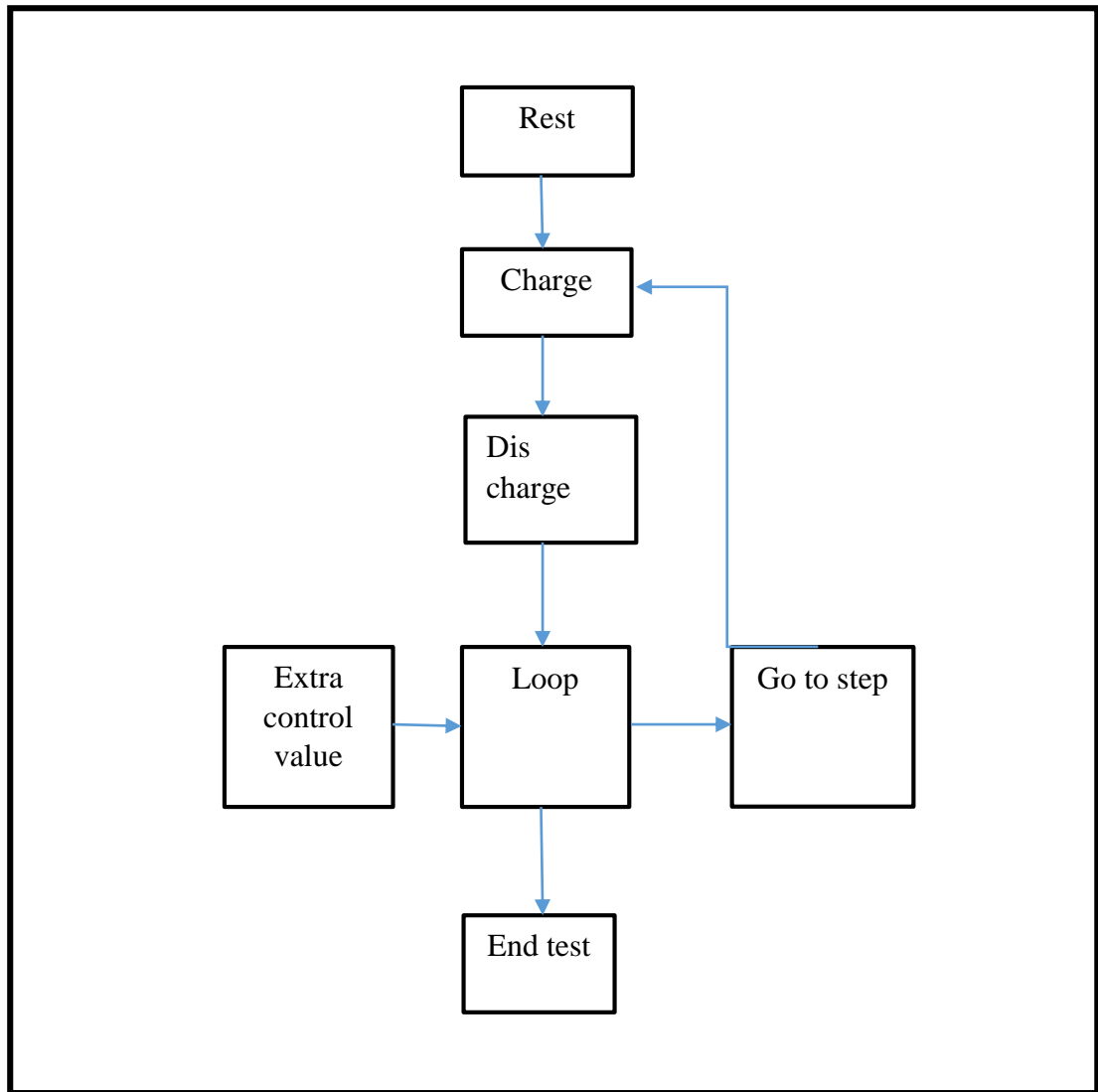


Figure 6.2 Steps of input command for MITS pro schedule file

Batteries are critical and important part of any energy storage application so it is necessary to select good battery. So battery testing system should be highly précised.

6.4.1 The charging and discharging behavior of single cell battery

Programmable DC gadgets load (Circuit-experts Inc. AZ and electronic battery analyzer, west mountain radio, WI) utilized for leading release tests and record profiles. Charge input was fixed at 105% of the past release limits esteems for all cells [8].

Schedule File Window > SLA_1K.sdu -

File Edit Print View Settings Help

Step Label	Number Of Limits	Control Type	Control Value	Extra Control Value 1	Extra Control Value 2	Current Range	Extended Definition	Extended Definition 1	Log Clock Stretch
1 Rest	2	Rest							
Log Limit	Step Limit	Goto Step	Variable1	Operator1	Value1	Variable2	Operator2	Value2	Operator3
<input checked="" type="checkbox"/>	<input checked="" type="checkbox"/>	Next Step	PV_CHAN_St	>=	00:05:00				
		Next Step	DV_Time	>=	00:02:00				
2 Charging	2	Current(A)	1			Medium			
Log Limit	Step Limit	Goto Step	Variable1	Operator1	Value1	Variable2	Operator2	Value2	Operator3
<input checked="" type="checkbox"/>	<input checked="" type="checkbox"/>	Next Step	PV_CHAN_Vo	>=	6.9				
		Next Step	DV_Time	>=	00:02:00				
3 Rest	2	Rest							
Log Limit	Step Limit	Goto Step	Variable1	Operator1	Value1	Variable2	Operator2	Value2	Operator3
<input checked="" type="checkbox"/>	<input checked="" type="checkbox"/>	Next Step	PV_CHAN_St	>=	00:05:00				
		Next Step	DV_Time	>=	00:02:00				
4 Discharge	2	Current(A)	-1			Medium			
Log Limit	Step Limit	Goto Step	Variable1	Operator1	Value1	Variable2	Operator2	Value2	Operator3
<input checked="" type="checkbox"/>	<input checked="" type="checkbox"/>	Next Step	PV_CHAN_Vo	<=	4.5				
		Next Step	DV_Time	>=	00:02:00				
5 Loop	1	Set Variable	Reset	Increment	Decrement				
Log Limit	Step Limit	Goto Step	Variable1	Operator1	Value1	Variable2	Operator2	Value2	Operator3
<input checked="" type="checkbox"/>	<input checked="" type="checkbox"/>	Charging	PV_CHAN_Cy	<=	50				
6 Step_F	2	Rest							
Log Limit	Step Limit	Goto Step	Variable1	Operator1	Value1	Variable2	Operator2	Value2	Operator3
<input checked="" type="checkbox"/>	<input checked="" type="checkbox"/>	Next Step	PV_CHAN_St	>=	00:05:00				
		Next Step	DV_Time	>=	00:02:00				
7 Step_G	2	Current(A)	1			Medium			
Log Limit	Step Limit	Goto Step	Variable1	Operator1	Value1	Variable2	Operator2	Value2	Operator3
<input checked="" type="checkbox"/>	<input checked="" type="checkbox"/>	End Test	PV_CHAN_Vo	>=	6.9				
		End Test	DV_Time	>=	00:02:00				

Global Step / Limit Edit

Hint

Figure 6.3 Schedule file window of MITS pro software

6.4.2 Rate of Charge and discharge

A simple way to convey battery capacity is to give it as a function of time, i.e. how long it would take to fully charge and fully discharge the battery. (practically battery cannot be fully discharged). This time taken by battery is expressed as rate of charge and discharge and it is demonstrated as “C”. Battery can work at different rates (C/5, C/2, C, 2C, 5C etc.) [9], for example we have a battery having capacity 5Ah. At 1C rate it will charge or discharge at 5A and Charged or discharged 1 hr. At 2C it will charge or discharge at 10A and ½ hr. At 5C it charges or discharge at 25A and 12 mints. At C/2 which shows slow charge discharge rate so it charges or discharge at 2.5 A and for 2 hrs. At C/5 it charges or discharge at 1A and 5 hrs [5].

This experiment is conducted at charge discharge rate of C/2 and C/5 for single cell. Charging and discharging profiles are shown below. Cut off voltage for charging is 2.5 V for single cell. And cut off voltage for discharging is 1.5V for single cell [10].

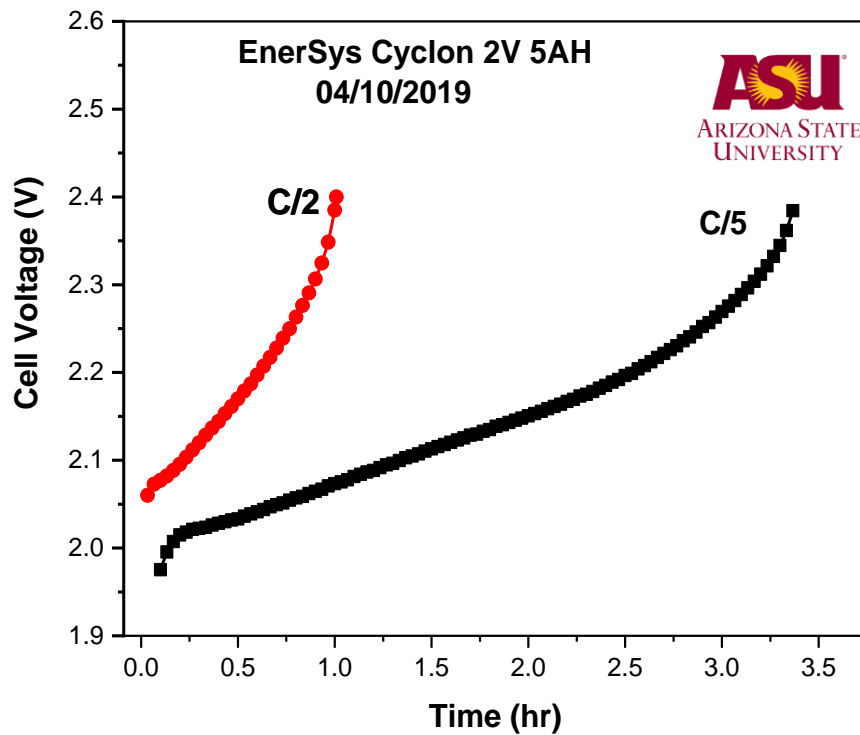


Figure 6.4 Charging curve (rate C/2 and C/5: upto 2.4 V) for single cell battery

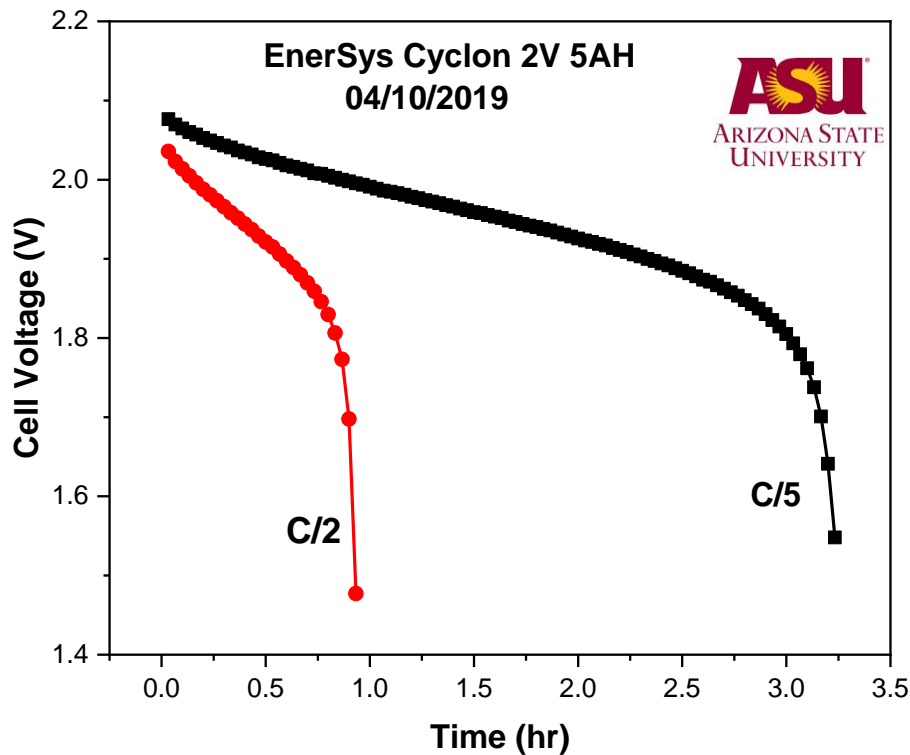


Figure 6.5 Discharge curve (rate C/2 and C/5) for single cell battery after charging up to 2.4V.

The discharging curve shows that the battery can be discharge up to 70% of its full capacity after about three hours. Current and voltage measurement of battery stack is recorded at C/2 discharge rate and charges with C rate. Battery discharges at 2.5A and charges at 1 A. maximum voltage is 6.5 V while charging and 4.5 V while discharging. Batteries charging and discharging patterns can be evaluated at different rates of charging and discharging, depends on applications of batteries. Where power density is required battery will discharge at higher C rates, while on the other case it will discharge at lower C rates.

6.4.3 Electrochemical Impedance spectroscopy (EIS)

The electrochemical impedance was recorded of cell at completely energized state by utilizing PARSTAT 2273 impedance analyzer with a recurrence range 10 μ Hz to 1 kHz. All impedance calculations were performed in the impedance analyzer at room

temperature with the voltage plentifulness (8 % of the phone voltage) of the sinusoidal symbol [3].

Impedance spectroscopy is more reliable to measure SOH rather than SOC, Conductance measurement at frequency range performed at batteries for quality control and provide information about state of health [11-12].

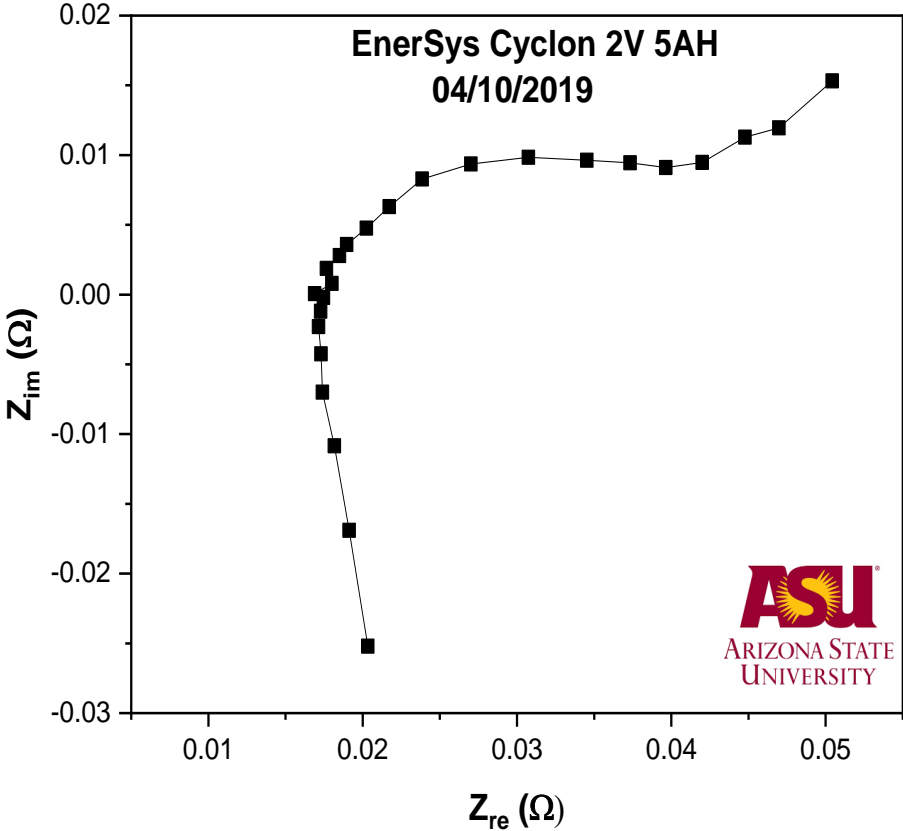


Figure 6.7 Impedance of single cell in charge condition after 10 cycles of charging and discharging cycle

EIS testing is carried out for estimating life of a cell. Impedance is sum of resistance, conductance and inductance collectively, EIS graphs shows relation between real and imaginary Impedance. As battery is used under different charge and discharge rates [13],

its impedance increased due to which life of cell reduced over no of cycles of charging and discharging [9].

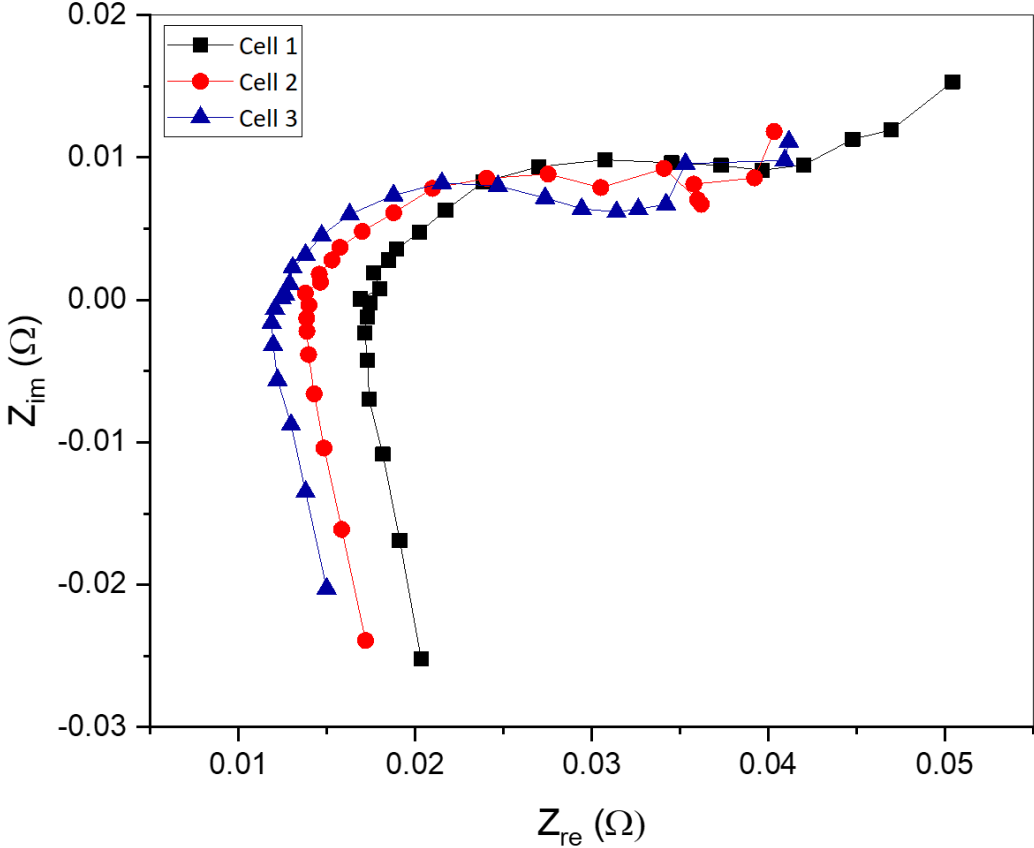


Figure 6.8 Impedence of 3 cells in charge condition after 10 cycles of charging and discharging

Summary of chapter

In this chapter methods to determine State of charge and state of health of Lead acid batteries were discussed . Arbins system was used to estimate SOC and SOH at different rate of charging and dischrnging as well at different temperatues and cycles . program was set in MITs Pro software.then batteries were put under testing on provided conditions and commands. MITS pro software is used to give command to Arbin battery cycling unit Current and voltage measurement of battery stack is recorded at different C rates . EIS was performed to estimate battery life.

References

- [1] A. Allam, E. Catenaro, and S. Onori, “Pushing the Envelope in Battery Estimation Algorithms,” *iScience*, vol. 23, no. 12, p. 101847, 2020, doi: 10.1016/j.isci.2020.101847.
- [2] M. Murnane and A. Ghazel, “A Closer Look at State of Charge (SOC) and State of Health (SOH) Estimation Techniques for Batteries,” *Analog devices*, 2017, [Online]. Available: <http://www.analog.com/media/en/technical-documentation/technical-articles/A-Closer-Look-at-State-Of-Charge-and-State-Health-Estimation-Techniques-....pdf>.
- [3] K. Vignarooban *et al.*, “State of health determination of sealed lead acid batteries under various operating conditions,” *Sustain. Energy Technol. Assessments*, vol. 18, pp. 134–139, 2016, doi: 10.1016/j.seta.2016.10.007.
- [4] L. Tang, G. Rizzoni, and A. Cordoba-Arenas, “Battery Life Extending Charging Strategy for Plug-in Hybrid Electric Vehicles and Battery Electric Vehicles,” *IFAC-PapersOnLine*, vol. 49, no. 11, pp. 70–76, 2016, doi: 10.1016/j.ifacol.2016.08.011.
- [5] P. Krivík, “Methods of SoC determination of lead acid battery,” *J. Energy Storage*, vol. 15, pp. 191–195, 2018, doi: 10.1016/j.est.2017.11.013.
- [6] F. Zhang, G. Liu, and L. Fang, “A battery state of charge estimation method using sliding mode observer,” *Proc. World Congr. Intell. Control Autom.*, pp. 989–994, 2008, doi: 10.1109/WCICA.2008.4593055.
- [7] D. Wang, F. Yang, Y. Zhao, and K. L. Tsui, “Battery remaining useful life prediction at different discharge rates,” *Microelectron. Reliab.*, vol. 78, pp. 212–219, 2017, doi: 10.1016/j.microrel.2017.09.009.
- [8] E. Björklund, E. Wikner, R. Younesi, D. Brandell, and K. Edström, “Influence of state-of-charge in commercial $\text{LiNi}_{0.33}\text{Mn}_{0.33}\text{Co}_{0.33}\text{O}_2/\text{LiMn}_2\text{O}_4$ -graphite cells analyzed by synchrotron-based photoelectron spectroscopy,” *J. Energy Storage*, vol. 15, pp. 172–180, 2018, doi: 10.1016/j.est.2017.11.010.

- [9] A. J. Salkind, P. Singh, A. Cannone, T. Atwater, X. Wang, and D. Reisner, “Impedance modeling of intermediate size lead-acid batteries,” *J. Power Sources*, vol. 116, no. 1–2, pp. 174–184, 2003, doi: 10.1016/S0378-7753(02)00690-0.
- [10] M. Rampazzo, M. Luvisotto, N. Tomasone, I. Fastelli, and M. Schiavetti, “Modelling and simulation of a Li-ion energy storage system: Case study from the island of Ventotene in the Tyrrhenian Sea,” *J. Energy Storage*, vol. 15, pp. 57–68, 2018, doi: 10.1016/j.est.2017.10.017.
- [11] S. Piller, M. Perrin, and A. Jossen, “Methods for state-of-charge determination and their applications,” *J. Power Sources*, vol. 96, no. 1, pp. 113–120, 2001, doi: 10.1016/S0378-7753(01)00560-2.
- [12] I. S. Kim, “The novel state of charge estimation method for lithium battery using sliding mode observer,” *J. Power Sources*, vol. 163, no. 1 SPEC. ISS., pp. 584–590, 2006, doi: 10.1016/j.jpowsour.2006.09.006.
- [13] S. Q. Fan *et al.*, “Ordered multimodal porous carbon as highly efficient counter electrodes in dye-sensitized and quantum-dot solar cells,” *Langmuir*, vol. 26, no. 16, pp. 13644–13649, 2010, doi: 10.1021/la1019873.

Chapter 7

Conclusions and Future Recommendations

7.1 Conclusions

- Bismuth vanadium oxide microspheres were successfully synthesized by using hydrothermal method as indicated by XRD, SEM/EDX and UV-Vis spectroscopy results.
- Bismuth-based nanomaterials have been proposed as possible PEC water splitting candidates and Dye degradation because of their limited band distance and suitable band positions
- The critical problems associated with bismuth based material systems are rapid charge recombination and photocorrosion
- Due to broad surface area and lateral flow of charges, nanostructure synthesis requires facet and morphology regulation. Heterojunctions are also an efficient technique to minimize the charge recombination rate of charge carriers and photo corrosion, different doping is performed to improve intrinsic properties and to increase the charge separation
- It is observed that Photo electrochemical response was increased with addition of hole scavenger
- The $\text{Bi}_{25}\text{VO}_{40}$ structure is stable by yttrium doping as high as 5% yttrium.
- Yttrium doped $\text{Bi}_{25}\text{VO}_{40}$ nanograins decolorized 84.4 % Dye in 180 mins of irradiation while pristine $\text{Bi}_{25}\text{VO}_{40}$ degraded 66 % MB in 180 mins
- The optimal 3% Y^{+3} doping showed significantly improved photocurrent response in comparison to the pristine material. It is important to note that no change in phase and

morphology yet a noticeable change in absorption behavior and reduction in recombination rate with yttrium doping in $\text{Bi}_{25}\text{VO}_{40}$ was noted, that in turns leads to better photocurrent density for water splitting

- 3% Y doped Bismuth vanadate showed 4.12 mA Cm^{-2} at 1 V vs Ag/AgCl. Which shows it is potential candidate for photoelectrochemical water splitting.

7.2 Future Recommendations

To enable active commercialization of Photocatalytic water splitting for hydrogen production and waste water treatment of industrial effluents, need to improve efficiency of harnessing solar photon's energy for these applications. Bismuth vanadate photocatalysts can be used in real waste water as it is visible light active so it can degrade range of pollutants under sun light.

7.2.1 Employing use of different morphologies of Bismuth vanadium oxide

Using various synthesis methods and optimizing the synthesis conditions, various structures such as Nano rods, nanotubes etc. can be synthesized. Photo anode formation using nanoparticles based on structures can produce better photo anode properties and lead to enhanced photocatalytic degradation, Photoelectrochemical water splitting, improved mechanism of conduction, and successful electron transport. In order to further enhance their properties, these structures can be doped with distinct non-metals and metals, thereby enhancing performance and efficiency.

7.2.2 Optimization of Coating processes

The low-cost coating techniques based on the solution can be optimized to create better films. For better activity of the photo anode, better properties and morphology of semiconductor thin films are advantageous. Vacuum based techniques are costly, but they provide the films with the best compositional control. In order to equal the quality of films coated by costly processes, attempts should be made to improve the quality of solution-based thin films. For better and low-cost thin film coatings, optimizing electrochemical methods can be one alternative.

7.2.3 Development of Technique to understand Chemical changes

Next plan for researchers is to develop a technique in order to understand how material changes chemically while operating as a photo anode in PEC system.

7.3 Future Experimentation for better photocatalytic performance of Bismuth Vanadium oxide

Yttrium doped Bismuth vanadium oxide was synthesized by two step solution based hydrothermal synthesis technique and heterojunction with Titania to use photons energy of both visible and UV spectra. And to enhance structural stability. This experiment is currently undergoing. Synthesis procedure is given in Chapter 4, Effect of these heterojunction photo anodes would be tested on different Dyes in order to measure photocatalytic activity. Further we can apply photocatalytic attributes of Bismuth vanadate heterojunctions on different type of pollutants such as pharmaceutical elements. As Bismuth vanadate is visible light active so sunlight can also be used instead of artificial solar light which is step towards commercialization.

Bismuth vanadate will find extensive applications on industrial level owing to its ongoing progress. Mostly degradation products are CO_2 and H_2O . Complete degradation is almost impossible. More degradation products are need to be investigated along with their toxicity. Which will enhance commercialization of this electrochemical system.

